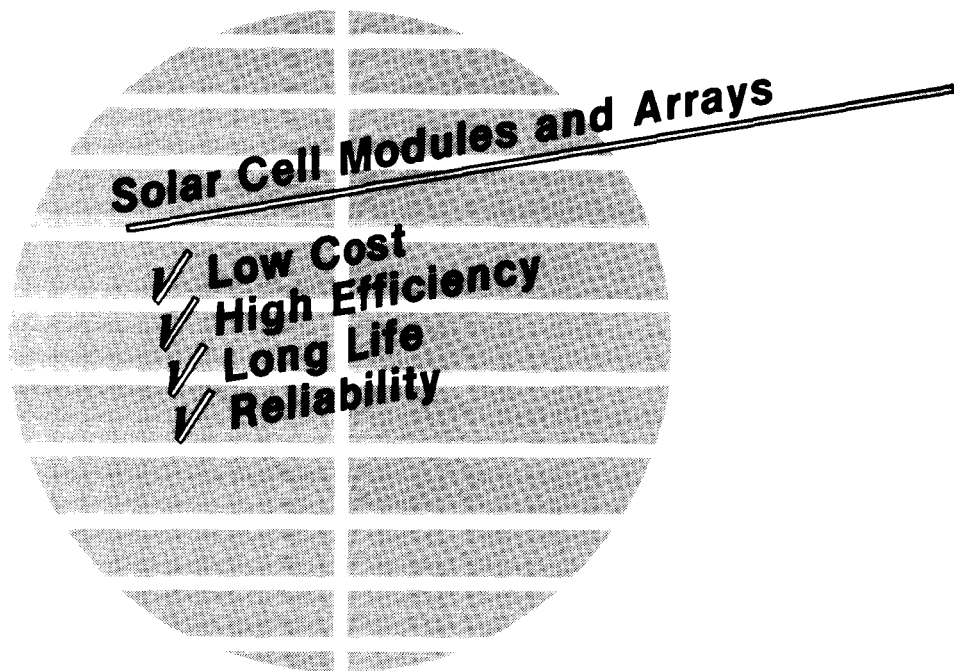


Electricity from Photovoltaic Solar Cells

**Flat-Plate Solar Array Project  
Final Report**

**Volume IV: High-Efficiency Solar Cells**

11 Years of Progress



October 1986

(NASA-CR-180662) FLAT-PLATE SOLAR ARRAY  
PROJECT. VOLUME 4: HIGH-EFFICIENCY SOLAR  
CELLS Final Report (Jet Propulsion Lab.)  
68 p

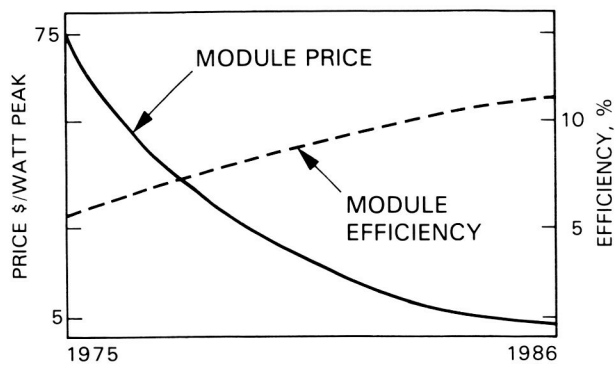
CSCI 10A

N87-20649

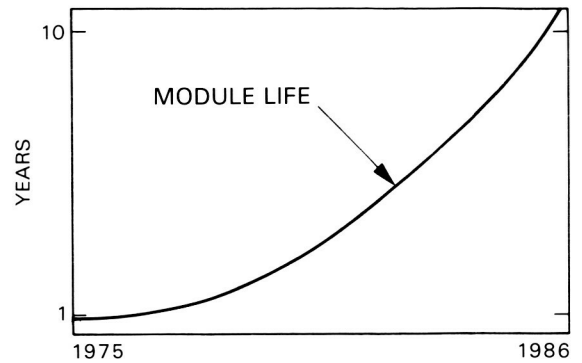
Unclas  
G3/44 45414

Project Managed by the Jet Propulsion Laboratory for the U.S. Department of Energy

# Photovoltaic Module Progress



Flat or non-concentrating module prices have dropped as module efficiencies have increased. Prices are in 1985 dollars for large quantities of commercial products.

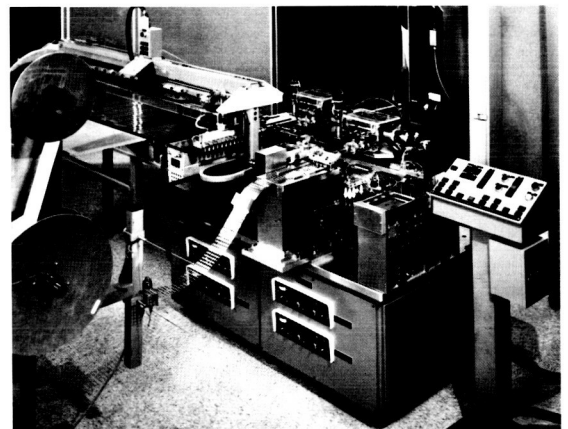


Typical module lifetimes were less than 1 year but are now estimated to be greater than 10 years. (Ten-year warranties are now available.)

## Technology advancement in crystalline silicon solar cells and modules (non-concentrating).



Union Carbide Corporation (UCC) funded the now operational silicon refinement production plant with 1200 MT/year capacity. DOE/FSA-sponsored efforts were prominent in the UCC process research and development.



The automated machine interconnects solar cells and places them for module assembly. The second-generation machine made by Kulicke and Soffa was cost shared by Westinghouse Corporation and DOE/FSA.



A Block I module (fabricated in 1975), held in front of four Block V modules, represents the progress of an 11-year effort. The modules, designed and manufactured by industry to FSA specifications and evaluated by FSA, rapidly evolved during the series of module purchases by DOE/FSA.

More technology advancements of the cooperative industry/university/DOE/FSA efforts are shown on the inside back cover. Use of modules in photovoltaic power systems are shown on the outside back cover.

5101-289  
Flat-Plate  
Solar Array Project

DOE/JPL-1012-125  
Distribution Category UC-63b

Electricity from Photovoltaic Solar Cells

# **Flat-Plate Solar Array Project Final Report**

## **Volume IV: High-Efficiency Solar Cells**

**M. Leipold  
L. Cheng  
T. Daud  
A. Mokashi  
D. Burger**

11 Years of Progress

October 1986

Prepared for  
U.S. Department of Energy  
Through an Agreement with  
National Aeronautics and Space Administration  
by  
Jet Propulsion Laboratory  
California Institute of Technology  
Pasadena, California

Project Managed  
by the  
Jet Propulsion Laboratory  
for the  
U.S. Department of Energy's  
National Photovoltaics Program

JPL Publication 86-31

# Final Report Organization

This FSA Final Report (JPL Publication 86-31, 5101-289, DOE/JPL 1012-125, October 1986) is composed of eight volumes, consisting of an Executive Summary and seven technology reports:

- Volume I: Executive Summary.
- Volume II: Silicon Material.
- Volume III: Silicon Sheet: Wafers and Ribbons
- Volume IV: High-Efficiency Solar Cells.
- Volume V: Process Development.
- Volume VI: Engineering Sciences and Reliability.
- Volume VII: Module Encapsulation.
- Volume VIII: Project Analysis and Integration.

Two supplemental reports included in the final report package are:

*FSA Project: 10 Years of Progress*, JPL Document 400-279, 5101-279, October 1985.

*Summary of FSA Project Documentation: Abstracts of Published Documents, 1975 to 1986*, JPL Publication 82-79 (Revision 1), 5101-221, DOE/JPL-1012-76, September 1986.

Upon request, this FSA Final Report (JPL Publication 86-31) and the two supplemental reports (JPL Document 400-279 and JPL Publication 82-79) are individually available in print from:

National Technical Information Service  
U.S. Department of Commerce  
5285 Port Royal Road  
Springfield, VA 22161

# Abstract

The Flat-Plate Solar Array (FSA) Project, funded by the U.S. Government and managed by the Jet Propulsion Laboratory, was formed in 1975 to develop the module/array technology needed to attain widespread terrestrial use of photovoltaics by 1985. To accomplish this, the FSA Project established and managed an Industry, University, and Federal Government Team to perform the needed research and development (R&D).

The High-Efficiency Solar Cells Task was assigned the objective of understanding and developing high-efficiency solar cell devices that would meet the cost and performance goals of the FSA Project. The need for research dealing with high efficiency devices was considered important because of the role efficiency plays in reducing the price per watt of generated energy.

This document is a summary of the R&D efforts conducted during the period 1982 to 1986 to provide understanding and control of energy conversion losses associated with crystalline-silicon solar cells. New levels of conversion efficiency (greater than 20%) were demonstrated. Major contributions were made both to the understanding and reduction of bulk and surface losses in solar cells. For example, oxides, nitrides, and polysilicon were all shown to be potentially useful surface passivants. Improvements in measurement techniques were made and Auger coefficients and spectral absorption data were obtained for unique types of silicon sheet. New modeling software was developed including a program to optimize a device design based on input characteristics of a cell. Although considerable progress was made in this Task, several elements of research were incomplete at the conclusion of the Project.

# Foreword

Throughout U.S. history, the Nation's main source of energy has changed from wood to coal to petroleum. It is inevitable that changes will continue as fossil fuels are depleted. Within a lifetime, it is expected that most U.S. energy will come from a variety of sources, including renewable energy sources, instead of from a single type of fuel. More than 30% of the energy consumed in the United States is used for the generation of electricity. The consumption of electricity is increasing at a faster rate than the use of other energy forms and this trend is expected to continue.

Photovoltaics, a promising way to generate electricity, is expected to provide significant amounts of power in years to come. It uses solar cells to generate electricity directly from sunlight, cleanly and reliably, without moving parts. Photovoltaic (PV) power systems are simple, flexible, modular, and adaptable to many different applications in an almost infinite number of sizes and in diverse environments. Although photovoltaics is a proven technology that is cost-effective for hundreds of small applications, it is not yet cost-effective for large-scale utility use in the United States. For widespread economical use, the cost of generating power with photovoltaics must continue to be decreased by reducing the initial PV system cost, by increasing efficiency (reduction of land requirements), and by increasing the operational lifetime of the PV systems.

In the early 1970s, the pressures of the increasing demand for electrical power, combined with the uncertainty of fuel sources and ever-increasing prices for petroleum, led the U.S. Government to initiate a terrestrial PV research and development (R&D) project. The objective was to reduce the cost of manufacturing solar cells and modules. This effort, assigned to the Jet Propulsion Laboratory, evolved from more than a decade-and-a-half of spacecraft PV power-system experience and from recommendations of a conference on Solar Photovoltaic Energy held in 1973 at Cherry Hill, New Jersey.

This Project, originally called the Low-Cost Solar Array Project, but later known as the Flat-Plate Solar Array (FSA) Project, was based upon crystalline-silicon technology as developed for the space program. During the 1960s and 1970s, it had been demonstrated that photovoltaics was a dependable electrical power source for spacecraft. In this time interval, solar-cell quality and performance improved while the costs decreased. However, in 1975 the costs were still much too high for widespread use on Earth. It was necessary to reduce the manufacturing costs of solar cells by a factor of approximately 100 if they were to be a practical, widely used terrestrial power source.

The FSA Project was initiated to meet specific cost, efficiency, production capacity, and lifetime goals by R&D in all phases of flat-plate module (non-concentrating) technology, from solar-cell silicon material purification through verification of module reliability and performance.

The FSA Project was phased out at the end of September 1986.

# Acknowledgments

A Solar Cell Advisory Committee, under the direction of T. Daud and M. Leipold and chaired by M. Wolf, was established to assist in directing the technology development related to solar cells. It met 22 times on an approximately triannual basis. Its members included R. Davis (deceased), P. Iles, F. Lindholm, J. Loferski, E. Ralph, B. Ross (deceased), G. Schwuttke, and C. Wrigley.

Jet Propulsion Laboratory (JPL) staff members were involved in laboratory research, technology critiques, process and problem analyses, and the technical management of contracts. A. Kachare was Manager of this program to which the following JPL engineers contributed: P. Alexander, D. Burger, L. Cheng, R. Cockrum, G. Crotty, T. Daud, K. Dumas, B. Gallagher, P. Grunthaner, S. Hyland, M. Leipold, A. Mokashi, P. Seshan, R. Stirn, G. Turner, and O. von Roos (deceased).

Greatly appreciated is the assistance of E. Christensen, J. Murry, and I. Bengelsdorf in editing this document, and of S. Montanez, V. Guzman, and M. Koop in its typing.

This document reports on work done under NASA Task RE-152, Amendment 419, DOE/NASA IAA DE-A101-85CE89008.

# FSA Project Summary

The Flat-Plate Solar Array (FSA) Project, a Government-sponsored photovoltaic (PV) project, was initiated in January 1975 with the intent to stimulate the development of PV systems for economically competitive, large-scale terrestrial use. The Project's goal was to develop, by 1985, the technology needed to produce PV modules with 10% energy conversion efficiency, a 20-year lifetime, and a selling price of \$0.50/W<sub>p</sub> (in 1975 dollars). The key achievement needed was cost reduction in the manufacture of solar cells and modules.

As manager, the Jet Propulsion Laboratory organized the Project to meet the stated goals through research and development (R&D) in all phases of flat-plate module technology, ranging from silicon-material refinement through verification of module reliability and performance. The Project sponsored parallel technology efforts with periodic progress reviews. Module manufacturing cost analyses were developed that permitted cost-goal allocations to be made for each technology. Economic analyses, performed periodically, permitted assessment of each technical option's potential for meeting the Project goal and of the Project's progress toward the National goal. Only the most promising options were continued. Most funds were used to sponsor R&D in private organizations and universities, and led to an effective Federal Government-University-Industry Team that cooperated to achieve rapid advancement in PV technology.

Excellent technical progress led to a growing participation by the private sector. By 1981, effective energy conservation, a leveling of energy prices, and decreased Government emphasis had altered the economic perspective for photovoltaics. The U.S. Department of Energy's (DOE's) National Photovoltaics Program was redirected to longer-range research efforts that the private sector avoided because of higher risk and longer payoff time. Thus, FSA concentrated its efforts on overcoming specific critical technological barriers to high efficiency, long life, reliability, and low-cost manufacturing.

To be competitive for use in utility central-station generation plants in the 1990s, it is estimated that the price of PV-generated power will need to be \$0.17/kWh (1985 dollars). This price is the basis for a DOE Five-Year Photovoltaics Research Plan involving both increased cell efficiency and module lifetime. Area-related costs for PV utility plants are significant enough that flat-plate module efficiencies must be raised to between 13 and 17%, and module life extended to 30 years. Crystalline silicon, research solar cells (non-concentrating) have been fabricated with more than 20% efficiency. A full-size experimental 15% efficient module also has been fabricated. It is calculated that a multimegawatt PV power plant using large-volume production modules that incorporate the latest crystalline silicon technology could produce power for about \$0.27/kWh (1985 dollars). It is believed that \$0.17/kWh (1985 dollars) is achievable, but only with a renewed and dedicated effort.

Government-sponsored efforts, plus private investments, have resulted in a small, but growing terrestrial PV industry with economically competitive products for stand-alone PV power systems. A few megawatt-sized, utility-connected, PV installations, made possible by Government sponsorship and tax incentives, have demonstrated the technical feasibility and excellent reliability of large, multimegawatt PV power-generation plants using crystalline silicon solar cells.

## Major FSA Project Accomplishments

- Established basic technologies for all aspects of the manufacture of nonconcentrating, crystalline-silicon PV modules and arrays for terrestrial use. Module durability also has been evaluated. These resulted in:
  - Reducing PV module prices by a factor of 15 from \$75/W<sub>p</sub> (1985 dollars) to \$5/W<sub>p</sub> (1985 dollars).
  - Increasing module efficiencies from 5 to 6% in 1975 to more than 15% in 1985.
  - Stimulating industry to establish 10-year warranties on production modules. There were no warranties in 1975.
  - Establishing a new, low-cost high-purity silicon feedstock-material refinement process.
  - Establishing knowledge and capabilities for PV module/array engineering/design and evaluation.
  - Establishing long-life PV module encapsulation systems.
  - Devising manufacturing and life-cycle cost economic analyses.
- Transferred technologies to the private sector by interactive activities in research, development, and field demonstrations. These included 256 R&D contracts, comprehensive module development and evaluation efforts, 26 Project Integration Meetings, 10 research forums, presentations at hundreds of technical meetings, and advisory efforts to industry on specific technical problems.
- Stimulated the establishment of a viable commercial PV industry in the United States.

# High-Efficiency Solar Cells Summary

At the inception of the Flat-Plate Solar Array (FSA) Project in 1975, the energy-conversion efficiency goal for photovoltaic (PV) modules was 10%, as had been recommended by the 1973 Cherry Hill conferees. Conventional terrestrial crystalline silicon solar cells in 1975 were capable of achieving 10% conversion efficiency, while modules had a 5 to 6% efficiency. By the end of the Project, these efficiencies were expected to increase gradually to 13% or more for cells and to 10% for modules. This was anticipated to be adequate for widespread use of photovoltaics. For this reason, initial emphasis in the Project on solar cell development was directed toward reductions in manufacturing cost through process simplification, automation, and better process control and product yields.

In the period following 1979, analysis of the costs to produce electricity with terrestrial PV power systems made it clear that greater improvements in cell and module efficiency would be necessary. The early emphasis on residential rooftop and intermediate installations changed to emphasize central station applications. For this central station use, land-area related costs of PV systems were recognized to be more important than previously thought. Thus, there was need for higher efficiencies. These considerations are discussed more extensively in Volume VIII: Project Analysis and Integration.

The efficiency goal established in the 1983 U.S. Department of Energy (DOE) Five-Year Plan was 15% for low-cost modules. Of course, even higher module efficiencies would be of greater benefit to the development of terrestrial PV applications. Low-cost modules with 15% efficiency require conversion efficiencies of individual cells to be greater than 17%. In 1982, in response to requirements for increased conversion efficiency, the High-Efficiency Solar Cells Task (also known within the FSA Project as the Device Research Task) was established within the Project. The primary responsibility of this Task was to define, understand, and develop techniques to reduce the energy-conversion losses associated with existing or new solar cell designs.

At the beginning of the Task, every aspect of a crystalline silicon solar cell was thought to require improvement. Ultimately, four technical areas for research were selected because they offered the greatest potential for enhancement of solar cell performance: (1) bulk losses in the silicon, (2) surface losses, (3) design and fabrication of high-efficiency solar cells, and (4) modeling and measurements.

A major cause of poor performance of solar cells results from carrier losses that arise from recombination in the bulk. Carrier diffusion lengths of the order of the thickness of the solar cell (about 150 to 300  $\mu\text{m}$ ) were found to be necessary. The Task produced considerable understanding of the sources and effects of several bulk losses such as dislocations and chemical impurities. Means to reduce these losses were demonstrated.

Another large source of losses in silicon solar cells involves losses at the surfaces and interfaces. In the case of a free (external) surface, knowledge derived from complementary metal-oxide silicon technology indicated that the use of silicon dioxide ( $\text{SiO}_2$ ) on the cell's surface was effective in reducing carrier losses at the surface. However, no understanding existed for a process to be used on unconventional, low-cost types of silicon sheet used for photovoltaics, as opposed to the conventional Czochralski and float-zone (FZ) silicon sheet. The use of  $\text{SiO}_2$  on heavily doped surfaces also had not been evaluated. The Task successfully demonstrated that  $\text{SiO}_2$  was effective as a surface passivant as were other compounds, e.g., silicon nitrides. A novel double-layer, antireflective coating was developed that also was effective as a surface passivant. At the conclusion of the Project, a good foundation for understanding surface passivation had been developed, but the potential for significant improvement remains.

Those cell areas where metal makes contact with the silicon must be passivated if solar cell performance of greater than 20% is to be achieved. The deposition of fine-grained polysilicon layers on these areas, before metallization, was investigated, and initial results were encouraging. This aspect of the program was largely incomplete at the conclusion of the Project. Additional research will be required to provide more definitive answers.

Evaluation of the effectiveness of loss-reduction approaches and novel device designs required the fabrication of solar cells and measurement of their performance. A state-of-the-art solar cell laboratory was established at the Jet Propulsion Laboratory. In conjunction with other existing laboratories, it served to make the above-described evaluations. Among the various concepts evaluated, a novel floating emitter design was developed and showed promise. A 4-cm<sup>2</sup> solar cell with more than 20% conversion efficiency was made, and its simple design holds promise for commercial production. Data were generated describing the energy-conversion efficiency of cells made from the unconventional sheet forms developed in the Sheet Task. These data were invaluable in evaluating the performance potential of cells fabricated from silicon prepared by low-cost sheet growth methods.

The fourth element in the Task included both modeling and measurement activities. New methods for the modeling of solar cell performance by computer simulation were developed and used separately and in conjunction with existing programs. This modeling ultimately provided a means to focus on the elements of a solar cell most

critical to its performance. Modeling also provided a means to evaluate research approaches before they were attempted and provided direction to the other research elements within the Task. Several specific computer programs were developed, including one to optimize predicted solar cell performance. These programs and programs obtained from other sources were installed in JPL computers. Specific analyses of existing solar cells were made and agreement of model calculations with measured performance successfully demonstrated the validity of the modeling. Calculations for theoretical solar cell designs were made and used to direct the Task research.

Specialized measurement techniques were developed to permit measurement of specific loss-parameters as well as the electrical output of a solar cell. The measurement of carrier lifetime and surface recombination velocity in the thin, highly doped emitter region was especially important. Determination of characteristics such as Auger coefficients and absorption coefficients for the unconventional types of silicon sheet also were made.

The Task made numerous important contributions to the understanding and improvement of silicon PV devices. The overall effectiveness of these studies best can be demonstrated by the increase in measured crystalline-silicon solar cell performance from 17% to >22% during the period of the Task's existence. Although all of the improved cells were not produced under direct support of this Task, the contribution of the Task is clear. These improved cells demonstrate that the fabrication of very high performance, crystalline silicon cells is feasible, although the cells are of small size, and used expensive processes and high-cost float-zone silicon for their production. Clearly, these developments must be extended to include silicon sheet, processes and sizes that are consistent with large-scale low-cost production processes.

Therefore, at the conclusion of the Project, some Task activities must be described as incomplete. Principally, the detailed nature of the bulk and surface loss mechanism requires better understanding and application of the understanding to the unconventional types of silicon sheet. All of the highest performance solar cells use FZ silicon wafers, a high-cost source of silicon sheet. Replacement of this source by a lower cost material that will still yield these highest efficiency cells is needed. Better as-grown sheet quality and/or better means of reducing losses are required. Additional research is necessary to complete these studies. Technical developments will continue after the conclusion of the FSA Project with part of the support, at least, coming from DOE.

# Contents

I.	INTRODUCTION .....	1
A.	BACKGROUND .....	1
B.	TASK ACTIVITIES: 1982 to 1986 .....	2
II.	BULK LOSSES .....	7
A.	INTRODUCTION .....	7
B.	LIMITS TO BULK LOSS IN HIGH-EFFICIENCY SILICON SOLAR CELLS: C.T. SAH ASSOCIATES .....	8
C.	OXYGEN AND CARBON IN SILICON: STATE UNIVERSITY OF NEW YORK AT ALBANY .....	8
D.	STRUCTURAL AND CHEMICAL DEFECTS: CORNELL UNIVERSITY .....	10
E.	HEAVY DOPING AND OTHER BULK EFFECTS IN HIGH-EFFICIENCY SILICON SOLAR CELLS: UNIVERSITY OF FLORIDA .....	11
F.	HEAVY DOPING EFFECTS IN EMITTER: STANFORD UNIVERSITY .....	11
G.	SILICON SHEET BY MOLECULAR BEAM EPITAXY: UNIVERSITY OF CALIFORNIA, LOS ANGELES .....	12
H.	HYDROGEN PASSIVATION: PENNSYLVANIA STATE UNIVERSITY .....	13
I.	STRUCTURAL DEFECTS: JET PROPULSION LABORATORY .....	14
J.	ABSORPTION COEFFICIENT MEASUREMENT: JET PROPULSION LABORATORY .....	17
K.	PRESENT STATUS .....	17
L.	KEY ACCOMPLISHMENTS .....	17
M.	FUTURE NEEDS .....	17
III.	SURFACE LOSSES .....	19
A.	INTRODUCTION .....	19
B.	SILICON SURFACE PASSIVATION BY SILICON NITRIDE: JOINT CENTER FOR GRADUATE STUDY AT THE UNIVERSITY OF WASHINGTON .....	19
C.	SURFACE PASSIVATION BY HEAVILY DOPED POLYCRYSTALLINE SILICON: UNIVERSITY OF FLORIDA .....	21
D.	INTERFACIAL BARRIERS: STANFORD UNIVERSITY .....	22
E.	MICROCRYSTALLINE SILICON HETEROJUNCTION: APPLIED SOLAR ENERGY CORP. AND BOSTON COLLEGE .....	23
F.	X-RAY PHOTOEMISSION SPECTROSCOPY: JET PROPULSION LABORATORY .....	24
G.	TRANSPARENT CONDUCTING POLYMERS: JET PROPULSION LABORATORY .....	25
H.	PRESENT STATUS .....	26
I.	KEY ACCOMPLISHMENTS .....	26
J.	FUTURE NEEDS .....	27

IV. ADVANCED SOLAR CELL DEVICES AND PROCESSES .....	29
A. INTRODUCTION .....	29
B. HIGH-EFFICIENCY CELLS PREPARED FROM WEB SILICON: WESTINGHOUSE .....	29
C. FLOATING EMITTER CELL DESIGN: APPLIED SOLAR ENERGY CORP. ....	30
D. EVALUATION OF LOW-COST SHEET FOR CELL EFFICIENCY: APPLIED SOLAR ENERGY CORP. ....	31
E. RAPID THERMAL PROCESSING: NORTH CAROLINA STATE UNIVERSITY .....	34
F. HIGH-EFFICIENCY SOLAR CELL PROCESSING: JET PROPULSION LABORATORY .....	34
G. PRESENT STATUS .....	37
H. KEY ACCOMPLISHMENTS .....	37
I. FUTURE NEEDS .....	37
V. MODELING AND MEASUREMENTS .....	39
A. INTRODUCTION .....	39
B. CPU-EFFICIENT DEVICE MODELING CODE: RESEARCH TRIANGLE INSTITUTE .....	40
C. OPTIMIZATION METHODS FOR SOLAR CELL NUMERICAL MODELS: UNIVERSITY OF CALIFORNIA, LOS ANGELES .....	40
D. MEASUREMENT OF RECOMBINATION LIFETIME AND SURFACE RECOMBINATION VELOCITY: UNIVERSITY OF FLORIDA .....	41
E. CRYOGENIC LASER CALORIMETRY FOR IMPURITY ANALYSIS: UNIVERSITY OF SOUTHERN CALIFORNIA .....	41
F. LOSS MEASUREMENT IN HEAVILY DOPED EMITTERS: UNIVERSITY OF PENNSYLVANIA .....	42
G. DEVICE MODELING: JET PROPULSION LABORATORY .....	42
H. ELECTRON-BEAM INDUCED CURRENT CHARACTERIZATION OF SOLAR CELLS: JET PROPULSION LABORATORY .....	44
I. ELECTRON-BEAM INDUCED CURRENT MEASUREMENTS OF MINORITY CARRIER RECOMBINATION: JET PROPULSION LABORATORY .....	45
J. MINORITY CARRIER LIFETIME IN SILICON SHEETS: JET PROPULSION LABORATORY .....	46
K. PRESENT STATUS .....	47
L. KEY ACCOMPLISHMENTS .....	47
M. FUTURE NEEDS .....	47
VI. OVERVIEW STATUS .....	49
A. KEY ACCOMPLISHMENTS .....	49
B. ADDITIONAL RESEARCH NEEDED .....	49

VII. REFERENCES .....	51
-----------------------	----

## APPENDIXES

APPENDIX A: ACQUISITION OF REFERENCES .....	A-1
---	-----

APPENDIX B: GLOSSARY .....	B-1
----------------------------	-----

## Figures

1. Crystalline Silicon Solar Cell .....	3
2. Current-Voltage Curve of a High-Efficiency Solar Cell .....	3
3. Key Factors that Influence Cell Efficiency .....	3
4. High Resolution TEM Picture of the (552)/(552) Tilt Boundary of Silicon .....	10
5. Calculated AM0 Efficiency of a Cascade Cell Versus Interface Recombination Velocity .....	13
6. Rutherford Backscattering Data in the Channeling and Random Mode from Silicon Samples Subjected to Low-Energy Ion Beams .....	14
7. EBIC Photographs of an Area of a Dendritic Web Ribbon Solar Cell .....	15
8. EBIC Photographs Taken from Three Different Areas of a Cross-Section of an "as-grown" Silicon Dendritic-Web Ribbon at Room Temperature .....	16
9. Schematic of PECVD System .....	20
10. Valence Band of 13 Å SiO <sub>2</sub> Over Si [100] .....	23
11. Conduction Band of 13 Å SiO <sub>2</sub> Over Si [100] .....	24
12. XPS Si 2p Spectra Obtained as a Function of Silicon Nitride Thickness .....	25
13. Typical Conducting Polymers and Structure with Dopant and Range of Conductivities .....	25
14. Electrochemical Synthesis of Poly(Pyrrole) .....	26
15. Model Calculations for the Effect of Electrical Activity of the Twin Plane on V <sub>OC</sub> in 0.2 Ω-cm Web Cells .....	31
16. Twin Planes in Web Showing Impact of Dislocations on Efficiency .....	32
17. LBIC Scans of Beveled Sample Prepared from Cell 17C (9.5% AM1) .....	33
18. Floating Emitter Solar Cell Transistor .....	33
19. Baseline Process Sequence .....	35
20. Calculated Solar Cell Parameters for Dot Junctions with 100-μm Separation (S) .....	36
21. (a) Electronic Circuit Used in the SCCD Method, (b) Schematic Illustration of the Current Decay Displayed on a Log Scale .....	41
22. Contour Plot of the rms Data (the ASLBIC Method) .....	43
23. Schematic Cross-Section of a Passivated Thin Silicon Solar Cell Design .....	44
24. Sensitivity of Efficiency of Solar-Cell Thickness for Various Minority Carrier Lifetime Values .....	44
25. Impact of Practical Barriers on Silicon Cell Performance .....	45

26. Impact of Shadowing and Surface Recombination Velocities on Silicon Solar Cell Performance . . . . .	46
27. High-Low Junction Voltage, (measured) Versus Cell Applied Voltage . . . . .	46

## Tables

1. Theoretical Limits and Typical Losses in High-Efficiency Solar Cells . . . . .	2
2. Contractor List for High-Efficiency Device Task . . . . .	4
3. Performance of Silicon Solar Cells as a Function of Various Loss Mechanisms . . . . .	9
4. Performance of Molecular-Beam Epitaxy Silicon Solar Cells . . . . .	13
5. Comparison of Optical Constants Determined from Ellipsometry and Ordinary Reflectance . . . . .	21
6. Summary of Measured Parameters at 28 °C Without Antireflective Coating . . . . .	22
7. Flat Band Potentials of p-Si as a Function of Conducting Polymers . . . . .	26
8. Comparison of the Light I-V Data of the Silicon Solar Cells Passivated by SiO <sub>2</sub> and TiO <sub>x</sub> /Al <sub>2</sub> O <sub>3</sub> . . . . .	35
9. Dot Junction Solar-Cell Results and Corresponding Efficiency . . . . .	36

## SECTION I

# Introduction

In 1975, terrestrial photovoltaic (PV) modules with 6% efficiency were available from conventional, crystalline silicon, solar cell technology. But, in the late 1970s, as various research and development (R&D) efforts in the Flat-Plate Solar Array (FSA) Project proceeded, it was seen that the original Project goal of 10% *module efficiency* would be met as a result of the ongoing FSA efforts. It was anticipated this would occur as *solar cell efficiencies* improved and as module packing factors increased (more active solar cell area per unit of module area). Obviously, cell efficiency should increase as cell design and fabrication technology matured. Module packing factors of 0.90 were thought to be achievable, up from the 0.60 to 0.70 common in 1975.

By the early 1980s, numerous economic analyses of large PV power systems indicated that module efficiency must be about 15% for photovoltaics to be economically competitive. These analyses were based on the premise that central station PV installations would be the first widespread application of photovoltaics in the United States. The achievement of 15% efficiency production modules requires the repeatable fabrication of large-area laboratory solar cells with 20% or greater efficiency. This would demonstrate that high-efficiency solar cell principles are understood. Present-day cells in this high-performance range are too small to be considered for practical solar modules. This knowledge then must be converted into a technology of low-cost cell production that would yield uniform quality production cells of 17 to 18% efficiency needed to yield modules with efficiencies of 15%.

Thus, the objective of the High-Efficiency Solar Cell Task<sup>1</sup> was to perform research to identify and resolve key generic limitations to increasing efficiency of crystalline-silicon solar cells.

The goal of the High-Efficiency Device Task was to establish solar cell technology required for repeatable fabrication of laboratory, crystalline-silicon solar cells with greater than 20% efficiency.

### A. BACKGROUND

The need for high-power output from spacecraft solar cell arrays initially motivated research for higher efficiency cells. The research broadened with the realization that photovoltaics had the potential to become a practical terrestrial power source. Consequently, the efficiency of silicon solar cells has been gradually

increasing as a result of: systematic efforts to better understand how solar cells function, better understanding of their internal loss mechanisms, better cell designs, and improved processing. Many relatively small advances through the years have added to the knowledge of solar cell technology and to increased cell efficiency. Early progress in cell designs and process techniques was largely empirical. This has subsequently been strengthened by better theoretical understanding of the underlying principles of cell operation. These activities have led to a general agreement regarding the factors that limit cell performance and to those that can be changed to increase the efficiency of crystalline-silicon solar cells. Table 1 shows losses in cells that occur as a result of a variety of effects and that have an influence on all of the performance parameters. The difference between a measured parameter and its theoretical maximum provides an excellent guide to the key problems to be addressed.

In selecting loss mechanisms for study within this Task, careful attention was paid to the fundamental nature of the problem and its understanding. For example, several significant losses of both cells and modules were not considered because they are well understood and their solution is largely a matter of engineering development and technology. These include multiple layer antireflective (AR) coatings and module design considerations such as cell packing factor, cell shape, module size, etc. Other tasks in the FSA Project developed these aspects of the technology. Results of these efforts can be found in Volume V: Processing Development, Volume VI: Engineering Sciences and Reliability, and Volume VII: Module Encapsulation.

Present solar cell conversion efficiencies are:

- (1) Production cells made from Czochralski (Cz) wafers for use in space (about 18%).
- (2) Production cells made from Cz wafers for low-cost terrestrial use (up to 14%).
- (3) Production cells, made from silicon ribbons, (greater than 13%).
- (4) Research cells made from float-zone (FZ) silicon (22%). (The predicted theoretical limit of efficiency for crystalline-silicon cells is about 30%, and the probable maximum achievable limit of efficiency is about 25%).

---

<sup>1</sup> Within the FSA Project, this Task was known as the Device Research Task.

Table 1. Theoretical Limits and Typical Losses in High-Efficiency Solar Cells

Loss	Values of Loss (%)		
	Ideal Cell	Demonstration Cell	Production Cell
In light-generated current (theoretical limit = 44 mA/cm <sup>2</sup> ) by:			
Optical reflection	0	3.0	5.0
Contact coverage	0	3.0	3.0
Incomplete absorption } Recombination }	0	5.0	12.0
Dead layers	0	0	0
Achieved current (mA/cm <sup>2</sup> )	44.0	39.3	35.7
In open circuit voltage (theoretical limit = 0.837 V) <sup>a</sup> by:			
Recombination (bulk, surface, contacts)	0	15.0	35.0
Bandgap narrowing, current leakage	0	0 <sup>b</sup>	0 <sup>b</sup>
Achieved voltage (V <sub>OC</sub> ) <sup>c</sup>	0.837	0.71	0.54
Fill factor			
Same losses as open-circuit voltage, above	0	13.0	15.0
Recombination in depletion zone	0	1.0	2.0
Series/contact resistance	0	1.0	2.0
Achieved fill factor <sup>c</sup>	0.96	0.82	0.78
Resultant efficiency % (AM1)	35.0	22.8	17.1

<sup>a</sup>AM0; black body cell.  
<sup>b</sup>With appropriate doping levels.  
<sup>c</sup>Amount remaining after application of losses to theoretical limits.

## B. TASK ACTIVITIES: 1982 TO 1986

A general technical approach was established to increase solar cell efficiency to greater than 20%. The changes required in certain cell parameters to achieve this high efficiency have been identified. The exact cell parametric changes and the cell design modifications required to fabricate large-area 20% laboratory cells consistently, however, have not been devised.

The main features of a crystalline silicon solar cell are shown in Figure 1. For more than a decade, there have been significant improvements in crystalline solar cell performance, mainly as a result of successful

attempts to increase cell short-circuit current ( $I_{SC}$ ) output. Figure 2 is a current-voltage (I-V) curve showing the current and voltage of a typical solar cell. Improvements have resulted through use of shallow junctions, back-surface fields (BSFs), back-surface reflectors (BSRs), textured surfaces, and multilayer AR coatings. There is some potential for further improvements in cell  $I_{SC}$ , but that potential is limited. Single-junction crystalline-silicon cell performance can be improved substantially, however, by increasing the cell open-circuit voltage ( $V_{OC}$ ). Losses in the  $V_{OC}$  derive largely from recombination at the surfaces of the cell and at recombination centers distributed throughout the bulk of the silicon material. The surface-related losses

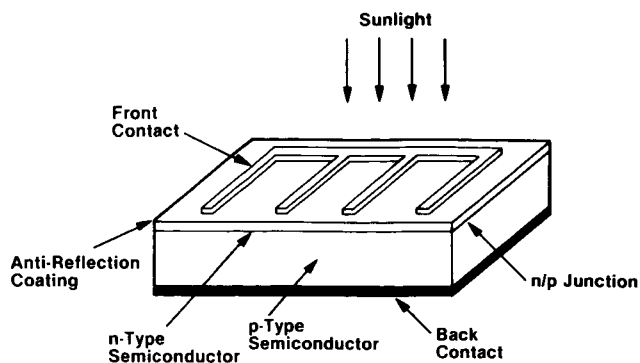


Figure 1. Crystalline Silicon Solar Cell

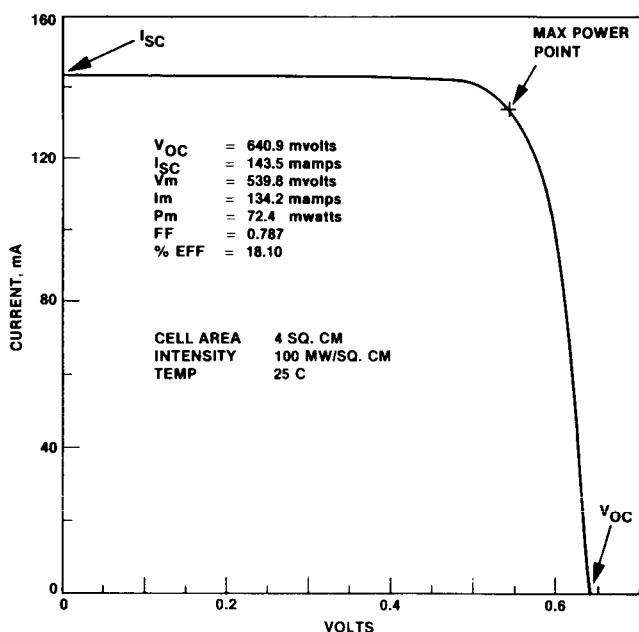


Figure 2. Current-Voltage Curve of a High-Efficiency Solar Cell

result primarily from cell design and processing, and the internal recombination centers are largely a result of the original growth process of the silicon crystal. Surface losses provide the major portion of  $V_{oc}$  losses.

Primary thrust of the FSA high-efficiency efforts was directed toward reducing solar cell losses in both bulk and surfaces, with specific focus on reducing the minority carrier recombination rates throughout the cell. Methods used involved increasing minority carrier lifetime by reducing the volume for bulk recombination and reducing surface recombination. Experiments are possible to reduce recombination in the thin emitter region and at the cell surface by obtaining silicon sheet in which the recombination rates in the bulk material did not dominate cell performance. Future cells are likely to be multilayer structures with each layer designed according to its properties and those of other layers. Figure 3 describes the factors that influence efficiency of a solar cell.

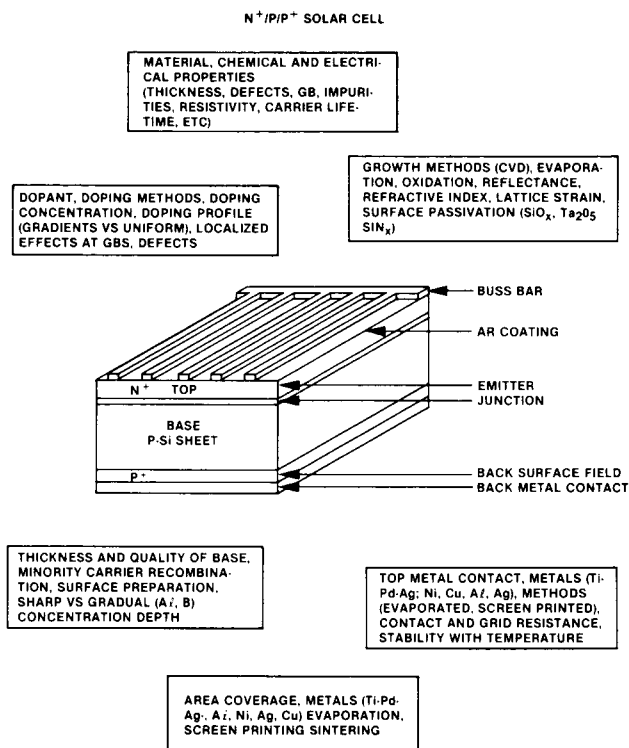


Figure 3. Key Factors that Influence Cell Efficiency

Within the Task, efforts were directed toward better understanding of the physics of carrier losses. This knowledge permits these losses to be overcome through the use of comprehensive modeling, the development and use of new and improved measurement techniques, and the investigation of a variety of surface passivation approaches including transparent conducting materials. Much of this work was performed by contractors and a list of the research topics and contractors is given in Table 2.

The surface recombination velocity of charge carriers within a solar cell is in the vicinity of  $10^5$  cm/s. An effort to reduce the velocity to less than  $10^3$  cm/s addressed problems of controlling recombination losses at surfaces and interfaces. To better understand and control surface and interface phenomena, surface passivants (such as  $\text{SiN}_x$ ), polycrystalline silicon, and ultrathin silicon dioxide layers were investigated. Reliable measurement techniques were developed to characterize passivants, surfaces, and interfaces. As part of surface loss investigations, work on transparent conducting materials emphasized study of the interaction of a polymer with a silicon surface and the resultant effects on optical and electrical characteristics.

Studies to understand and control bulk-loss mechanisms by improvements in silicon sheet structural, electrical, and chemical properties are leading to improved minority carrier diffusion lengths. A study of the impact of specific metallic impurities on cell performance is reported in Volume II: Silicon Material. The complicated and varied nature of silicon sheet is a function of its growth conditions and its processing,

*Table 2. Contract List for High-Efficiency Device Task*

Contract Number and Title	Contractor, Address
<b>Bulk Losses</b>	
956289: Study of Relationship of Material Properties and High-Efficiency Solar Cell Performance on Material Composition	C.T. Sah Associates Urbana, Illinois
956989: Studies of Oxygen and Carbon-Related Defects in Silicon Solar Cells	State University of New York Albany, New York
956525: Surface and Allied Studies in Silicon Solar Cells	University of Florida Gainesville, Florida
956233: Silicon Sheet with Molecular-Beam Epitaxy for High-Efficiency Solar Cells	University of California, Los Angeles, California
957159: Carrier Transport in Heavily Doped Silicon	Stanford University Stanford, California
956126: Hydrogen Implantation	Pennsylvania State University University Park, Pennsylvania
956046: Electrical, Structural, and Chemical Characterization of Silicon Sheet Material	Cornell University Ithaca, New York
<b>Surface Losses</b>	
956960: Interfacial Studies	Stanford University Stanford, California
956614: High-Efficiency Cell Surface Passivation	University of Washington Richland, Washington
956525: Surface and Allied Studies in Silicon Solar Cells	University of Florida Gainesville, Florida
956369: Microcrystalline Silicon Growth for Heterojunction Solar Cells	Applied Solar Energy Corporation City of Industry, California, with subcontract to Boston University, Boston, Massachusetts
<b>Modeling and Measurements</b>	
956290: High-Efficiency Cell Modeling	University of Pennsylvania Philadelphia, Pennsylvania
957170: Silicon Optimization Methods and Silicon Solar Cell Numerical Methods	University of California Los Angeles, California
956741: Comprehensive Computer Modeling of Silicon Solar Cell	Research Triangle Institute Research Triangle Park, North Carolina
956290: Development and Analysis of Silicon Solar Cells of Near 20 % Efficiency	University of Pennsylvania Philadelphia, Pennsylvania
956467: Time-Resolved Spectroscopic Measurements	University of Southern California Los Angeles, California

Table 2. (Cont'd)

Contract Number and Title	Contractor, Address
Cell Processes	
955080: Silicon Solar Cell Process Development, Fabrication, and Analysis	ASEC City of Industry, California
957098: High-Efficiency Emitter Design	ASEC City of Industry, California
956786: High-Efficiency Cell Surface and Bulk	Westinghouse R&D Pittsburgh, Pennsylvania
957175: Rapid Thermal Processing of Ion Implanted Cells	North Carolina State University Raleigh, North Carolina

including solar cell fabrication. Studies within this Task served to monitor sheet quality and the influence of various sheet parameters on cell performance. Characterization of bulk material and solar cell performance evaluation used a variety of measurement techniques for chemical, structural, and electrical

characterization. These techniques included optical, electron and ion beam analysis, x-ray characterization, light and dark I-V relationships, spreading resistance, surface photovoltage, scanning electron microscopy, deep-level transient spectroscopy, secondary ion microprobe spectroscopy, and Zeeman spectroscopy.

## Bulk Losses

## A. INTRODUCTION

Bulk loss in crystalline silicon, a critical and generic issue for the development of better solar cells, is caused mainly by recombination of photo-generated minority carriers at the crystal imperfections. Examples of imperfections are structural defects and chemical impurities in the materials. Recombination reduces minority carrier diffusion length and enhances leakage current. Consequently, both  $I_{SC}$  and  $V_{OC}$  deteriorate. The presence of structural defects and impurities also can reduce carrier mobilities in the material by means of defect and impurity scattering. As a result, series resistance is increased and the fill factor (FF) is decreased. To understand the origin of bulk losses in solar cells, recombination phenomena have to be investigated. The origin of recombination centers in currently available silicon sheet, and their relationship with crystal growth and cell fabrication processing, must be understood.

The two categories of recombination processes in silicon, intrinsic and extrinsic (listed with their energy exchange partners), are (Reference 1):

- (1) Intrinsic mechanisms (interband transitions).
  - (a) Thermal recombination: phonons (lattice vibrations).
  - (b) Radiative recombination: photons.
  - (c) Auger recombination: third electron or hole.
- (2) Extrinsic mechanisms (band-bound transitions).
  - (a) Thermal recombination [Shockley-Reed-Hall (SRH)]: phonons.
  - (b) Radiative recombination: photons.
  - (c) Auger recombination: third electron or hole.

The fundamental differences between intrinsic and extrinsic recombination mechanisms can be described as follows:

- (1) For the intrinsic processes, the carrier recombination occurs via band-to-band transitions. Because the energy gap between the bands is relatively large, these processes are less significant than the extrinsic mechanisms.
- (2) For the extrinsic processes, the initial or final state is a bound state localized at a lattice imperfection (either an impurity or defect site) in the gap and the other is an unlocalized band state. Because the largest phonon

energy available in solids is about 60 meV, which is much smaller than the energy band-gap in silicon, the intrinsic thermal recombination is extremely small, but the extrinsic processes can be very large. The radiative recombination in silicon also is very small because silicon is an indirect bandgap crystal. Because the Auger recombination depends on the presence of a third electron or hole, the intrinsic Auger recombination cannot be completely eliminated. Intrinsic processes, therefore, cannot be eliminated in a silicon crystal, even if the crystal contains no imperfections.

In silicon materials available to date, the extrinsic recombination is the dominant process, mainly because the materials always contain imperfections. The extrinsic thermal (SRH) recombination is the most important mechanism. The Auger recombination can be a major contributor in heavily-doped materials. The recombination rate of the SRH mechanism is proportional to the density of impurities and defects. These imperfections can be unintentionally, but readily introduced during crystal growth as well as during cell fabrication. In principle, these imperfections can be eliminated by improving techniques of present-day crystal growth and cell fabrication. If these techniques are successful in the elimination of imperfections, the impact can be large on the development of high-efficiency silicon solar cells (greater than 20% AM1).

In an early phase of the FSA project, the approach was to investigate low-cost solar grade silicon materials and their allowable metallic impurity contents in low-cost terrestrial solar cells. This study is discussed in greater detail in Volume II: Silicon Material. These results demonstrated that high-purity silicon was a necessary, but not a sufficient requirement for high-efficiency cells. Devices of 13 to 15% efficiency could be produced from semiconductor purity silicon in which other defects are present. Higher efficiency can be achieved only by controlling other bulk defects such as dislocations, carbon and oxygen content, dopant species, and the complex interactions among them.

The FSA Project increased its effort to reduce the bulk losses in solar cells. One specific research activity included development of an understanding of the loss mechanisms that limited the ultimate performance in silicon solar cells (C.T. Sah and Associates). Other research investigated the bulk mechanisms in solar cells made of currently available silicon sheet materials, including: single crystal wafers [State University of New York at Albany (SUNYA)], cast polycrystalline wafers [Cornell University and Jet Propulsion Laboratory (JPL)], dendritic web (DW), and edge-defined film-fed growth (EFG) ribbons (Cornell University and JPL). Efforts also

have included studies of heavy doping effects using dopant concentrations greater than those used in most conventional semiconductors (University of Florida and Stanford University). An examination was made of the potential of a new silicon growth method, Molecular-Beam Epitaxy (MBE) [University of California, Los Angeles, (UCLA)], and the utility of hydrogen passivation (Pennsylvania State University). In principle, it was found that it is possible to eliminate most of the bulk losses in the solar cell by improving the crystal growth and cell processing techniques.

Details of these results, reported by the above-mentioned contributing organizations, are presented in the following sections.

#### B. LIMITS TO BULK LOSS IN HIGH-EFFICIENCY SILICON SOLAR CELLS: C.T. SAH ASSOCIATES

C.T. Sah Associates has investigated the relationship of material properties to high-efficiency solar cell performance. The investigation included basic studies of the material parameters that limit the performance of high-efficiency silicon solar cells. The work also dealt with identification of the barriers that prevent the achievement of the ultimate efficiency of silicon solar cells.

These fundamental studies led to quantification of many of the required features of the ideal cell. It was shown that the ideal cell has the lowest intrinsic recombination losses (interband radiative and interband Auger recombination losses), and has no surface and interface recombination losses. Study by C.T. Sah Associates of an ideal silicon cell with the common  $n^+ - p - p^+$  device structure shows that the ultimate efficiency, limited by radiative recombination alone, is about 25% at AM1 and 28°C. The Auger recombination limits were computed for low and high injection levels, and both are close to the 25% radiative limit. The results give the condition at which SRH recombination loss will become important to lower the ultimate efficiency. Thus, although a SRH recombination lifetime of 100  $\mu$ s gives a 23% efficiency, the SRH base lifetime must be greater than about 1 ms to reach 25%. This is at the limit of the state of the art for very large scale integration-grade (VLSI) silicon crystal. Table 3 shows the performance of silicon solar cells, including the effect of surface recombination and other losses. Details of the calculation are available (References 1 and 2).

The investigations of C.T. Sah and Associates lead to the conclusion that, among the recombination processes, the intrinsic Auger and radiative mechanism pose the ultimate limit and the extrinsic SRH mechanism is the current technology limit. The latter can be eliminated by means of R&D to improve understanding of the behavior of impurities and structural defects in silicon as well as crystal growth and cell fabrication. Innovative cell structure designs also must be incorporated to alleviate dependence on stringent processing technology requirements.

#### C. OXYGEN AND CARBON IN SILICON: STATE UNIVERSITY OF NEW YORK AT ALBANY

Researchers at the State University of New York at Albany (SUNYA) investigated the presence of oxygen and carbon in silicon and their influence on solar cell performance. This was generic research to understand the behavior of oxygen and carbon in silicon and their relationships to bulk losses in silicon solar cells. The importance of the presence of oxygen and carbon in silicon photovoltaics is not obvious, and a brief discussion of its relevance is given below.

Oxygen is a ubiquitous impurity in silicon material, whether the silicon is single crystalline, polycrystalline, or amorphous. In Cz-grown single crystalline and cast polycrystalline silicon, the oxygen concentration is typically about  $10^{18}$  atoms/cm<sup>3</sup>, which is approximately the solubility limit of oxygen in silicon near the melting point. Even though in FZ silicon, the concentration is about  $10^{15}$  to  $10^{16}$  atoms/cm<sup>3</sup>, that amount is still sufficient to cause complications, especially following various high temperature fabrication processes. It is known that the existence of active recombination centers involving oxygen concentrations of the order of  $10^{13}$  to  $10^{14}$ /cm<sup>3</sup> can drastically reduce the minority carrier lifetime in silicon. The existence of oxygen in concentrations several orders of magnitude higher is likely to have noticeable effects on the recombination in silicon via some indirect means.

In as-grown silicon, oxygen is uniformly distributed throughout the material in the form of isolated oxygen atoms as bonded interstitials in a puckered configuration between two silicon atoms. Using the stress-induced dichroism technique, the movement of oxygen in silicon can be detected at temperatures as low as about 300°C. Experimental evidence has shown that the behavior of oxygen is very complicated. It is known that oxygen-related donors are formed during thermal annealing at 450 to 650°C. Oxygen can interact with vacancies and self-interstitials to form complexes that are often mobile at these temperatures. Details of this behavior, however, are not clear at present.

Carbon, which occupies substitutional sites in as-grown silicon, is electrically neutral, but can be detected by infrared (IR) absorption. Typically, the carbon concentration in silicon is about  $10^{15}$  to  $10^{16}$  atoms/cm<sup>3</sup>, except in EFG ribbon which is saturated with carbon. It is known that carbon interacts with intrinsic defects such as vacancies and interstitials, dislocations, oxygen, and acceptor impurities at elevated temperatures. From experimental observations, it is expected that carbon can influence the minority carrier lifetime in silicon, but its detailed influence is not clear at present.

It is obvious from the above that improvement of the present-day understanding of the effects of oxygen and carbon on high-efficiency silicon solar cell performance is needed for the development of high-efficiency and low-cost silicon solar cells for terrestrial applications. The effects of oxygen and carbon could

Table 3. Performance of Silicon Solar Cells as a Function of Various Loss Mechanisms

Limiting Source	Input Parameters Used				Results			
	$J_i$ , A	m	$J_i/q$	$S_{eff}$ , cm/s	$I_{sc}$ , mA	$V_{oc}$ , mV	Fill Factor	Efficiency, %
Radiation Recombination	$5.0 \times 10^{-16}$	1	$C^0 n_i^2 x_B$	3.1	36.0	817	0.86	25.4
Auger H	$3.0 \times 10^{-22}$	2/3	$C_H^a x_B n_i^3$	0.33	36.0	786	0.90	25.4
Auger L	$2.3 \times 10^{-15}$	1	$C_L^a x_B n_i^2 N_B$	14	36.0	776	0.86	24.0
SRH L	$8.0 \times 10^{-15}$	1	$\tau_B^{-1} x_B n_i^2 N_B^{-1}$	50	36.0	746	0.85	23.0
Ohmic L	$6.4 \times 10^{-13}$	1	$D x_B^{-1} n_i^2 N_B^{-1}$	4000	36.0	634	0.83	19.1
SRH H	$8.0 \times 10^{-8}$	2	$\tau_B^{-1} x_B n_i$	50	36.0	666	0.74	17.8
Ohmic H	$6.4 \times 10^{-6}$	2	$D x_B^{-1} n_i$	4000	36.0	442	0.66	10.6

$J_i$  = dark leakage current of the ideal Shockley p/n junction diode

$S_{eff}$  = effective surface recombination velocity

Injection level: L = low; H = high

Temperature = 24°C

Cell area = 1 cm<sup>2</sup>

$\tau_B$  = base lifetime = 100  $\mu$ s

Power Input = 100 mW (AM1.5)

$n_i$  = intrinsic carrier density =  $10^{10}$  cm<sup>-3</sup>

$x_B$  = base layer thickness = 50  $\mu$ m

$N_B$  = base carrier concentration =  $10^{17}$  cm<sup>-3</sup>

$D$  = carrier diffusion coefficient = 20 cm<sup>2</sup>/s

$m$  = reciprocal slope of non-ideal junction diode

$q$  = electronic charge

$C^0 n_i^2$  =  $0.62 \times 10^6$ ;  $C_L^a = C^n = 2.8 \times 10^{-31}$  cm<sup>6</sup>/s

$C_H^a = C^n + C^p = 3.8 \times 10^{-31}$  cm<sup>6</sup>/s

be indirect through complicated interactions with other impurities and defects. The contract activities at SUNYA were directed toward this goal and considerable progress was made. The final report reviews process-induced defects in silicon, especially oxygen-related defects and their complicated evolution from

isolated interstitial oxygen (Reference 3). SUNYA also carried out experimental investigations on effects of stresses on the formation of oxygen thermal donors in silicon (Reference 4) and theoretical studies on thermal donor formation kinetics (References 5 and 6). SUNYA performed theoretical and experimental studies to

improve the understanding of the influence of oxygen and carbon-related defects on minority carrier lifetime in silicon.

#### D. STRUCTURAL AND CHEMICAL DEFECTS: CORNELL UNIVERSITY

Structural defects and impurities in silicon dictate the electrical properties of the material. Scientists at Cornell University (see Table 2) have investigated the physical and chemical nature of structural defects in thin silicon sheets (such as web and EFG ribbons) as well as polycrystalline wafers. They have made significant contributions to the improved understanding of the nature of structural defects and impurities in these silicon sheets and of their influence on electrical properties. Their work has covered a wide range of materials and characterization tools. The following are several illustrations of their accomplishments.

Understanding the influence of carbon on various properties of the ribbon is very important to the development of advanced silicon technology for PV applications because carbon is the major impurity in EFG ribbons. Because the carbon content in Cz-grown silicon is too low for carbon to precipitate out, carbon-based gettering has not been considered in the past. The gettering mechanism, however, is important for an understanding of the behavior of EFG ribbon. The contractor developed a model for electrical activity of carbon-self-interstitial agglomerates (Reference 7). The model used the assumptions that the self-interstitial content of these agglomerates determines their electrical activities and that compressive stresses (high, self-interstitial content) and tensile stresses (low, self-interstitial content) give rise to electrical activity of the agglomerates. The self-interstitial content of carbon-related agglomerates may be reduced by appropriate high-temperature treatment, and enhanced by supersaturation of self-interstitials generated during formation of the p-n junction of solar cells. It has been suggested that oxygen present in supersaturation in carbon-rich silicon may be reduced to form  $\text{SiO}_2$  precipitates by self-interstitials generated during phosphorus diffusion. It has been proposed that the Si-SiO<sub>2</sub> interface of the precipitates gives rise to a continuum of donor states. These interface states are responsible for at least a part of the light enhancement effects seen after phosphorus diffusion into oxygen-containing EFG silicon.

A considerable amount of work has been done on characterization of structural defects in a variety of silicon sheet materials for solar cell applications. The tools used included chemical etching, electron-beam-induced current (EBIC), and transmission electron microscopy (TEM). Emphasis has been on the correlation of data obtained and identification of defects. For example, results have shown that the coherent twin boundaries in silicon are often electrically inactive, but unsymmetrical tilt boundaries are strongly active. EBIC results also have illustrated that exposure to hydrogen

plasma increases charge collection efficiency (Reference 8). The oxygen content in silicon dendritic web ribbons also was studied. Results have shown that oxygen content in the ribbon is similar to that in Cz-grown silicon (Reference 9). An investigation of the interactions of twin boundaries and dislocations in solar silicon also was made (Reference 10).

The contractor also performed a detailed structure study of  $\langle 110 \rangle$  tilt boundaries in silicon using high-resolution TEM. These boundaries are common in solar cell materials such as EFG ribbons, dendritic web ribbons, and cast polycrystalline silicon wafers. The contract work has observed several symmetric tilt boundaries. Figure 4 shows a high-resolution TEM picture of the (552)/(552) tilt boundary and a schematic representation of the boundary (Reference 11). The schematic shows a repeat pattern of 7-atom and 5-atom ring structures. There are no dangling bonds along the boundary, however, suggesting the boundary is not electrically active. This is consistent with EBIC experimental results. This type of boundary often has some recombination activity at some isolated places along the boundary, indicating the existence of structural complications along the boundary, probably caused by interactions with other structural defects and impurities.

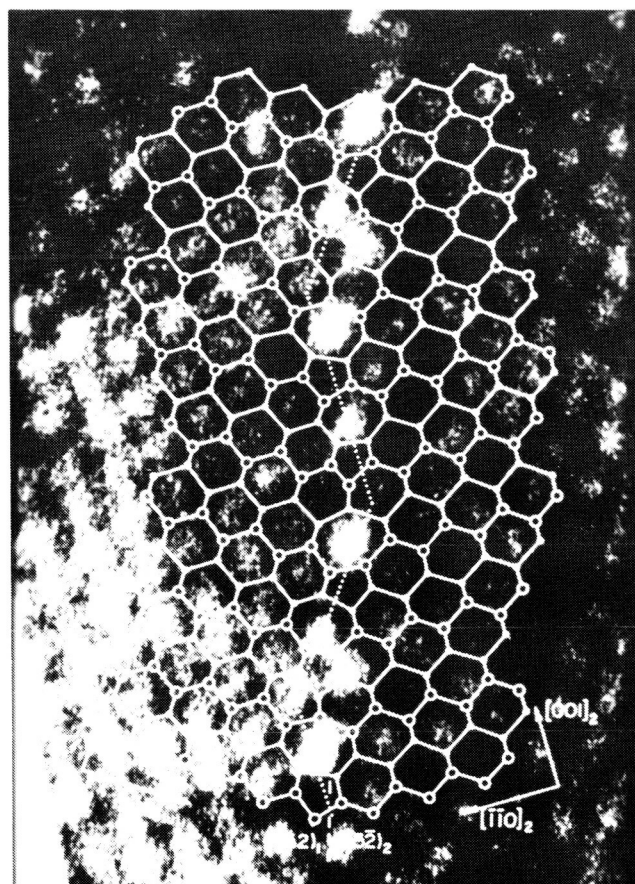


Figure 4. High Resolution TEM Picture of the (552)/(552) Tilt Boundary of Silicon

## E. HEAVY DOPING AND OTHER BULK EFFECTS IN HIGH-EFFICIENCY SILICON SOLAR CELLS: UNIVERSITY OF FLORIDA

In silicon solar cells, the base region usually consists of good quality silicon with a long minority carrier lifetime compared to the thickness. This causes minority carriers to recombine at the back contact, which results in increased dark current and reduced open circuit voltage. To reduce the effective surface recombination velocity, a high-low junction is formed at the back surface to act as a minority carrier reflector. This effect then manifests itself as effective surface recombination velocity ( $S_{eff}$ ) at the high-low junction.

The emitter in the solar cell generally is a very thin layer (1000 to 3000 Å thick) of heavily doped n-type material. Heavy doping in emitter (and base) causes two detrimental physical phenomena that are important for solar cell operation. They are Auger recombination (causing lower minority carrier lifetime) and narrowing of the bandgap (causing higher leakage currents and an electric field gradient in a direction to push the minority carriers away from the junction).

The University of Florida initially developed a transient method called Electrical Short-Circuit Current Delay (ESCCD) for the measurement of  $\tau_n$  and  $S_{eff}$  (References 12 and 13). This method is more accurate than the open-circuit voltage decay (OCVD) or the Junction Reverse Recovery (JRR) methods, because of quicker removal of injected charge in the space charge region.

Additional efforts were devoted to determination of the bulk properties of heavily doped silicon. Measurement of the activation energy for arsenic-doped silicon at  $10^{20}$  atoms/cm<sup>3</sup> gave evidence for values of minority-hole diffusivity,  $D$ , and mobility,  $\mu$ , that are significantly lower than the majority-carrier  $D$  and  $\mu$  (Reference 14). Measurement of the transit time for boron-doped silicon at  $10^{20}$  atoms/cm<sup>3</sup>, using s-parameter techniques, gave similar results for minority electron  $\mu$  and  $D$  (see Reference 3). These results differ from those from research at Stanford University. An improved determination of bandgap narrowing from activation energy, however, gave results consistent with Stanford results. Further work may be needed to obtain an explanation for the two sets of data obtained at the two universities.

Theoretical investigations of solar cells, including the effects and mechanisms of the effects in heavily doped silicon, started with an improved model for bandgap narrowing (Reference 15). It was determined that neither a real inhomogeneity, nor the presence of a high surface recombination velocity reduced accuracy. Auger lifetime,  $\tau_{au}$ , was determined using photoluminescence decay, provided one observed the tail of the response. This treatment led to a precise definition of the tail. The overall conclusion is that the Dziewior-Schmid values of  $\tau_{au}$  do not suffer from inadequacy of theoretical interpretation. This lends greater credibility to these values because they had been challenged by

other workers. A generalized reciprocity theorem was presented (Reference 16) that enables calculation of internal quantum efficiency based on a non-illuminated analysis. Other applications of this analysis could involve measurements of various device parameters. Thus, interfacial surface recombination velocity at a polysilicon contact could be measured by using steady-state or transient photons or mass-particle radiation. The mathematical foundation underpinning the analysis of impact Auger lifetime led to an exact solution of three-dimensional transport problems for solar cells without solving the actual boundary-value problem. In this theoretical work (Reference 17), recombination current, transit time, and open-circuit voltage are determined not by solving the actual three-dimensional boundary-value problems, but rather by introducing auxiliary one-dimensional models.

The earlier work on the generalized reciprocity theorem led to the first detailed attempt to systematize the design of silicon solar cells. Design principles follow from three theorems. Several optimal designs are derived from the theorems, one of which involves a three-dimensional morphology in the emitter region. A multiple integral series solution was derived for nonuniformly and heavily doped emitter regions (Reference 18). By truncation, this approach yields many different orders of approximation. It is believed that the simplest of these approximations, called the quasineutral-quasiequilibrium approximation, enables hand calculations to have an accuracy comparable to detailed computer solutions provided that the emitter is thin ( $< 3 \mu\text{m}$ ) and has a low surface recombination velocity ( $< 10^5 \text{ cm/s}$ ).

From additional experimental studies, evidence was presented for excess carrier storage. This phenomenon was connected to a bandgap narrowing (80 mV or three thermal voltages for a density of  $4 \times 10^{18}$  atoms/cm<sup>3</sup>), not in heavily doped silicon but rather in highly excited silicon (Reference 19) in which approximately equal numbers of holes and electrons exist in densities above  $10^{17}$  atoms/cm<sup>3</sup>. These findings have implications for solar cells in concentrated illumination, both in the quasineutral and junction regions. A detailed interpretation was presented to explain why the apparent transient photoconductivity lifetime can considerably exceed the steady-state lifetime.

## F. HEAVY DOPING EFFECTS IN EMITTER: STANFORD UNIVERSITY

The Solid State Electronics Laboratory of Stanford University performed an investigation of minority carrier transport in heavily doped p-type silicon. The objective was to improve the understanding of minority carrier transport in the heavily doped emitter region of silicon solar cells.

From first principles, the contractor demonstrated that there are three transport and recombination parameters in heavily doped n-type silicon: (1) hole equilibrium concentration,  $P_0$ , (2) lifetime,  $\tau$ , and (3) diffusion

length,  $L$ . In steady state, however, only combinations or derivations of these three fundamental parameters are relevant. The two parameters of interest are the diffusion length and the product of the hole equilibrium concentration and the diffusion coefficient, where the diffusion coefficient is derived from the equation  $D = L^2/\tau$ . These two parameters have been measured in heavily phosphorus-doped silicon fabricated by epitaxy. Good quality epitaxial layers were grown with doping levels up to  $1.6 \times 10^{20}$  atoms/cm<sup>3</sup>. The measurement was done on test structures with vertical and lateral bipolar transistors fabricated with the epitaxial layers. The diffusion length in the  $n^+$  epitaxial region was measured from the collector characteristics of identical  $p^{++}-n^+-p^{++}$  lateral transistors with different base widths. Simultaneously, the hole equilibrium concentration/diffusion coefficient product was extracted from the collector characteristics of  $p^{++}-n^+-p$  vertical transistors. A doping range of two orders of magnitude was covered. Previous steady-state measurements of the hole transport and recombination parameters by other authors were reviewed. The original measurements of the two relevant parameters were reconstructed from the reported data. Agreement within a factor of two was obtained among this work and other published data.

Based on Stanford's recent measurements of hole lifetime in  $n$ -type silicon, values for hole mobility and hole equilibrium concentration were obtained from the measured parameters. The hole mobility is found to be two times larger than its  $p$ -type silicon value. The equilibrium hole concentration is about a factor of two larger than predicted from values of bandgap narrowing measured by photoluminescence.

Using only the two measured parameters, the work also revealed that modeling of the current injected into heavily doped regions is possible in steady-state. As an illustration, the emitter saturation current of several bipolar transistors was calculated and the value, without any adjustable parameters, was within 30% of the experimentally measured data. A simple and accurate analytic approximation to internal quantum efficiency of heavily doped emitters also was developed.

Functional doping dependence of hole lifetime, hole mobility, and bandgap narrowing were determined. These values should be useful for device modeling (References 19, 20, and 21). The contractor also conducted similar research on heavily doped  $p$ -type silicon.

#### G. SILICON SHEET BY MOLECULAR-BEAM EPITAXY: UNIVERSITY OF CALIFORNIA, LOS ANGELES

This effort was to apply the capabilities of the new technique of Molecular-Beam Epitaxy (MBE) at UCLA to the growth and fabrication of high-efficiency silicon solar cells. UCLA was to use MBE to grow and characterize silicon films and  $p$ - $n$  junctions to determine the

MBE film quality. It then was planned to fabricate various prototype high-efficiency solar cell designs such as front- and back-surface field, cascade cells, etc., and then model and characterize these cells.

The UCLA MBE System consisted of a modified stainless steel Varian station capable of obtaining a base pressure of  $5 \times 10^{-11}$  Torr. Surface analysis included low energy electron diffraction (LEED), Auger electron spectroscopy (AES), and quadrupole mass spectroscopy (QMS) for in situ surface studies. A molybdenum crucible with a 6 kW electron bombardment gun was used for pure silicon evaporation. The beams of gallium ( $p$ -type dopant) and antimony ( $n$ -type dopant) were generated by resistance-heated, pyrolytic, boron nitride effusion cells.

Normal operation consisted of cleaning the substrate by heating to 1200°C for 1 to 2 min and checking the cleanliness by LEED pattern. Silicon films then were grown by molecular beam epitaxial deposition at substrate temperatures of 650°C. Doping was obtained by controlled coevaporation of either Ga or Sb. Silicon substrates and MBE-grown  $p$ - and  $n$ -type layers were evaluated before and after cleaning within the chamber and after growth of each layer. Solar cells were made from the  $p$ -type grown layer by conventional thermal diffusion of phosphorus and application of a Ti-Pd-Ag contact.

It was found that the cleaning procedure (heating the substrate to 1200°C under  $<10^{-9}$  Torr pressure) did not degrade the minority carrier lifetime in the substrate. Solar cells made from the grown  $p$ -layer ( $\sim 1 \mu\text{m}$  thick), however, showed very poor performance, as compared to control cells.

Scanning Ion Microprobe Spectroscopy (SIMS) on these samples showed a gradual rise of doping in the grown layer rather than a plateau after a steeper doping rise. Also, carbon contamination was observed at the substrate-epi interface. Oxygen and carbon were detected within the thickness of the epi-layer. Corrective actions such as argon bombardment prior to growth, etc., were not very successful.

Saturation current is a very sensitive test for the quality of diodes. Mesa diodes were etched on the epitaxial layer samples and a measurement of the reverse current characteristics showed that the central region was slightly better than the end regions near the holding clamps. This was thought to be a result of stresses introduced by the clamping arrangement. Minority carrier lifetime derived from the reverse saturation current measurements on  $p$ - $n$  junctions have been in the nanosecond range instead of the microsecond range normally obtained with good quality silicon.

A new substrate holder with a radiative heating element was designed with no clamping required. This holder gave better uniformity of heating and eliminated any mechanical stresses. Problems of quality of film, however, remained unsolved.

Hall mobility studies on both p- and n-type layers showed that MBE-grown silicon matched bulk mobility values except at doping levels  $> 10^{18}/\text{cm}^3$ . TEM studies of the films showed some areas where dislocation density was  $< 10^3/\text{cm}^2$ . Major areas had dislocation densities of  $10^5/\text{cm}^2$ , however, with moderate levels of stacking fault densities.

To overcome the problem of smearing of doping profile, a modified technique of amorphous silicon evaporation was done at  $575^\circ\text{C}$  with substrate at room temperature, with coevaporation of dopant and crystallization of the film in a solid phase epitaxial regrowth. This worked extremely well and gave sharp doping profiles and dopant levels reaching above solid solubility limits (Reference 22).

Fabrication of p-n junctions by MBE resulted in very poor performance. Conventional fabrication of solar cells on p-type MBE-grown layers gave efficiencies up to 4.8% without AR coating. Table 4 lists some of the cell characteristics.

Table 4. Performance of Molecular-Beam Epitaxy Silicon Solar Cells

Sample	$J_{sc}$ , $\text{mA}/\text{cm}^2$	$V_{oc}$ , $\text{mV}$	Fill Factor	Efficiency, %
MBE 9	27.0	380.0	0.55	2.8
JPL 109	21.9	454.9	0.707	4.7
JPL 110	23.5	486.7	0.713	4.8
JPL 102	Shorted	—	—	—
JPL 103	Shorted	—	—	—
JPL 112	Lost in processing	—	—	—
JPL 113	Lost in processing	—	—	—

Computer modeling was done for a two-junction, all-silicon cell that was expected to give nearly twice the voltage of a single junction cell. The two-junction cell had an interspersed tunneling junction contact. The concept and the model were developed originally at JPL, but a more detailed study was carried out at UCLA. It was shown that with different bulk dopings of the front and rear cells, a higher efficiency of the cascade cell was obtainable (by 1 to 2 percentage points). This was achieved if the interface recombination velocity at the tunneling junction was below  $5 \times 10^3 \text{ cm/s}$ , as compared to a single junction conventional cell (Reference 23). Figure 5 shows this result where  $S_{eff}$  is the effective interface recombination velocity at the  $p^+ - n^+$  tunneling junction, and the resistivities are those of the base regions of each solar cell.

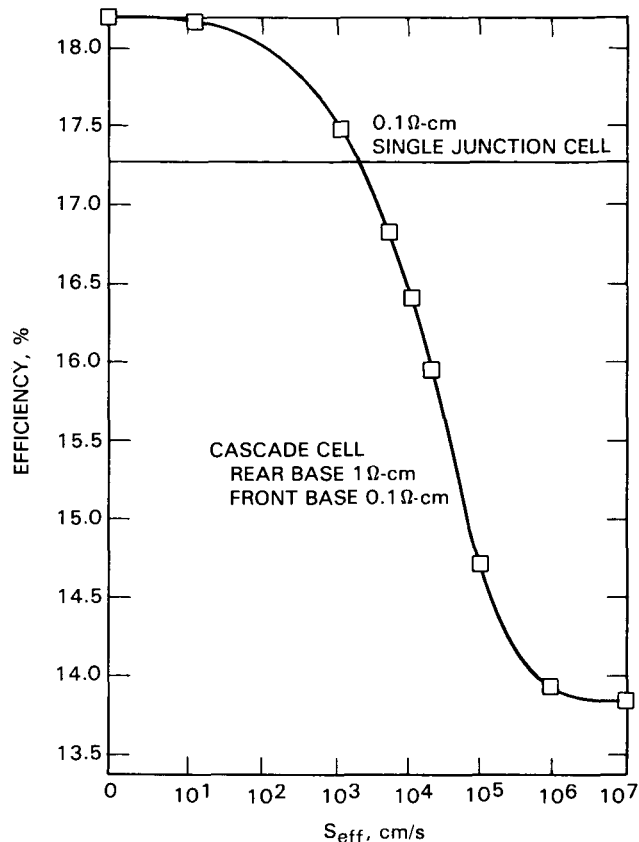


Figure 5. Calculated AM0 Efficiency of a Cascade Cell Versus Interface Recombination Velocity

During this effort, nearly 30 samples of different structures were made. About 10 solar cells were attempted, and the best efficiencies were 4.8% at  $100 \text{ mW}/\text{cm}^2$  illumination without AR coating. Other samples were used for layer characterization, diode characterization, and SIMS analysis.

Even though the MBE technique has the advantage of achieving sophisticated solar cell structures, problems of quality of the layers need to be solved before the technique can be usefully applied to the fabrication of research solar cells.

#### H. HYDROGEN PASSIVATION: PENNSYLVANIA STATE UNIVERSITY

At Pennsylvania State University (Reference 24), researchers have established that low-energy hydrogen implants can result in hydrogen-caused effects in all three parts of a solar cell: emitter, space-charge region, and base. This work studied:

- (1) The effect of low-energy hydrogen implants on surface properties.
- (2) The possible role of hydrogen in silicon regrowth and diffusion.

- (3) Emitter, space-charge region, and base passivation.
- (4) Hydrogen passivation of bulk silicon impurity levels.
- (5) The use of hydrogen ion implants for high-efficiency Cz, FZ, and DW silicon solar cells.

The significant results of these studies were:

- (1) Low-energy ion beams were found to introduce structural damage at the silicon surface. This damage manifested itself as a positive surface charge and drastically affected the characteristics of metal/ion-beam-damaged silicon contacts.
- (2) Structural damage at the silicon surface by energetic  $H^+$  ions was found to be more extensive than damage introduced by inert gas ions, e.g.,  $Ar^+$  (Figure 6). Note that as the energy of the incident ions is increased, more damage is introduced at the silicon surface. Note also that  $H^+$  ions introduce more lattice damage than do  $Ar^+$  ions. It was found that  $H^+$ , however, could passivate its self-induced structural damage, provided the sample was allowed to thermally float during the processing. If the processing temperature was restricted, then the self-induced damage could not be passivated.
- (3) Enhanced interstitial population during ion bombardment can lead to enhanced diffusivity of deep-level impurities. This, in turn, can

modify the concentration of these centers in the bulk.

- (4) Hydrogen, bonded to residual defects in the silicon lattice, is stable up to temperatures around 600°C.
- (5) Low-energy hydrogen implants can result in hydrogen-caused effects in all three parts of a solar cell: emitter, space-charge region, and base. In web, Cz, and FZ material, low-energy hydrogen ion implants reduced surface recombination velocity and also passivated space charge region recombination centers.
- (6) Hydrogen implants can alter the diffusion properties of some ions implanted in silicon e.g., boron (but not others, e.g., arsenic).

#### I. STRUCTURAL DEFECTS: JET PROPULSION LABORATORY

The effect of structural defects on bulk losses is an important issue for the performance of all polycrystalline silicon solar cells. The polycrystalline materials include DW ribbons, EFG ribbons, and cast silicon wafers. Line and two-dimensional structural defects, such as dislocations and grain boundaries, are the main concern because they are commonly recombination active. There has been considerable effort at JPL to improve understanding of the behavior of these defects and their influence on silicon solar cell performance. Following is a brief illustration of the progress made through in-house research at JPL.

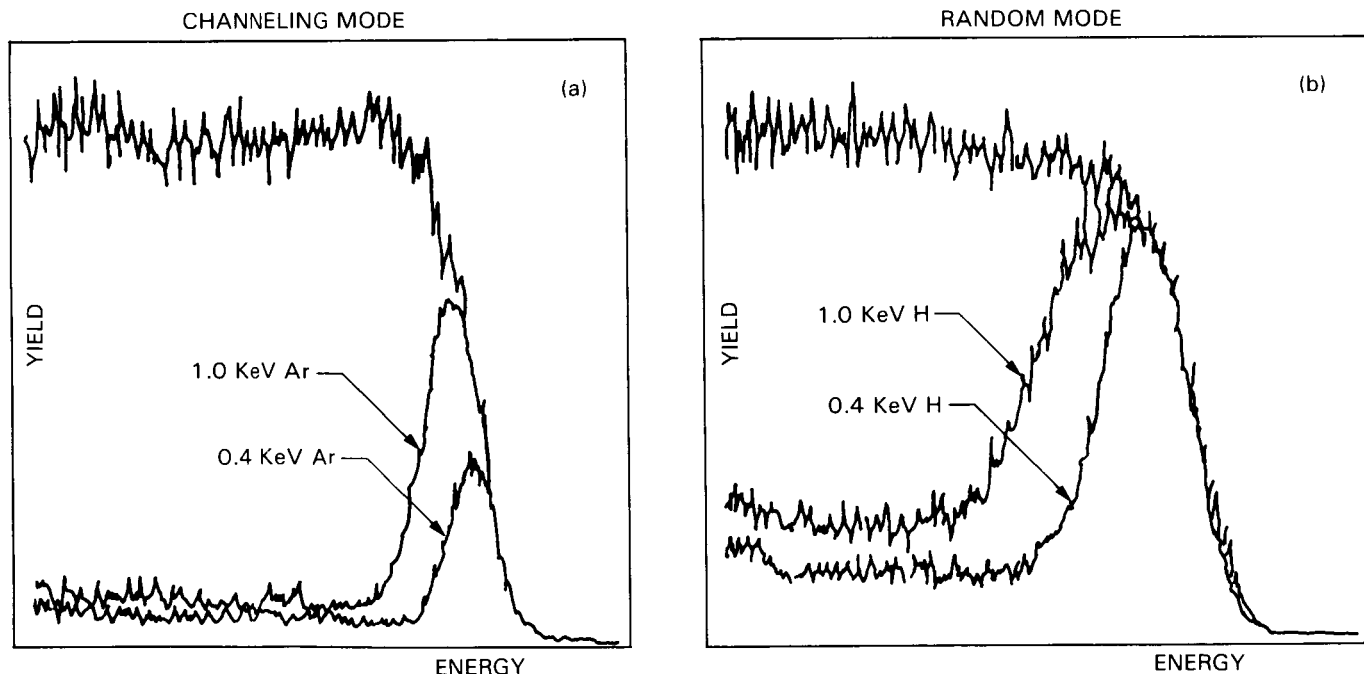


Figure 6. Rutherford Backscattering Data in the Channeling and Random Mode from Silicon Samples Subjected to Low-Energy Ion Beams

Silicon dendritic web ribbon is grown along a  $\langle 211 \rangle$  crystal orientation with  $[111]$  surfaces. Structurally, the ribbon consists of two thin sheets of single crystals twinned to each other. The twin plane consists of an odd number of closely spaced, coherent twin boundaries. The existence of the twin boundary parallel to the ribbon surfaces is needed for stable growth of the dendrites. There also are dislocations and, occasionally, a few planar defects (mainly twins) in the ribbon. There are two types of dislocations: (1) grown-in dislocations along the  $\langle 211 \rangle$  or  $\langle 110 \rangle$  axes (mainly in and near the twin plane), and (2) slip dislocations formed because of plastic deformation during the cooling stage of growth. To understand the basic material quality influence on the performance of solar cells made from web dendritic silicon, the FSA Project has carried out in-house research on properties of these structural defects.

The distribution of slip dislocations in silicon dendritic ribbons was studied using the technique of chemical etching and optical microscopy. The results show the existence of two distinguishable stress regions across the ribbon formed during the plastic deformation stage: shear stress at the ribbon edges and tensile stress at the middle (Reference 25). This observation is consistent with the theoretical analysis of thermal stress distribution done by Westinghouse (References 26 and 27) and JPL (C.F. Shih, private communication). Studies have further illustrated that the magnitude of thermal stress caused by plastic deformation during the cooling phase can be estimated from the density of etching pits (Reference 28).

Recombination properties of the slip dislocations in web ribbons were studied using the EBIC in a scan-

ning electron microscope (C.F. Shih, private communication). Figure 7 shows two EBIC pictures of the same area of a web solar cell taken at 298 and 110 K. The picture at 298 K is almost featureless, except for a number of small black dots, probably caused by dust particles on the surface. The EBIC picture taken at 110 K, however, reveals interesting features: many black dots and lines at which EBIC signals are considerably lower than those in the bulk. The two black lines that are aligned along the ribbon growth axis are probably caused by low-angle grain boundaries formed by the agglomeration of slip dislocations. A significant number of the black dots are preferentially aligned along two directions about 30 deg off the growth axis. It is known from previous investigations of etching pits that slip dislocations in the middle of the web ribbon are likely to be aligned in the same pattern (see Reference 25). This and further experimental results led to the conclusion that these black dots are caused by slip dislocations (Reference 29). The temperature dependence measurements of EBIC signals at slip dislocations indicated that recombination activities at slip dislocations are not the same, but depend on the complexity of their structures. When two or more dislocations aggregate together, the recombination activity increases significantly. It was concluded that some dislocations have weak EBIC signals at low temperatures and the signal disappears at 160 K, whereas other dislocations disappear gradually over a wide temperature range and can be active at room temperature. The difference between the two types is not understood.

An investigation of recombination-active structural defects observed in the cross section of web ribbons has been carried out (see Reference 28). Figure 8 shows EBIC pictures of three different areas of a cross

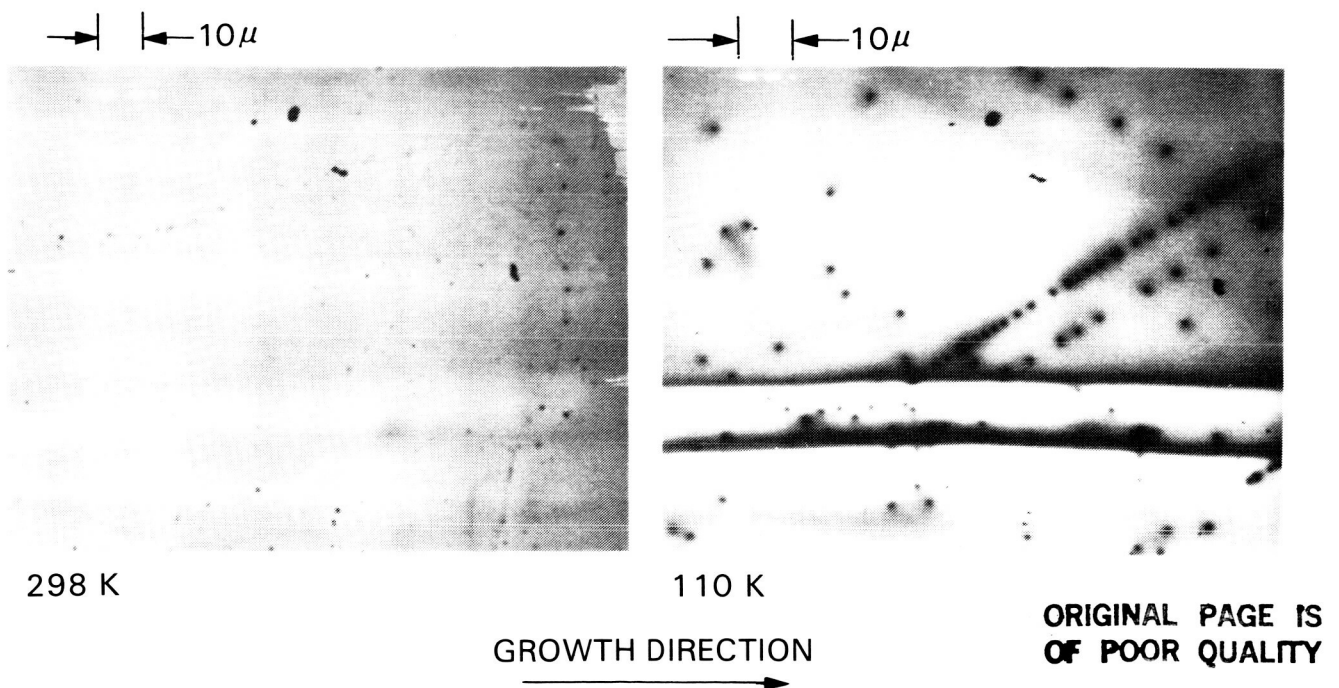


Figure 7. EBIC Photographs of an Area of a Dendritic Web Ribbon Solar Cell

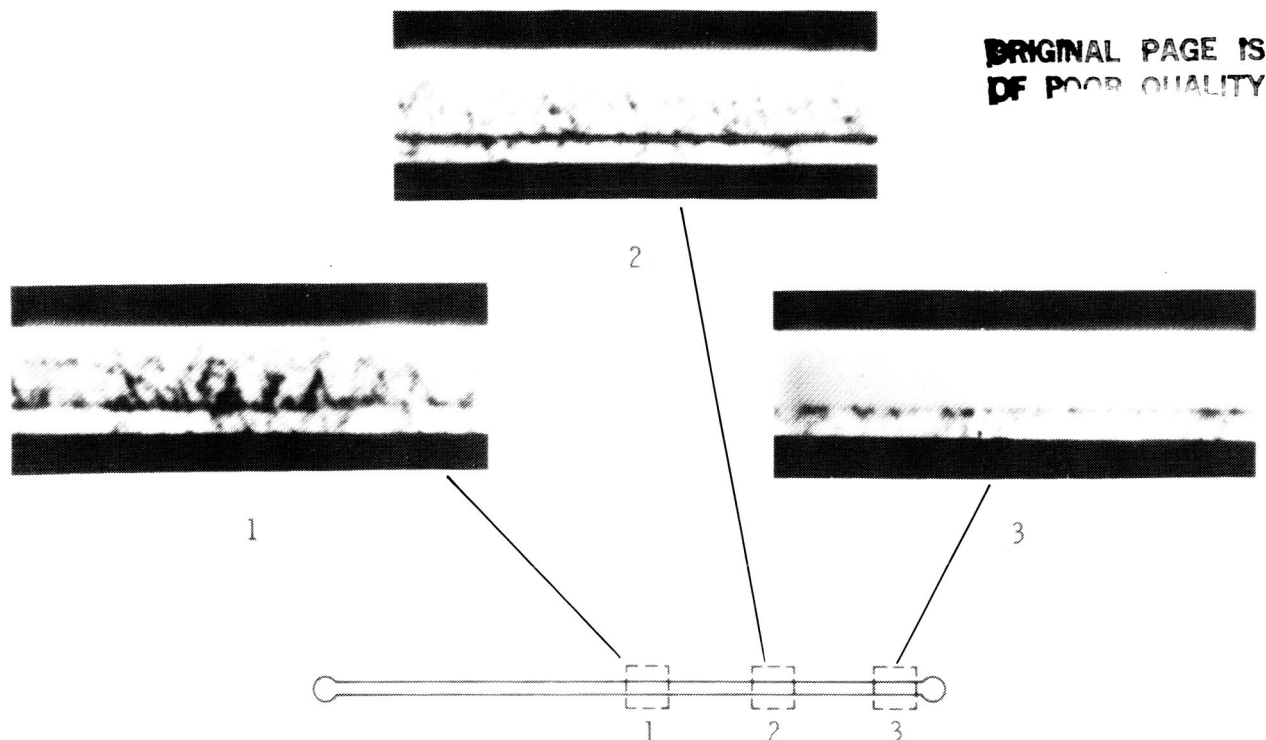


Figure 8. EBIC Photographs Taken from Three Different Areas of a Cross-Section of an "as-grown" Silicon Dendritic Web Ribbon at Room Temperature

section of an as-grown ribbon sample perpendicular to the growth direction. These pictures illustrate several important observations of recombination-active defects in the ribbon. The distribution of these defects not only varies significantly across the thickness of the ribbon, but also along the width of the ribbon. The variations are believed to be related to the growth condition. The defects are mainly concentrated in the inner part of the ribbon, specifically at and near twin planes, whereas the region near the surface often has significantly fewer defects. This observation could be related to two possible mechanisms occurring during growth. The first observation is the fact that the twin plane can act as a source for the creation of structural defects and the surface can act as a sink for defects. The second observation is related to the thought that, during growth, the silicon material near the ribbon surface often solidifies first because of the cooler environment around the ribbon. As a consequence of these two mechanisms, more structural defects are expected to be formed in the inner part of the ribbon. The variation of defect densities along the width and thickness also can be related to some uncontrolled fluctuations of the existing growth condition.

The dark straight line parallel to the ribbon surfaces in Figure 8 is caused by recombination activity at the twin plane. It is known that a perfect, coherent twin boundary is not recombination-active. This observation illustrates that the twin plane is often heavily decorated with recombination-active structural defects. There are several clearly observable segments of the twin plane, however, at which no recom-

bination activities are observed. This observation indicates that a perfect, coherent twin plane without defect decoration could exist in the web ribbon.

All known experimental results have suggested that dislocations are the most likely candidates for these recombination-active structural defects. This is consistent with a recent TEM observation by the Westinghouse group. A previous study on slip dislocations in ribbon has revealed that, at room temperature, simple slip dislocations are not recombination-active and only dislocation complexes are active (see Reference 6). The structures of these dislocations at the twin plane, therefore, are believed to be more complex than those of simple dislocations. This is because of the complicated nature of multiple interactions among dislocations, twin boundaries and, possibly, impurities.

It was reported that phosphorus diffusion at 850°C can reduce the recombination activities of twin boundaries and structural defects in polycrystalline silicon at room temperature (Reference 30). An experiment was carried out to check the phosphorus diffusion effect on recombination at the twin plane and dislocation complexes in the ribbon. The result revealed that phosphorus diffusion at 850°C can reduce the recombination activity of structural defects at room temperature, but not completely remove the defects (see Reference 28). This result is similar to that seen for twin boundaries in cast polycrystalline silicon (see Reference 30). In other words, the behavior of the twin plane is expected to be the same as that of twin boundaries in polycrystalline silicon.

An investigation was carried out of the effects of thermal annealing at 850 °C on the minority carrier lifetime of web ribbon stressed at different levels. The results revealed a large improvement in the lifetime came from the samples with low residual stress. This observation is consistent with the thought that the as-grown defects in high-stress samples have more complex structures and are less amenable to being annealed out (Reference 31).

#### J. ABSORPTION COEFFICIENT MEASUREMENT: JET PROPULSION LABORATORY

Because it provides a prediction of the energy conversion efficiency that may be attained in the final solar cells, the minority carrier diffusion length is widely used to characterize the quality of silicon solar cell material before it is processed into solar cells. The surface photovoltage (SPV) technique is a convenient, nondestructive method of measuring the minority carrier diffusion length. This method, however, relies on an accurate knowledge of the optical absorption coefficient of the silicon.

Previously published values for the optical absorption coefficient of silicon differ enough so that their values result in a substantial uncertainty in the minority carrier diffusion length determined by the SPV technique. A study in the wavelength range specifically required for SPV analysis (0.8 to 1.0  $\mu$ ) (Reference 32) was done to measure the optical absorption coefficient of single-crystal silicon produced by three low-cost growth methods [Cz, DW, and heat exchange method (HEM)].

The absorption coefficients obtained are slightly lower than those reported by Runyan,<sup>2</sup> with the greatest disagreement at long wavelengths. Minority carrier diffusion lengths computed using the new absorption coefficients are approximately 16% greater than those calculated using the older data.

#### K. PRESENT STATUS

Major contributions have been made to the understanding and control of losses in the bulk of a crystalline-silicon solar cell. These findings have contributed measurably to the present performance demonstrations of efficiencies greater than 20% (AM1). More work is needed, however, especially in the use of this knowledge in the preparation of crystals and in the processing of solar cells. The interaction of various defects is especially important, e.g., dislocations, metals, carbon, and oxygen, etc. More specific findings and needs are given below.

#### L. KEY ACCOMPLISHMENTS

Key accomplishments are:

- (1) Identified present-day technology barriers to the achievement of the theoretical efficiency.
- (2) Determined specific effects of processing on oxygen behavior and the complicated evolution of oxygen complexes and precipitates from super-saturated isolated interstitial oxygen in silicon.
- (3) Identified several  $\langle 110 \rangle$  tilt boundaries in silicon using high-resolution TEM and described dislocation motions and their interactions with other structural defects in silicon.
- (4) Developed theories and performed experiments that improved the understanding of heavy doping effects in silicon.
- (5) Performed the first direct measurement of minority electron transit time in a heavily boron-doped p-type transparent layer.
- (6) Correlated the distribution of slip dislocations in silicon dendritic web ribbons with stress patterns formed during the plastic deformation stage of growth.
- (7) Advanced the knowledge of the recombination activities of dislocations and twin boundaries in silicon dendritic web ribbons and polycrystalline wafers by using the EBIC technique in a scanning electron microscope.
- (8) Established that low-energy hydrogen implantation can result in detectable effects in all three parts of a silicon solar cell, namely, emitter, space-charge region, and base.

#### M. FUTURE NEEDS

The need for continuing research in bulk losses cannot be entirely reduced to a list of specific experiments because bulk losses and their relationship to defect behavior in silicon are very complicated phenomena and still are far from being completely understood. The recombination-active centers are influenced by many complicated factors such as the thermal and stress history of crystal growth and cell fabrication. For cells to have an efficiency greater than 20%, elimination of residual recombination impurities and defect centers remains a very important question that must be

---

<sup>2</sup>W.R. Runyan, Southern Methodist University Report SMU 83-13, 1967, also NASA CR 93154 from NTIS (N68-16510).

resolved. Although the concentration of recombination centers required to damage the material is very small, about  $10^{11}$ - $10^{13}/\text{cm}^3$ , the characterization of these defects requires substantial improvement of currently available characterization tools. With proper tools, one can improve the understanding of residual recombination centers and develop methods to avoid them. This effort will require close collaboration among crystal growers, cell makers, and materials scientists.

The following describes the kind of research needed to be done for reduction of bulk losses in high-efficiency cells:

- (1) Improve the fundamental understanding of the behavior of residual impurities and defects as

well as the interactions among them (defect chemistry).

- (2) Develop effective characterization tools for detailed investigations of residual impurities and structural defects and their correlation with minority carrier lifetime.
- (3) Improve the understanding of structural defects, the origin of their recombination activities, and their relationships with crystal growth and cell processing conditions (including stress/strain which is important to all silicon materials, but especially for silicon ribbons).

## SECTION III

# Surface Losses

### A. INTRODUCTION

Experimentally, the collection efficiency of photo-generated carriers in a crystalline-silicon solar cell has reached near theoretical values. The  $I_{SC}$  in experimental solar cells reached 36 to 40 mA/cm<sup>2</sup>, which was close to the theoretical maximum of 44 mA/cm<sup>2</sup>. However,  $V_{OC}$ , which is affected by the lowering of the dark saturation current, remains in the 600+ mV range, far away from the theoretical limit of almost 850 mV.<sup>3</sup> The predominant contribution to the dark current is the recombination at the front and back surfaces, especially the front surface.

One of the major thrusts of the High-Efficiency Device Research Task, therefore, was to study the surface loss mechanisms and develop suitable surface passivation techniques for high-efficiency silicon solar cells. To that end, efforts were initiated for the development of surface passivation techniques and measurement of surface interface structure and properties. Most of the efforts were supported by contracts with universities. JPL in-house research also was conducted to supplement and support the contract activities.

It is well known that silicon surface passivation can be achieved by growth of a thermal oxide. Studies, therefore, were made using angle-resolved x-ray photoelectron spectroscopy (XPS) and Brehmstrahlung Isochromat Spectroscopy (BIS) to understand the silicon-oxygen bonding at the surface, and the nature of conduction band density of states at the thin silicon-silicon dioxide interface.

Another passivation approach that was evaluated used the passivation caused by silicon nitride deposited on silicon using a plasma-enhanced chemical vapor deposition (PECVD) system. Because the Si<sub>3</sub>N<sub>4</sub> layers also act as an AR coating, they were analyzed for optical properties as well.

In addition to studies of passivation at bare silicon surfaces, surfaces under the contact also were examined. For a good ohmic contact, it is necessary to have a metal-silicon contact with infinite surface recombination velocity for the majority carriers. This makes the minority carrier recombination also very high, thereby increasing the dark current component (or leakage) and lowering the photo-generated current component. A study, therefore, was initiated on the passivation under the contact by heavily arsenic-doped polycrystalline silicon. The arsenic was deposited by chemical vapor deposition (CVD) at

about 670°C. Various test structures, including solar cells, were fabricated and tested.

Another approach was to explore the use of a microcrystalline<sup>4</sup> silicon (m-Si) film on single-crystalline silicon (c-Si) for solar cell applications. The approach evaluated m-Si/c-Si as a heterojunction or m-Si as a window layer on a c-Si p-n junction to enhance cell performance. This was deemed possible because m-Si has an optical band gap of 1.7 eV, a crystal size of 100 Å, and a good lattice match to c-Si. This could potentially enhance  $V_{OC}$  by reducing interface recombination velocity for minority carriers.

Because of their metal-like conductivity and modest environmental stability, three types of conducting polymers were tried as current collectors and surface passivants for silicon solar cells: (1) Poly(pyrrole), (2) Poly(azulene), and (3) Poly(isothionaphthalene). Evidence has suggested that some conducting polymers exhibit metallic conductivities of 500 (Ω-cm)<sup>-1</sup>, and can passivate surface states present on semiconductors such as WSe<sub>2</sub>, MoSe<sub>2</sub>, etc. Conducting polymers were deposited onto the p-type silicon surface electrochemically in the dark and their properties were evaluated. Conductivities as high as 200 to 1000 (Ω-cm)<sup>-1</sup> were obtained for poly(acetylene) with Li and ClO<sub>4</sub>-dopants. AC impedance measurement techniques showed flat band voltages in the range of 0.15 to 10-4 V.

Details of these investigations and participating organizations are described in the following sections.

### B. SILICON SURFACE PASSIVATION BY SILICON NITRIDE: JOINT CENTER FOR GRADUATE STUDY AT THE UNIVERSITY OF WASHINGTON

This program was developed to investigate the use of SiN<sub>x</sub> film grown by PECVD to passivate silicon surfaces and included the following areas of investigation:

- (1) Establishment of PECVD process parameters to grow SiN<sub>x</sub>, including surface pretreatment.
- (2) Optical characterization of SiN<sub>x</sub> films.
- (3) Characterization of SiN<sub>x</sub>/Si interface.
- (4) Determination of surface recombination velocity from photoresponse.

<sup>3</sup>To reach the theoretical limit of about 850 mV for the  $V_{OC}$  would require a reduction of dark current from its present value near  $5 \times 10^{-13}$  mA/cm<sup>2</sup> to the low  $10^{-17}$  mA/cm<sup>2</sup> range, a reduction of 4 orders of magnitude.

<sup>4</sup>Silicon with a grain size of 100 to 500 Å.

Procedures for growing  $\text{SiN}_x$  films, shown in Figure 9, were developed using a PECVD system on silicon wafers having a (100) orientation. Two basic silicon surface cleaning procedures were used: (1) an RCA cleaning procedure, and (2) a more abbreviated process that omits the RCA peroxide steps. Silicon wafers either had a native oxide or a thin oxide film (20 Å) formed by heat treating the wafer at 500°C for 20 min in oxygen. Wafer surfaces either were nitrided or not. Nitridation involved exposing a surface to an RF plasma and  $\text{NH}_3$  using 15 W radio frequency (RF) power, 70 standard cubic centimeters per minute (sccm)  $\text{NH}_3$  flow, and 270°C platen temperature. Thus, eight initial surface conditions were defined by the various combinations of two cleaning steps (RCA or abbreviated), two oxide films (room temperature or 500°C), and either nitrided or not.

After surface preparation,  $\text{SiN}_x$  films were deposited using the highest grades of silane and  $\text{NH}_3$  gases commercially available. A Freon-14/oxygen mixture was used for etching and clean-up, and argon was used as a carrier gas. The key deposition parameters for  $\text{SiN}_x$  films were:

- (1) Gas flow rates.
- (2)  $\text{NH}_3/\text{SiH}_4$  flow ratio.
- (3) Platen temperature.
- (4) RF power.
- (5) Chamber pressure.

Growth parameters were generally controlled to within 1% during deposition. A typical set of deposition parameters for film growth were:  $\text{SiH}_4$  flow, 10 sccm;  $\text{NH}_3$  flow, 20 sccm; argon flow, 30 sccm; RF power, 1200 W/m<sup>2</sup>; platen temperature, 270°C; total pressure, 0.48 torr; and deposition time, 300 s. The resultant film had a thickness of 670 Å with an index of refraction of about 2.0.

After growth, the optical properties of PECVD  $\text{SiN}_x$  films were determined. These are of interest because such a film can be used as an AR coating as well as a passivation layer for silicon solar cells. Two approaches (ellipsometry and reflectivity) were used to determine optical properties as a function of growth parameters. Ellipsometric measurements using optical filters were made at several wavelengths on  $\text{SiN}_x$  films. These measurements, however, yielded only two of the three parameters: the index of refraction (N), the extinction coefficient (K), and the film thickness.

Because only N and K can be determined, data obtained at 0.7 μm were analyzed assuming  $K = 0$  to determine thickness and N. This value of thickness then is used in analyzing the data for shorter wavelengths. Reflectance measurements were carried out from 0.36 to 1.2 μm. Results obtained for N and K with ellipsometry were compared to values for N and thickness from reflectance measurements.

By varying growth parameters, one could produce  $\text{SiN}_x$  films with high or low N values. Films with high N values were too absorptive. Table 5 gives a comparison of optical data obtained by ellipsometry and reflectance.

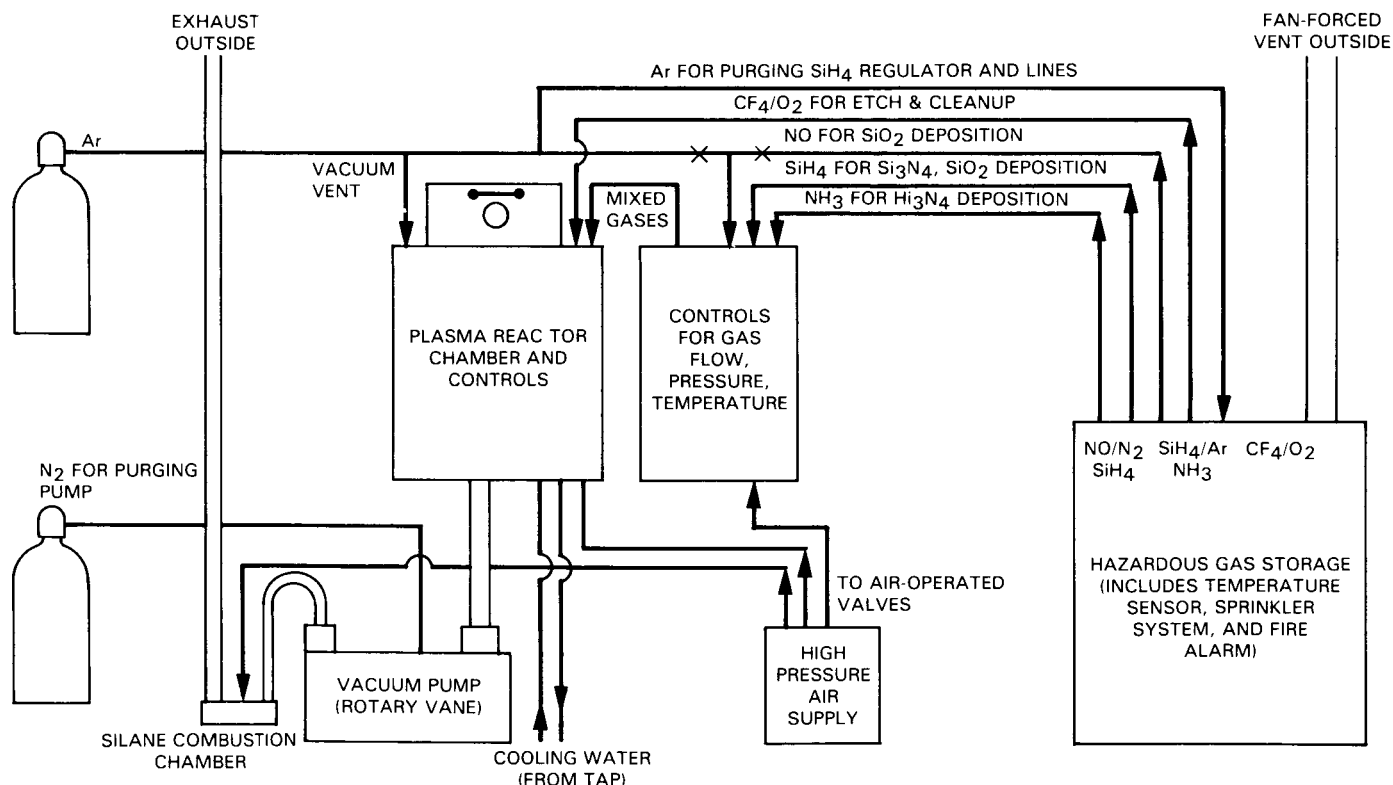


Figure 9. Schematic of PECVD System

Table 5. Comparison of Optical Constants Determined from Ellipsometry and Ordinary Reflectance

SiN <sub>x</sub> Film	Growth Parameters	Wavelengths, nm	Ellipsometry Reflectance				
			d	N	K	d	N
84-119	SiH <sub>4</sub> Flow: 10 sccm	400	374	2.45	0.188	360	2.35
	NH <sub>3</sub> Flow: 5.6 sccm	450	374	2.45	0.069	360	2.63
	T = 150°C	546	374	2.39	0.016	360	2.61
	Power = 75 W	700	374	2.25	0.000	360	2.42
84-151	SiH <sub>4</sub> Flow: 10 sccm	360	683	2.06	0.071	732	—
	NH <sub>3</sub> Flow: 10 sccm	400	683	2.01	0.006	732	1.99
	T = 270°C	450	683	2.03	0.000	732	1.95
	Power = 14 W	546	683	2.00	0.000	732	1.93
		700	683	1.95	0.000	732	1.93

The density of states at the SiN<sub>x</sub>/Si interfaces was determined by high-frequency capacitance voltage (C-V) analysis. A data acquisition program was used and CV data were gathered using a PAR-410 capacitance meter in conjunction with a computer. The method is accurate for surface state densities down to  $1 \times 10^{11}$  states per cm<sup>2</sup>/eV. Presently, SiN<sub>x</sub>/Si interfaces on moderately doped p-type silicon have been characterized by surface state densities below this value. A more accurate method with slow ramp capacitance versus voltage analysis was used to measure low surface state densities. It was observed that SiN<sub>x</sub> film deposited at lower power (10 to 20 W) led to lower surface state densities. Deposition of SiN<sub>x</sub> film at 270°C and nitriding the silicon surface prior to SiN<sub>x</sub> deposition also results in low surface state densities. Additional details are available in References 33 to 35.

#### C. SURFACE PASSIVATION BY HEAVILY DOPED POLYCRYSTALLINE SILICON: UNIVERSITY OF FLORIDA

Modeling and experimental studies have shown that high-efficiency silicon solar cells require a very low surface recombination velocity,  $S$  ( $S < 1000$  cm/s), at both front and back surfaces. In work at the University of Florida, the effectiveness of polycrystalline silicon to provide surface passivation at metal contacts was investigated. The polysilicon films were deposited using an atmospheric pressure CVD reactor at 670°C.

The following films were investigated:

- (1) 1500 Å: Undoped polysilicon (grain size 100 Å).

- (2) 1500 Å: In situ arsenic doped (grain size larger than about 400 Å).

- (3) Bilayer 1500 Å of undoped film followed by deposition of 1000 Å in situ doped film (grain size larger than about 300 Å). Wafers were etched in a buffered HF solution prior to polysilicon deposition.

A typical test structure consisted of a 0.06 Ω-cm p-type substrate with a thin ( $\sim 0.8$  μm) n-type epitaxial layer with doping density  $10^{16}$ /cm<sup>3</sup> grown on top, followed by polysilicon deposition. The solar cells also were subjected to various post-deposition heat treatments between 750 and 1000°C for 15 min to 64 h. Performance data are shown in Table 6.

A simple phenomenological model was developed to describe minority carrier transport in the polysilicon-mono-silicon interface. The CV characteristics of these solar cells were used to identify the parameters that determine the minority carrier transport in the interfacial layer and in the polysilicon film.

Correlation of the electrical results with the structural measurements using SIMS and TEM yielded the conclusion that minority carrier transport in the polysilicon-mono-silicon interface is controlled by a highly disordered layer within 100 Å of the interface characterized by very low minority carrier diffusivity. The effective surface recombination velocity at the interface was found to be  $\leq 10^4$  cm/s. A very low effective surface recombination velocity for the minority carriers at the polysilicon-silicon interface suggests that polysilicon can be used for surface passivation for both

Table 6. Summary of Measured Parameters of Solar Cells Without AR Coating (28°C)

Cell*	Base Type	Back Contact	$V_{OC}$ , mV	$I_{SC}$ (>0.6 $\mu\text{m}$ ), mA	L, $\mu\text{m}$	S, cm/s
1P	p	ohmic	573	63.0	310-350	—
2P	p	BSF	574	64.0	310-350	$4.2 \times 10^4$ to $5 \times 10^4$
5P	p	poly-Si BSF	583	67.7	310-350	1100-1500
1N	n	ohmic	566	62.7	190-250	—
2N	n	BSF	565	65.2	190-250	700-1000
5N	n	poly-Si BSF	591	65.5	190-250	100-160

\* These cells have area  $A = 4 \text{ cm}^2$  and thickness of about  $210 \pm 10 \mu\text{m}$  except for cell 2N which was  $330 \mu\text{m}$  thick. The results are averages obtained from 10 to 20 cells.

p- and n-type silicon. This suggestion is supported by the following considerations:

- (1) The minority carrier transport at the polysilicon-monosilicon interface, with no intentional insulating layer at the interface, is determined by the carrier transport within the polysilicon, rather than by tunneling through the native insulating layer.
- (2) The similarity of the electrical properties of the solar cells with in situ doping, and the bilayer polysilicon film, suggests a correlation between the electrical properties and the microstructure in the polysilicon film.
- (3) The observed lower dark current with polysilicon passivation compared to that without passivation can be explained by assuming the heavily doped interfacial layer must have properties significantly different from the properties of the monosilicon. The dominant mechanism for low dark current with polysilicon is more sensitive to the arsenic dopant concentration at the interface than to the carrier concentration at the interface.
- (4) The polysilicon-monosilicon interface acts as a very efficient barrier for minority carriers. This is mainly because of the very sudden transition from the orderly epitaxial single-crystal layer to the CVD-deposited polysilicon with randomly oriented grains of a few hundred angstroms in size. Thus, the polysilicon-monosilicon interface can be regarded as a region with a high degree of disorder. Such a heterojunction reduces recombination current by forming quasi-blocking contacts.

The potential of heavily doped polysilicon to replace the conventional high-low junction or BSF structure of silicon solar cells also was investigated. The resulting solar cells showed improvements in red spectral response and moderate improvements in  $V_{OC}$  when compared with control cells made with the BSF structure or with back ohmic contact structures. To assess the origin of these improvements, the effective surface recombination velocity,  $S$ , of the minority carriers in the polysilicon was measured as they enter the polysilicon layer. The measurements showed that  $S$  (polysilicon back) was less than  $S$  (BSF controls). This lowering of  $S$  is the mechanism responsible for the improvement in  $V_{OC}$  and red spectral response. Table 6 shows a summary of these results (References 36 to 38).

These results suggest a new class of silicon solar cell design that uses a thin base ( $\leq 150 \mu\text{m}$ ) of  $0.1 \Omega\text{-cm}$  resistivity p-type silicon contacted on the back by Al/Ti/Pd/Ag with a passivating layer of heavily doped polysilicon and a front surface passivated by oxide. This will attain high efficiency by reducing both front and back surface recombination velocities. To further reduce  $S$  values, heavily doped polysilicon can be used to passivate the front metal contact areas.

#### D. INTERFACIAL BARRIERS: STANFORD UNIVERSITY

To study the nature of interfacial barriers in high-efficiency silicon solar cells, XPS and BIS were used to examine Si/SiO<sub>2</sub> and Si/SiN<sub>x</sub> interfaces. XPS allows determinations of the bonding and valence band density of states, and BIS directly maps the conduction band density of states. Thus, XPS and BIS provide complementary information-measuring states at and above the Fermi level, respectively, in SiO<sub>2</sub> at the Si/SiO<sub>2</sub> interface.

XPS data on the Si/SiO<sub>2</sub> interface indicated that the interface is abrupt, and thermally grown oxides are chemically uniform beginning from 3 to 4 monolayers from the interface. It also was found that the strain in the near interfacial region of SiO<sub>2</sub> does not cause significant change in the nature of the Si-O bond.

BIS measurements showed that the conduction band for 13 Å oxide looks very much like the silicon conduction band. With thicker oxides, electron charging problems occurred. Figures 10 and 11 show the valence band by XPS and conduction band by BIS, respectively, for a 13 Å SiO<sub>2</sub> film on a silicon (100) surface.

XPS measurements on SiN<sub>x</sub> samples also were made. The SiN<sub>x</sub> films were deposited by plasma-enhanced CVD at the University of Washington and were subsequently annealed in argon ambient at 450 °C for 40 min. It was observed that SiN<sub>x</sub> films had oxidized and the film composition was more like SiO<sub>x</sub>N<sub>y</sub>. Some films were depth profiled by angle-resolved XPS and a gradient in nitrogen and oxygen concentrations was detected.

The XPS results indicated that the film surface was enriched with oxygen and was depleted of nitrogen. The bonding configuration of silicon also was observed to be changed across the film and becomes more like O-Si-O near the film surface, but it is like N-Si-O in the bulk of the film (References 39 to 40).

#### E. MICROCRYSTALLINE SILICON HETEROJUNCTION: APPLIED SOLAR ENERGY CORP. AND BOSTON COLLEGE

This effort to enhance cell performance was to explore the use of m-Si film on c-Si for solar cell applications, either as a m-Si/c-Si heterojunction or m-Si as a window layer on c-Si p-n junctions. This was deemed possible because m-Si has an optical bandgap of 1.7 eV, and a crystal size of 100 Å. Because of a good lattice match, m-Si could potentially enhance V<sub>OC</sub> by reducing interface recombination velocity. This program was a joint venture with Boston College using an evaporation scheme to deposit doped films of m-Si with in situ hydrogenation. The Applied Solar Energy Corp. (ASEC) was to supply suitable substrates and also make solar cells after m-Si deposition. Evaporated films and solar cells were to be characterized by both contractors.

Earlier experiments on non-silicon substrates had demonstrated microcrystal sizes of about 100 Å and an optical bandgap of 1.7 eV. The wavelength dependence of the absorption coefficient data for e-beam evaporated layers closely matched data obtained by glow discharge techniques. Work under this contract was concentrated, therefore, on making different cell structures and their characterizations. Nearly 40 deposition runs were made, with substrate temperatures varying from 572 to 652 °C, and layer

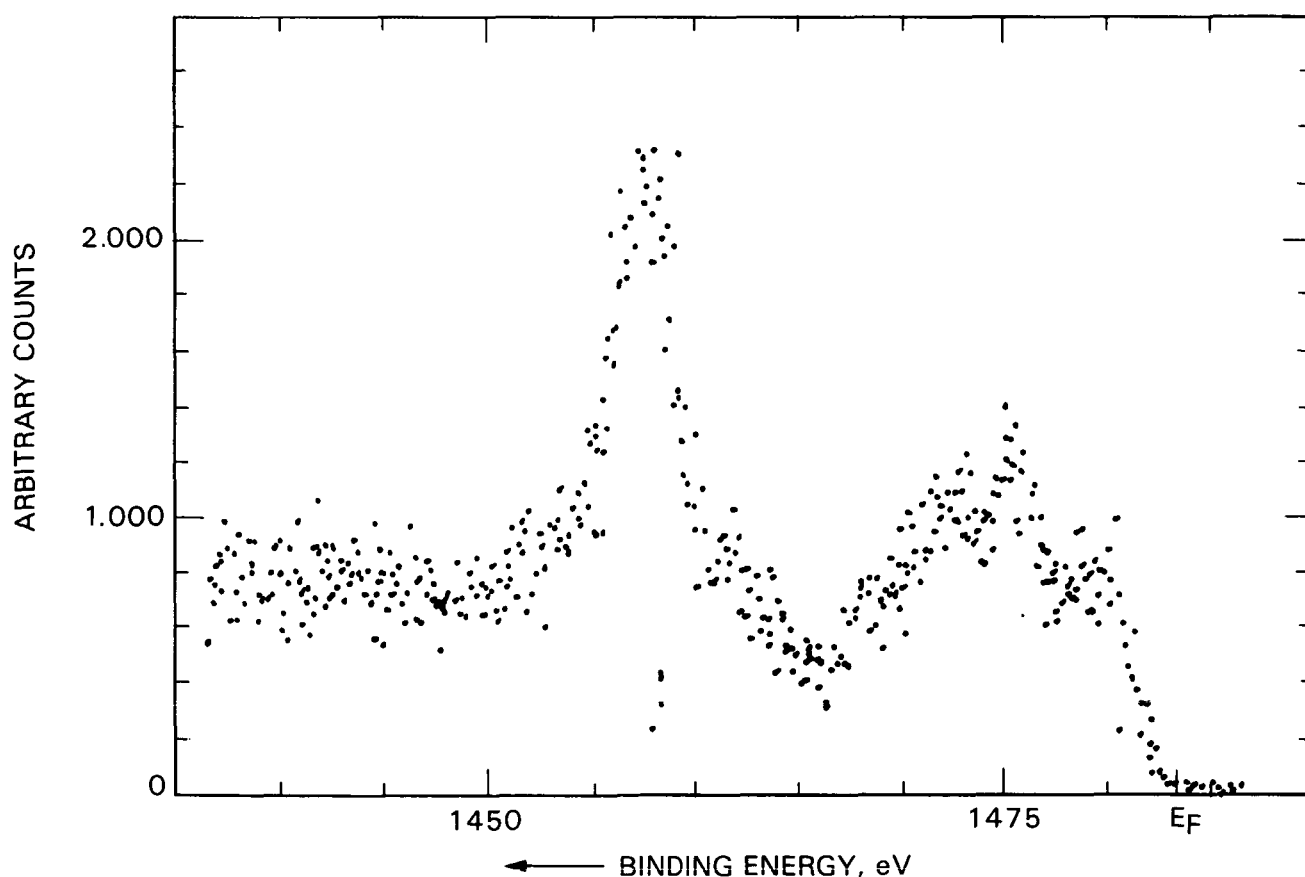


Figure 10. Valence Band of 13 Å SiO<sub>2</sub> Over Si [100]

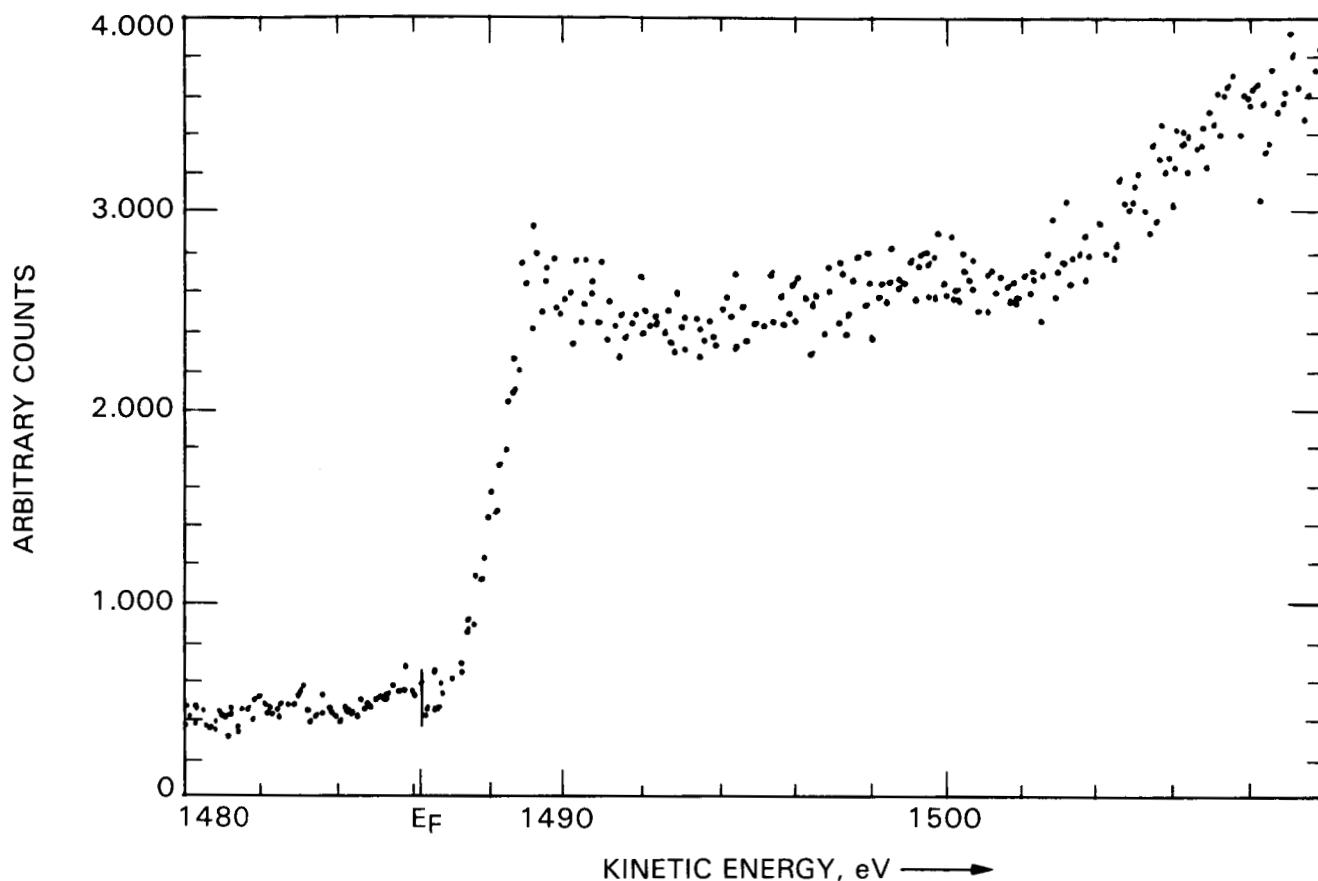


Figure 11. Conduction Band of 13 Å  $\text{SiO}_2$  Over Si [100]

thicknesses varying from a few tens of angstroms to slightly less than 1  $\mu\text{m}$ . Each run yielded five coated substrates, most of which were fabricated into cells.

The m-Si deposition system consisted of a vacuum chamber with an e-beam evaporation system using a graphite boat containing pure silicon. Boron and antimony as p- and n-type dopants could be co-evaporated by electrical heating. Both substrate heating and in situ cleaning with hydrogen plasma were provided. Hydrogen plasma also was used for in situ hydrogenation of the m-Si film either during or after growth.

Heterojunction structure was affected by interface and shunting problems and the best  $V_{OC}$  achieved was only 482 mV, well below that of single-crystal silicon homojunctions. The heterojunction structure of p-m-Si/p-n showed promise on some of the samples. The complementary structure did not show any improvement. Although several runs with different deposition conditions were made, the results were inconsistent. Any  $V_{OC}$  enhancement obtained was too small to compensate for the current loss because of the extra absorption and poor carrier transport properties of the m-Si film. A study of the m-Si/c-Si interface using a p-p or n-n heterojunction showed that m-Si did not always serve as a minority carrier barrier as expected. The  $V_{OC}$  in many samples was of opposite polarity from that predicted which indicated some degree of carrier

collection. This raised problems concerning the nature of the m-Si/c-Si interface. Cell efficiencies varied from 0.6 to 8.3% at 100  $\text{mW}/\text{cm}^2$  with AR coatings, signifying poor minority carrier lifetime and interface shunting.

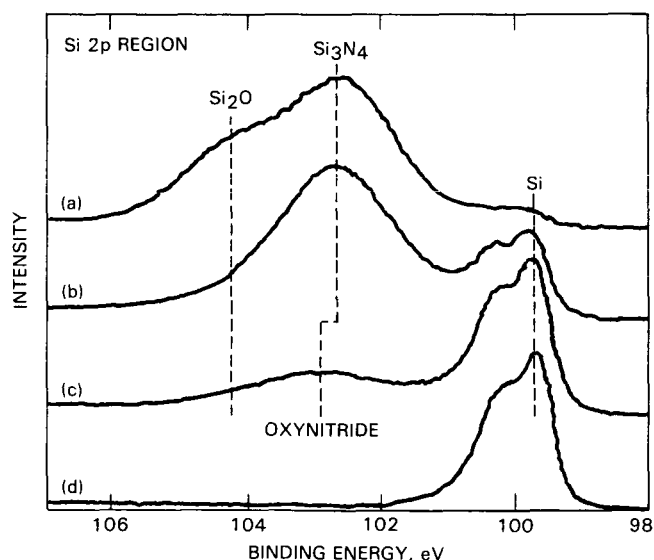
The SIMS study revealed carbon along the interface and within the layer. Replacement of the graphite boat with a boron nitride boat reduced the carbon content, but did not eliminate it. Copper and Mo also were discovered as contaminants. Photomicrographs showed uneven surfaces, bubbly areas, and etch pits, signifying poor quality of the film. For this approach to succeed, interface problems need to be solved, and quality of the deposited layer of m-Si needs to be improved (Reference 41).

#### F. X-RAY PHOTOEMISSION SPECTROSCOPY: JET PROPULSION LABORATORY

High-resolution x-ray photoemission spectroscopy was used for chemical analyses of some of the  $\text{SiN}_x$  films. These films were grown by PECVD at the Joint Center for Graduate Studies (JCGS) at 270°C (see Section III. B. for details). Surface passivation characteristics of these layers were investigated by measuring density of states ( $N_{ss}$ ) using a high-frequency CV technique.  $N_{ss}$  values were measured in the range of  $10^9$  to  $10^{12}$  states/ $\text{cm}^2$ .

Figure 12 shows XPS spectra of  $\text{SiN}_x$  films as a function of film thickness. As can be seen, these films were characterized by four compositional regions within the layer:

- (1) The topmost layer is composed primarily of  $\text{SiO}_2$ , produced possibly through exposure of the film at high temperatures to oxygen contamination during the pull process or through the long-term exposure of  $\text{SiN}_x$  to air.
- (2) The second region is composed of essentially stoichiometric  $\text{Si}_3\text{N}_4$  with the possibility of some oxygen incorporation.
- (3) The third layer is characteristic of an oxynitride.
- (4) The final layer at the  $\text{SiN}_x$ /silicon interface is essentially  $\text{SiO}_2$ . The role of this final layer in surface passivation in the  $\text{SiN}_x$  passivation scheme should not be overlooked. It is quite conceivable that the  $\text{SiO}_2$  is participating as a surface passivant, at least partially and perhaps totally. It is well known that it is extremely difficult to produce oxide-free silicon surfaces (Reference 42 and 43).



LEGEND:

- (a) AS-RECEIVED SURFACE, SHOWING PRESENCE OF SILICON DIOXIDE ON SURFACE.
- (b) SPECTRUM AFTER SILICON DIOXIDE LAYER HAS BEEN REMOVED, SHOWING PRESENCE OF SILICON NITRIDE.
- (c) SPECTRUM OBTAINED NEAR INTERFACE, SHOWING OXYNITRIDE LAYER OVER SILICON DIOXIDE.
- (d) CLEAN SILICON SUBSTRATE SPECTRUM.

Figure 12. XPS Si 2p Spectra Obtained as a Function of Silicon Nitride Thickness

## G. TRANSPARENT CONDUCTING POLYMERS: JET PROPULSION LABORATORY

Because of their metal-like conductivities and modest environmental stability, conducting polymers have generated widespread interest in a variety of important areas. The possible use of transparent conducting polymers as a solar cell front-side current collector is of interest. JPL evaluated the potentials of these types of polymers as current collectors and surface passivants in silicon solar cells.

Some of the well characterized conducting polymers exhibit metallic conductivities  $< 500 (\Omega\text{-cm})^{-1}$  (References 44 through 48), and there are speculations about the possible synthesis of polymers with conductivities higher than those of copper and silver (Reference 49). Their robustness to air oxidation combined with the metal-like conductivities prompted their consideration as possible replacement materials for metallic current collectors and back ohmic contacts in silicon solar cells. Claims by Bard (References 50 through 52) that polymers can passivate surface states, that are present especially on layer type compounds (References 53 through 55), prompted exploration of the potential of these conducting polymers as surface passivants in silicon solar cells. This exploration led to the investigation of the nature of the interfaces of a series of conducting polymers with single crystal p-Si semiconductor. Typical conducting polymers considered to have potential for this application are shown in Figure 13.

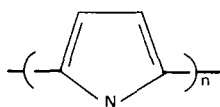
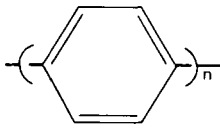
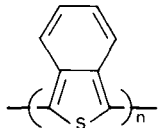
POLYMER	DOPANT	CONDUCTIVITY
 POLY(PYRROLE)	$\text{BF}_4^-$	~ 100 $\Omega^{-1}\text{cm}^{-1}$
 POLY(PARAPHENYLENE)	$\text{AsF}_5^-$	~ 500 $\Omega^{-1}\text{cm}^{-1}$
 POLY(ISOETHIANAPHTHENE)	$\text{Cl}^-$	~ 50 $\Omega^{-1}\text{cm}^{-1}$

Figure 13. Typical Conducting Polymers and Structure with Dopant and Range of Conductivities

The conducting polymers electrochemically were deposited onto the p-Si surface in the dark. The electrochemical experimental set-up used to deposit the conducting polymers and a typical deposition mechanism of poly-pyrrole are shown in Figure 14. After deposition, the interfacial properties of the p-Si conducting polymer were measured using an AC-impedance technique. The results of the AC-impedance measurements are given in Table 7 (References 56 and 57).

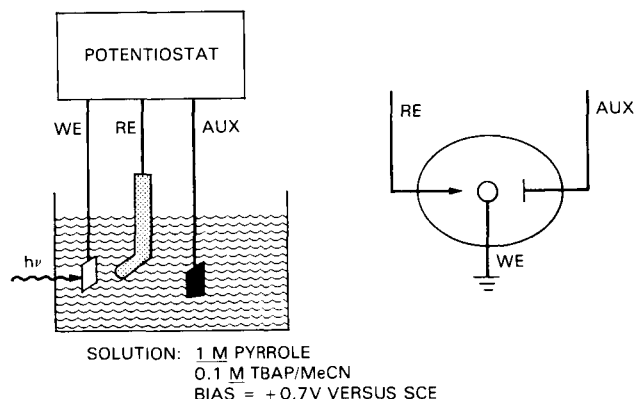


Figure 14. Electrochemical Synthesis of Poly(Pyrrole)

To form an ohmic contact between p-Si and a p-type degenerate organic semiconductor, such as perchlorate-doped polypyrrole  $PP(ClO_4^-)$ , the polymer's Fermi level should be more positive in the electrochemical potential scale than that of p-Si. Table 7 shows the flat-band ( $V_{fb}$ ) potentials of p-Si and a series of conducting polymers. For p-type materials, the  $V_{fb}$  is very close to the Fermi level. Thus, it is clear that  $PP(ClO_4^-)$  has the best chance of forming an ohmic contact with p-Si. This is indeed what was

Table 7. Flat Band Potentials of p-Si as a Function of Conducting Polymers<sup>a</sup>

Electrode	$V_{fb}^b$
p-Si	+0.15
Poly (pyrrole) doped with $ClO_4^-$ ion	+0.19
Poly (azulene) doped with $ClO_4^-$ ion	+0.1
Poly (isothianaphthene) doped with $ClO_4^-$ ion	-0.41 <sup>c</sup>

<sup>a</sup>All AC measurements were carried out in an acetonitrile solution containing tetra-n-butyl ammonium perchlorate as supporting electrolyte.

<sup>b</sup>Versus standard calomel electrode.

<sup>c</sup>Preliminary value inconsistent with typical results.

shown. Coupling these data with earlier referenced studies showing passivation effects suggests that organic semiconductors may have potential as passivating contacts. Additional development including preparation of cells is needed, however.

## H. PRESENT STATUS

Considerable progress was made in studies toward understanding and reducing losses associated with surfaces in silicon. Results, however, are far from complete. The value of various surface films (oxides, oxy-nitrides, and polycrystalline silicons) in reducing losses was empirically established. The detailed mechanisms of passivation, the relative stability of the passivation, and practical means of producing the layers as part of a cell manufacturing sequence are largely unresolved. Variations in passivation with process conditions are not all understood. Thus, the inclusion of a passivation process in a PV cell manufacturing sequence is not available.

In contrast to established empirical values of better understood films, other layers such as polymers and microcrystalline layers require development before their contribution can be evaluated. Preliminary results suggested potential, but better films are required.

## I. KEY ACCOMPLISHMENTS

The Task was unable to complete many aspects of the research that were needed to reduce surface losses in these PV devices. Thus, many of the accomplishments presented here are valid only for specific studies and do not lend themselves to broad application. Yet, the following specific accomplishments contribute substantially to our ability to reduce losses at the surfaces of devices.

XPS data indicated that the silicon/silicon oxide interface was abrupt, and thermally grown oxides were chemically uniform beginning at 3 to 4 monolayers from the interface. The strain at and near the interfacial region of  $SiO_2$  did not cause significant changes in the nature of Si-O bonding.

Silicon nitride was shown to be an effective surface passivant. A modified Rosier method was developed to measure density of surface states and surface recombination. A slow, ramp-capacitance voltage technique proved successful in measuring small values of interface surface state densities.

XPS data on silicon passivated with nitrides suggested: (1) the topmost layer was  $SiO_2$  (possibly from exposure of the film at high temperature to oxygen, or long-term exposure of  $SiN_x$  to air), (2) a second region consisted essentially of  $Si_3N_4$ , (3) the third layer showed characteristics of an oxynitride ( $SiN_xO_4$ ), and (4) the surface layer closest to silicon was essentially  $SiO_2$ .

A new silicon solar cell design was proposed having: (1) a thin base ( $> 150 \mu\text{m}$ ) of  $0.1 \Omega\text{-cm}$  p-type silicon with a shallow ( $0.2 \mu\text{m}$ ) junction, (2) contacts on the back and front in selected areas with an intermediate to heavily doped polycrystalline silicon layer of about  $1000 \text{ \AA}$  thickness, (3) the remaining contact surfaces passivated by growth of  $\text{SiO}_2$  at  $800^\circ\text{C}$ , and (4) a double layer AR coating used as in conventional cells for better optical absorption.

Microcrystalline silicon deposition was done in an e-beam evaporation chamber with co-evaporation of either boron or antimony as p- or n-type dopant and in situ hydrogen passivation by a plasma generator to passivate m-Si bonds and obtain a higher bandgap of  $1.7 \text{ eV}$ .

#### J. FUTURE NEEDS

Significant additional effort is needed in the application, understanding, and effectiveness of surface and interface passivation. It is clear that such effort is valuable because of the significant gains in  $V_{OC}$  to be

made using this approach. These efforts should be an important part of continued R&D in the field of photovoltaics.

A primary need is a detailed understanding of the chemical-structural bonding at the free silicon surface so that the impact of previous history, processing effectiveness, and reliability can be controlled. With this understanding, the complex and sensitive passivation step can be reoptimized each time the design, process, material, or process sequence is changed.

In addition to this general need for a better understanding of passivating layers, certain interesting layers still require development for full evaluation of their potential. Microcrystalline silicon, although similar to polycrystalline layers, may hold some advantages and could be further developed. The organic layers, because of low-temperature application, show promise. Additional polymer material composition and deposition developments are required before questions of optimum performance on solar cells and reliability can be addressed.

## SECTION IV

# Advanced Solar Cell Devices and Processes

### A. INTRODUCTION

This Task element addressed two main topics: (1) determination of the suitability of various prepared silicon sheets produced by diverse technologies to meet the FSA cost goals (conversion efficiency is a first-order determinant of cost), and (2) novel approaches to the achievement of very high ( $>20\%$ ) conversion efficiency in silicon solar cells. Both topics involved internal JPL research coupled with contractor support.

The major sheet technologies evaluated ranged from semicrystalline silicon to dendritic web. Baseline fabrication processes were established at ASEC and JPL, and were used to compare the competing sheet-growth materials. Cell output data, coupled with more fundamental measurements such as minority carrier diffusion length, were used to evaluate the progress in each material and to compare them to each other and against single-crystal Cz silicon.

A great deal of processing and measurement work was done on dendritic web material under a contract with Westinghouse. The advanced processes of surface passivation, multiple layer AR coatings, and back-surface reflectors were employed. Fundamental measurement techniques of deep-level transient spectroscopy (DLTS), EBIC, and TEM were used to assess the impact of growth parameter variations and post growth annealing on the minority carrier diffusion length of dendritic web. Cells were fabricated with conversion efficiencies of nearly  $17\%$ . Diffusion length improvements by more than a factor of three (to  $120\text{ }\mu\text{m}$ ) were attained in optimized dendritic-web material.

Cell processing schemes to advance the performance of all devices were predicated on feedback from the FSA modeling effort. Modeling identified the major loss mechanisms that limited the achievement of very high efficiency for cells fabricated from single-crystal silicon. Sophisticated solar cell designs were investigated aimed at reducing or eliminating the effect of surface recombination velocity and enhancing bulk collection.

The two major cell configurations evaluated in this work were the floating emitter solar cell transistor and the dot contact cell. The former cell was conceived by C.T. Sah and processed by ASEC. It aims at reducing the deleterious effect of high-emitter doping by an approach that allows the emitter to function effectively at a significantly lower doping concentration. This cell design also should make surface passivation much easier and allow enhanced bulk collection efficiency. The dot contact cell design, investigated by JPL, seeks to reduce the effect of surface recombination by use of a

geometry featuring small isolated emitters separated by well-passivated silicon. This reduces emitter recombination because of the reduced volume of the emitter.

Work on both cell designs ran into severe processing problems that prevented either approach from fulfilling its potential. The last processing runs dealing with the floating emitter cell, however, produced encouraging evidence that this design may be capable of achieving a greater than  $20\%$  conversion efficiency. Current densities as high as  $45\text{ mA/cm}^2$  were obtained and showed that the enhanced current collection postulated for this type of solar cell is valid. Further progress with the dot contact cell, however, requires improvements in photolithography and surface passivation techniques.

At JPL, an additional approach to obtain high-efficiency silicon cells involved the use of high-quality FZ silicon to fabricate cells. The FZ silicon was processed with the most sophisticated conventional fabrication processes such as shallow junctions, refined contact configurations, surface texturing, and multiple AR coatings. It seems that the AR coating process also acts to passivate the silicon surface. Using this approach, conversion efficiencies from  $18.6$  to  $22\%$  AM1 (depending on cell size) have been obtained.

A study at North Carolina State University was to evaluate: (1) use of the rapid thermal process (RTP) as a viable procedure to dissolve grown-in defects and nucleation sites for oxygen precipitation, and (2) the rapid junction activation procedure following ion implantation to prevent the occurrence of any subsequent defect nucleation or other lifetime-degrading processes. By dissolving grown-in defects and by preventing them from occurring subsequently, one can improve the minority carrier lifetime and thereby the efficiency. Studies continued to obtain optimum RTP and implant cycles with known precipitate denuded zones in the input material.

### B. HIGH-EFFICIENCY CELLS PREPARED FROM WEB SILICON: WESTINGHOUSE

This research was directed toward improving both silicon web material and processing techniques to produce high-efficiency cells (goal of  $18\%$ ). Westinghouse investigated the influence of twin planes, dislocations, trace impurities, and internal stress on bulk minority carrier lifetime. Processing investigations included annealing effects, cleaning effect, surface passivation, AR coatings, and BSRs.

One of the earlier experiments studied the effects of heat treatment and cooling rate on diffusion length. Diffusion length was shown to improve after an 800 to 900 °C heat treatment. Other data were inconclusive in that some showed a drop-off in diffusion length and others showed improvement at 1100 to 1200 °C heat treatment levels.

The effect of stress on web cell performance was investigated. The data indicated that stress has no appreciable influence on the minority-carrier diffusion length in web crystals in the as-grown condition. The diffusion length was found to be about  $30 \pm 10 \mu\text{m}$  in the web crystals with a stress level of 40 Mdyne/cm<sup>2</sup>. After heat treatment (boron diffusion), however, the low-stress web showed very significant improvement in the diffusion length. Diffusion lengths as high as 116  $\mu\text{m}$  were measured by a surface photovoltage technique in the low-stress web after heat treatment. The high-stress web, however, showed no appreciable change in the diffusion length after heat treatment.

The impurity twin-plane interaction was investigated by conducting DLTS measurements as a function of depth on titanium-doped web crystal. Results indicated that the grown-in titanium impurity tends to pile up near twin planes. There was about a factor of 5 increase in the titanium deep-level concentration near the twin planes relative to the web surface.

EBIC measurements, performed on beveled web samples to detect recombination activity at the twin planes within the web material, indicated that twin planes in web show higher recombination activity compared to the rest of the bulk. It was not clear whether this activity increase was caused by the accumulation of titanium impurities near the twin planes.

Model calculations were performed to observe the effect of twin-plane activity on  $V_{OC}$  as a function of resistivity of the web material. The calculations indicated that an active twin plane can lower  $V_{OC}$ . The impact of an active twin plane on 4  $\Omega\text{-cm}$  web cell efficiency is much more than on 0.2  $\Omega\text{-cm}$  web cells. This is because the  $V_{OC}$  of a 4  $\Omega\text{-cm}$  cell is base limited, whereas the emitter usually limits the  $V_{OC}$  in 0.2  $\Omega\text{-cm}$  cells.

Some process improvements made by Westinghouse to increase cell efficiency included: (1) surface passivation by surface oxidation to reduce surface recombination velocity, (2) development of a double-layer AR coating using ZnSe and MgF, and (3) development of an aluminum BSR to make use of the unabsorbed long wavelength photons. Cells were fabricated with these advanced features and efficiencies as high as 16.9% were obtained for a 1 cm<sup>2</sup> cell with web silicon of 0.37  $\Omega\text{-cm}$  resistivity. Compared to the counterpart baseline cell with no passivation, no AR coating, and no BSR, the combined effect of oxide passivation, evaporated double-layer AR coating, and BSR gave a 59% improvement in  $I_{SC}$  and a 69% increase in cell efficiency.

Westinghouse investigated the use of hydrogen ion implantation as a means of improving bulk properties and, hence, cell efficiencies. The data indicated that lower quality cells could be improved by hydrogen implantation and some samples showed absolute efficiency improvements from 8 to 10% (non-AR). Higher quality cells of more than 10% efficiency (non-AR), however, showed little improvement in efficiency after hydrogen ion implantation.

Figure 15 presents curves of model calculations of twin plane effects on  $V_{OC}$ 's of 0.2  $\Omega\text{-cm}$  web material. Figure 16 is a cross-sectional TEM view of a cell showing twin planes and dislocations. Figure 17 depicts light-beam-induced current (LBIC) scans of beveled surfaces that demonstrate, under certain growth conditions, twin planes can be decorated with defects causing recombination. Note the 50% decrease in photocurrent in Figure 17a and the dark bands in Figure 17b associated with the decorated twin plane.

More details on this effort on "Development of High-Efficiency Solar Cells on Silicon Web" is covered in the Westinghouse final report (Reference 58).

#### C. FLOATING EMITTER CELL DESIGN: APPLIED SOLAR ENERGY CORP.

A novel approach to a high-efficiency cell design was proposed by C.T. Sah Associates. A patent disclosure, Docket 16467, by Drs. Li-Jen Cheng, of JPL, and C.T. Sah describes the theory and operation of the solar cell called a Floating Emitter Solar Cell Transistor. ASEC was assigned the task to fabricate the floating emitter cell design by JPL. The emitter designs are shown in Figures 18a and 18b. Only the back-surface contact, vertical floating emitter, solar cell transistor (BSC-VFE-SCT) was fabricated by ASEC. The design proved difficult to fabricate and required two diffusion masking steps for the n<sup>+</sup> and p<sup>+</sup> layer formations: a photolithography masking step for metal patterning, and two CVD steps for the SiO<sub>2</sub> insulation layers.

Performance results of the fabricated cells from initial lots were not good. With a second lot, however, cell efficiencies ranged from 11% to more than 15%. The average cell efficiency was 13.2%, with one-third of the cells measuring more than 14% efficient.  $V_{OC}$ 's ranged from 575 to 605 mV. The best improvement was in the junction current density ( $J_{SC}$ ) values of the final lot which measured between 35 to 45 mA/cm<sup>2</sup> for the 4 cm<sup>2</sup> cells as compared to 2 to 25 mA/cm<sup>2</sup> for  $J_{SC}$ 's of the previous lots. It is proposed that this improved current collection efficiency results from reduction of the cell thickness from 8 to 4 mils, and an increase in the bulk resistivity from <10 to 50  $\Omega\text{-cm}$ .

Some of the processing problems encountered in fabrication of the floating emitter cells included mask alignment, oxide layers induced during boron diffusion, and nonuniformity of both the POCl<sub>3</sub> diffused layers and the passivated SiO<sub>2</sub> layers. No doubt, some of

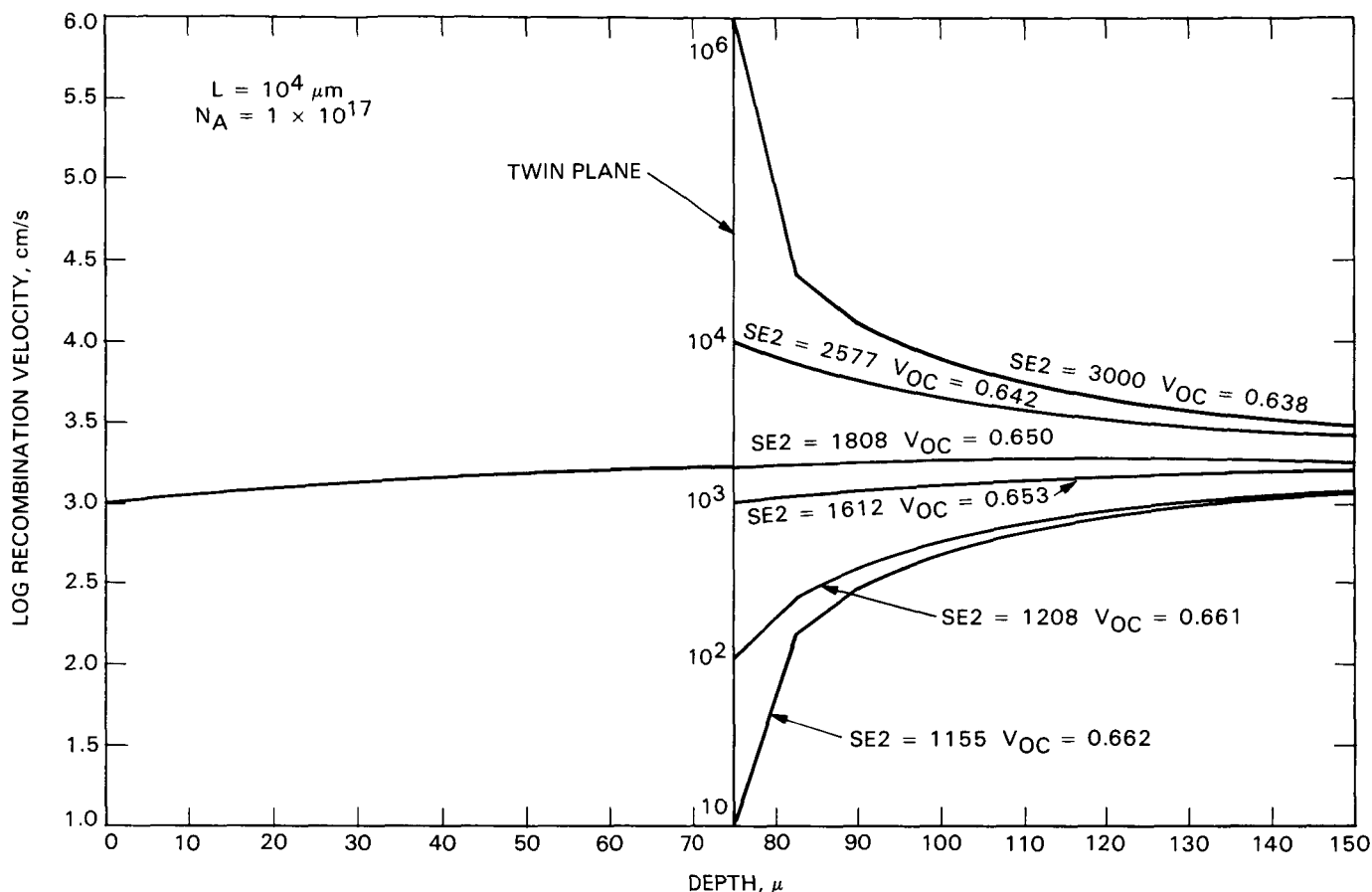


Figure 15. Model Calculations for the Effect of Electrical Activity of the Twin Plane on  $V_{OC}$  in 0.2  $\Omega$ -cm Web Cells

these problems contributed to the poor performance of some cells. The ASEC fabrication contract did not resolve the issue whether or not the floating emitter design is a viable solar cell design. It was not determined what effect the processing problems had on the overall cell performance. The improvement in performance of the final lot of cells was encouraging and suggested there might be a potential for the design to be a high-efficiency solar cell. It was concluded, therefore, that the floating emitter design needs more work both in analysis and processing before its full potential as a high-efficiency solar cell can be determined (Reference 59).

The design in Figure 18b is labeled FSC-VFE-SCT and functions similarly to the previously described BSC-VFE-SCT, differing only in that the  $n^+$  contact is moved to the front of the cell. The first acronym, therefore, was changed from BSC to front-surface contact (FSC). Construction of this design was not attempted prior to the conclusion of the FSA Project.

#### D. EVALUATION OF LOW-COST SHEET FOR CELL EFFICIENCY: APPLIED SOLAR ENERGY CORP.

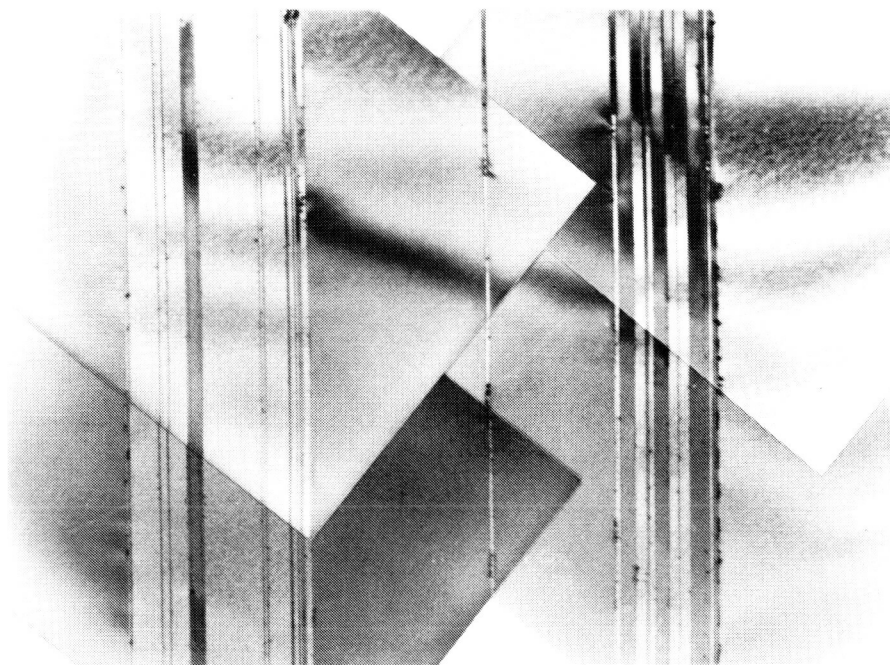
This study was an evaluation study of solar cells prepared from low-cost silicon materials, including EFG ribbons from Mobil-Tyco, dendritic web ribbons

from Westinghouse, cast ingots by HEM from Crystal Systems, and cast ingots by ubiquitous crystallization process (UCP) from Semix. The objective of this task was to investigate, develop, and use technologies appropriate and necessary for the improvement of the efficiency of solar cells made from these unconventional silicon sheets (Reference 60). Solar cells were fabricated using a baseline process typical of those used in the silicon solar cell industry. Process modifications were included to give indications of the possible improved performance obtainable from various sheets. These modifications included gettering by diffusion glasses, low temperature annealing, shallow junction formation, application of fine front gridlines, formation of BSF and BSR, and application of better AR coatings.

The solar cell parameters that were measured included short circuit current density, curve fill factor, and conversion efficiency. Also measured for selected cells were spectral response, dark I-V characteristics, minority carrier diffusion length, and photoresponse by fine light spot scanning. The results were compared to the properties of cells made from conventional Cz-silicon with an emphasis on statistical evaluation (see Reference 60).

The investigation found that EFG ribbons grown in a carbon-containing environment have better structural

# CELL 40C: LOW EFFICIENCY TWIN PLANE REGION

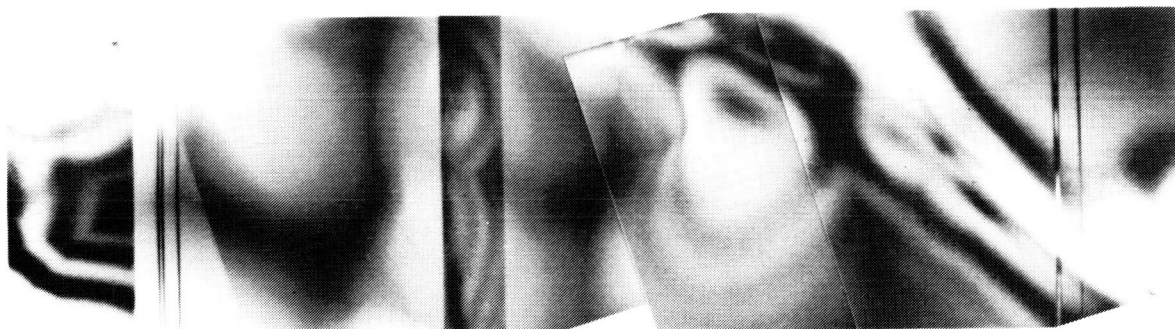


4.8  $\mu\text{m}$

TWIN PLANE VERTICAL  
TWIN PLANE REGION:  
NUMEROUS ALTERNATING TWINS

ORIGINAL PAGE IS  
OF POOR QUALITY

# CELL 69A: HIGH EFFICIENCY



8.7  $\mu\text{m}$

TWIN PLANE VERTICAL  
NO DISLOCATIONS  
ADJACENT TO  
TWIN PLANES;  
FEWER TWINS

TWIN PLANE TILTED

TWIN PLANE TILTED

Figure 16. Twin Planes in Web Showing Impact of Dislocations on Efficiency

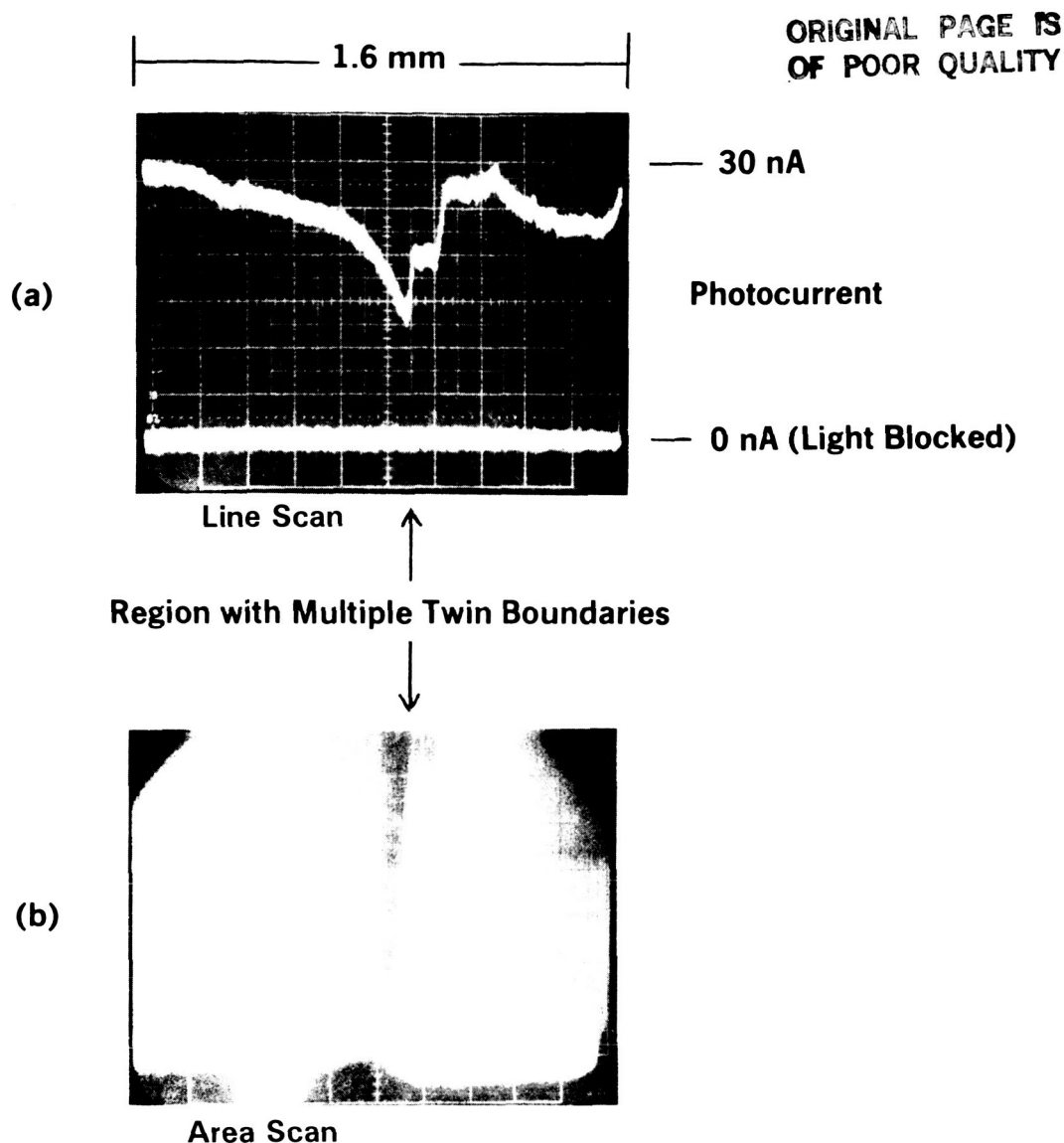


Figure 17. LBIC Scans of Beveled Sample Prepared from Cell 17C (9.5% AM1)

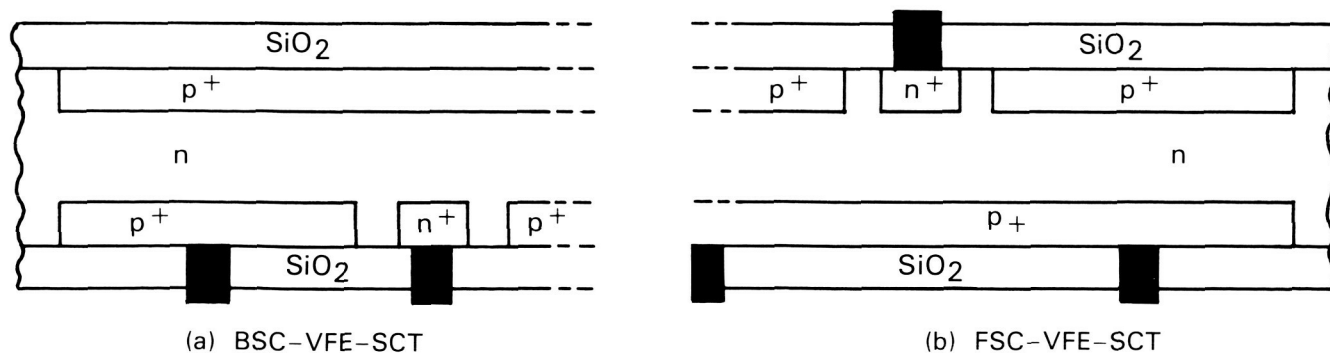


Figure 18. Floating Emitter Solar Cell Transistor

perfection, such as large grain, less dislocation density, and longer carrier diffusion length. Solar cells made from these specific EFG ribbons have higher efficiencies in comparison with cells prepared from earlier EFG ribbons. The best cell efficiency achieved by the advanced process was about 14%.

The evaluation of web ribbons suggested that web cells made using the baseline process have efficiencies slightly lower than those made of Cz silicon. Cell performance agreed with the data of dislocation densities in the ribbons.

The evaluation of cells made of HEM material had problems both of ingot reproducibility from run to run, and uniformity of sheet quality within an ingot. Junction shunting, which could be caused by particulate inclusions observed in the bulk, was a major result of these problems. Gettering and low-temperature annealing did not improve cell performance.

The evaluation of UCP cells prepared by the baseline process suggested that the quality of this silicon material was lower than that of Cz silicon. Overall cell performance was relatively uniform with the exception of a few cells that showed shunting problems caused by particulate inclusion.

It should be emphasized that the results reported here represent the somewhat immature state of development (1981) for these forms of silicon. No systematic comparisons of quality and performance have been made since 1981.

#### E. RAPID THERMAL PROCESSING: NORTH CAROLINA STATE UNIVERSITY

The objective of this study was to evaluate rapid thermal processing (RTP) as a viable procedure for: (1) Cz substrate modification using high-temperature dissolution treatments, and (2) rapid junction activation following ion implantation. The reason for the first treatment is to dissolve grown-in defects and nucleation sites for oxygen precipitation. The second treatment should be done as quickly as possible (e.g.,  $< 10$  s) to prevent the occurrence of any subsequent defect nucleation or lifetime-degrading processes.

The experimental approach for substrate evaluation used preferential chemical etching and x-ray topography to delineate defects which then are correlated with minority carrier lifetime. The x-ray delineation is enhanced by a lithium decoration procedure performed at temperatures less than  $450^{\circ}\text{C}$  both prior to and after a high temperature dissolution anneal. Silicon wafers examined have been as-grown as well as furnace and RTP annealed with various combinations of 1200, 1050, and  $750^{\circ}\text{C}$  thermal cycles.

Initial generation lifetime (Gg) maps did correlate Gg with defects delineated by x-ray topography. The raw data, obtained from samples with and without a RTP of  $1200^{\circ}\text{C}$  for 1 min prior to a  $1100^{\circ}\text{C}/80\text{-min}$  field oxide-growth, showed a significant improvement with the RTP treatment ( $10\ \mu\text{s}$  without, and  $35\ \mu\text{s}$  with an RTP cycle).

Results show that correlation between process-induced defects and values for Gg spans a range from 100 to  $1000\ \mu\text{s}$ , and recombination is generally a factor of 10 lower. Studies also were included to obtain optimum RTP and implant cycles with known precipitate-denuded zones as input materials (Reference 61).

#### F. HIGH-EFFICIENCY SOLAR CELL PROCESSING: JET PROPULSION LABORATORY

The JPL FSA Project was actively involved in the processing of silicon solar cells from 1980 to 1986. The solar cell processing capability was initiated to evaluate silicon sheet materials that were being developed by various FSA Project contractors. The facility also was used to support basic research on improving cell performance.

The baseline processing capability consisted of forming an  $n^{+}$  junction in p-type material by diffusing phosphorus at  $850^{\circ}\text{C}$  from a phosphine source for 20 min. This yielded a junction depth between 0.35 and  $0.4\ \mu\text{m}$ . Spreading resistance measurements indicated that the surface concentration was  $5 \times 10^{19}$  atoms/cm<sup>3</sup>. A metal tri-layer back contact of titanium, palladium, and silver then was evaporated on the back of the cell and sintered at  $600^{\circ}\text{C}$  in hydrogen to form an ohmic contact. The front contacts were formed by evaporating titanium, palladium, and silver through a shadow mask. The last step was to evaporate  $625\ \text{\AA}$  of  $\text{Ta}_2\text{O}_5$  on the front as an AR coating. The basic process flow is illustrated in Figure 19. A detailed description of JPL's baseline processing is described in Reference 62.

In 1984, a major effort was initiated to produce solar cells that would be comparable to the best cells available at that time. This required several changes to the baseline process. FZ wafers were purchased with respective resistivities of 1.0 to 2.0, 0.3 to 0.5, and 0.15 to  $0.25\ \Omega\text{-cm}$ . FZ wafers were used because their low oxygen content results in fewer defects and longer minority carrier diffusion lengths. This was especially important for lower resistivity materials. FZ material also would maintain its lifetime during thermal cycling caused by cell processing.

To increase the short wavelength (blue) response of the cells and decrease emitter recombination, the diffusion process was altered so that the junction depth was reduced to  $0.2\ \mu\text{m}$  and the surface concentration was lowered to  $1 \times 10^{19}$  atoms/cm<sup>3</sup>. To accomplish this, the diffusion temperature was lowered to  $800^{\circ}\text{C}$ . The diffusion time was retained at 20 min.

To improve the back contact,  $2000\ \text{\AA}$  of aluminum were added as the first layer for the back contact. When sintered at  $500^{\circ}\text{C}$  for 20 min in hydrogen, a heavily doped  $p^{+}$  contact was formed at the back. This resulted in a small increase in voltage and more consistent curve factors (Reference 63).

To achieve a further increase in current, it was necessary to improve on the single-layer AR coating. A single-layer coating produces about a 40% increase in current compared to the uncoated cell value. A double-layer AR coating, by comparison, theoretically would result in up to a 56% increase in current. Thus, a double-layer AR coating consisting of  $\text{TiO}_x$  and

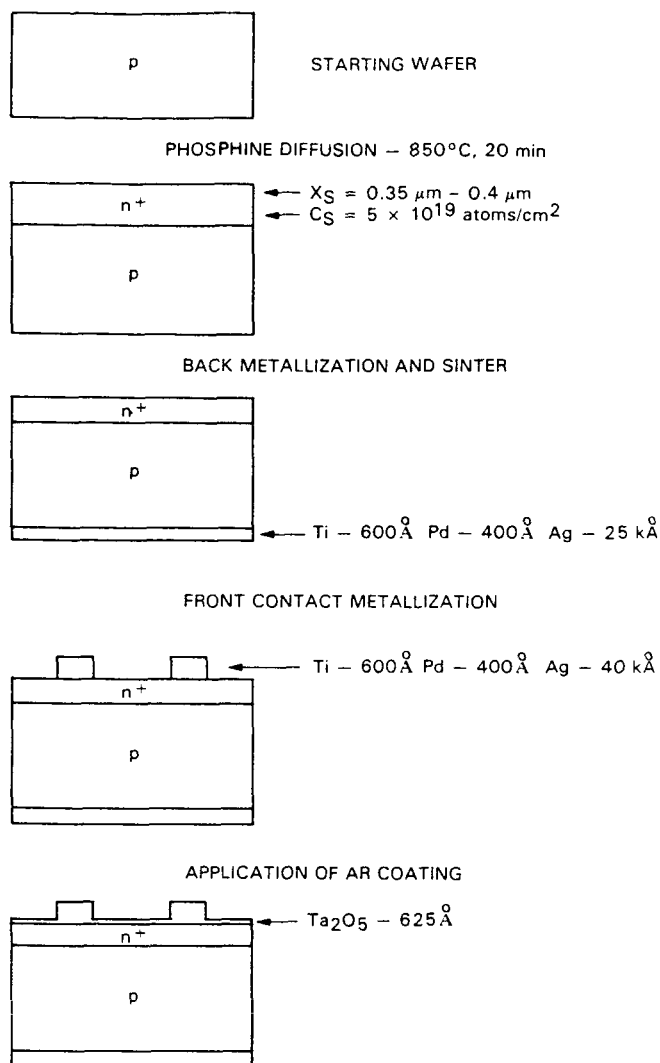


Figure 19. Baseline Process Sequence

$\text{Al}_2\text{O}_3$  was developed. It essentially is the same as the double-layer coatings used by the space PV industry. The  $\text{TiO}_x$  is applied, however, in a manner that differs from that used in the space industry. Typically,  $\text{TiO}_x$  is evaporated from  $\text{TiO}_x$  evaporation material. In the JPL process, the evaporation material is pure titanium metal that is evaporated in an oxygen-rich atmosphere. This yields coatings with refractive indices very close to that of  $\text{TiO}_2$ . The largest increase in current that has been achieved to date with this AR coating is 52%, which is close to the theoretical maximum. With these processing changes, solar cells processed on 1 to 2  $\Omega\text{-cm}$  Cz substrates resulted in 14% efficiency compared to values of 12% for cells fabricated with the baseline process (Reference 64).

To further improve cell voltages, lower resistivity materials were examined. As a result of the material and processing changes, cells processed from 0.15  $\Omega\text{-cm}$  material regularly achieved efficiencies of 17 to 17.5%, with  $V_{OC}$  of 640 mV and  $I_{SC}$  of 33.5 mA/cm<sup>2</sup>. To gain even further improvement in  $V_{OC}$  and  $I_{SC}$ , the front contact system was redesigned to lower the contact shadowing area from 4 to 2.5% and a texture etch was used to further reduce surface reflection and improve light-coupling by the cell. This has resulted in cell efficiencies as high as 20.1% for 4 cm<sup>2</sup> cells. These are the highest efficiency cells made at JPL to date, and represent a greater than 65% improvement over the earlier baseline cells.

As part of the cell improvement investigations, surface passivation was examined by growing thin ( $<100 \text{ \AA}$ ) thermal oxides over the front surface. It was found that comparable voltages could be obtained, however, with only the previously described  $\text{TiO}_x\text{-Al}_2\text{O}_3$  AR coating process. Table 8 summarizes results obtained for cells passivated with thermal oxides and with the double-layer  $\text{TiO}_x\text{-Al}_2\text{O}_3$  AR coating. This double-layer coating

Table 8. Comparison of the Light I-V Data of the Silicon Solar Cells Passivated by  $\text{SiO}_2$  and  $\text{TiO}_x/\text{Al}_2\text{O}_3$

Cell	Remarks	Sintered in $\text{H}_2$	$V_{OC}$ , mV	$J_{SC}$ , mA/cm <sup>2</sup>	Fill Factor	Efficiency, %	$J_{OE} \times 10^{13}$ A/cm <sup>2</sup>
1-a	No AR No $\text{SiO}_2$	No	605	22.3	0.79	10.7	12.3
1-b	AR No $\text{SiO}_2$	No	625	26.9	0.79	13.3	6.6
1-c	AR No $\text{SiO}_2$	Yes	646	33.3	0.81	17.5	3.2
2-a	No AR with $\text{SiO}_2$	No	627	22.4	0.79	11.1	4.8
2-b	AR with $\text{SiO}_2$	No	627	25.4	0.78	12.5	5.6
2-c	AR with $\text{SiO}_2$	Yes	643	31.9	0.81	16.6	3.6

technique has three advantages over the thermal oxide passivation technique: (1) the high-temperature thermal oxide process, which can adversely affect overall cell performance, is eliminated; (2) two process steps can be combined into one, simplifying overall processing; and (3) optical absorption losses are reduced by eliminating the oxide layer.

In 1984, SERI awarded a contract to JPL to develop dot junction silicon solar cells. The basic concept was that open-circuit voltage could be increased by reducing the emitter contribution to the reverse saturation current. It was proposed that this could be accomplished by limiting the total junction area. To achieve this, the  $n^+$  diffusion was limited to small areas or "dots" on the surface of the cell. The individual junctions were then interconnected by a metal contact grid. A model was developed in parallel with the processing work. Results of the model analyses are shown in Figure 20 (References 65 and 66).

As shown in Figure 20,  $V_{OC}$  increases as the ratio of junction to total cell area is reduced. Unfortunately, there is a simultaneous drop in current caused by the loss of photogenerated carriers before they can be collected at the junction. This indicates the bulk diffusion length would have to be much greater than the distance between the dots, and the surface between the dots must be very well passivated to obtain the full potential of this solar cell. Reduction of the dot spacing leads to problems with photolithography and increased metal coverage. A summary of solar cells made from FZ and Cz materials is shown in Table 9. The data corroborate the model as  $V_{OC}$  is increased for cells with reduced junction areas when compared with cells that have junctions covering the entire surface. There also is a decrease in  $I_{SC}$  for cells with reduced junction areas.

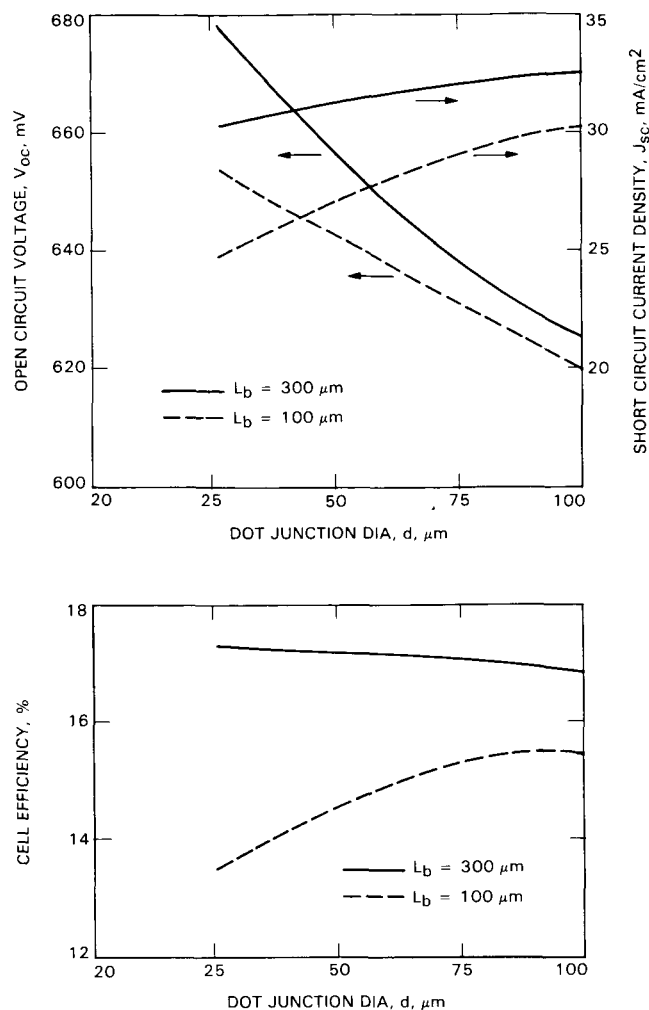


Figure 20. Calculated Solar Cell Parameters for Dot Junctions with 100- $\mu m$  Separation

Table 9. Dot Junction Solar-Cell Results and Corresponding Efficiency

Cell	Cell Configuration <sup>a</sup>	$V_{OC}$ , mV	$J_{SC}$ , mA	Fill Factor	Efficiency, <sup>b</sup> %	Junction/Area Ratio, %
036-1-1	282-50	585	30.5	0.568	10.24	2.5
036-1-2		594	31.5	0.554	10.37	2.5
036-1-3		590	30.9	0.580	10.57	2.5
036-0-4		597	31.4	0.588	11.02	2.5
036-2-1	141-50	585	28.9	0.689	11.66	10.0
036-2-2		548	29.0	0.565	8.97	10.0
036-2-3		531	29.8	0.561	8.87	10.0
036-2-4		577	29.4	0.679	11.53	10.0

<sup>a</sup>Refer to dot separation S and dot diameter d in microns, respectively, for 282-50, etc.

<sup>b</sup>Cells are 2 x 2 cm on 1 to 2  $\Omega$ -cm FZ substrates. Measurements made at 25 °C and 100 mW/cm<sup>2</sup>.

## G. PRESENT STATUS

Based on results to date, it seems there are several viable approaches to achieve a 20% conversion efficiency for silicon solar cells. It also is apparent that sophisticated processing will be required and that work must be continued to reduce these processes to practice. Once this has been accomplished, both the dot contact and floating emitter concepts should be revisited. The use of both thinner and lower resistivity material should be emphasized in any future work. A more thorough understanding of the mechanism associated with the passivating property of certain AR coatings is required to fully exploit this process in advanced cell-concept fabrication schemes. Dendritic web has been demonstrated to be the sheet material with the greatest potential for high efficiency with low cost.

The achievement of laboratory solar cell efficiencies of 20% in FZ silicon and 16.9% in dendritic web suggests that 22% conversion efficiency for silicon is a realistic goal. The progress made in significantly increasing the minority carrier diffusion length in dendritic web is even more reason for optimism with respect to this sheet material. Proven processes capable of a major reduction in surface recombination velocity, coupled with the high-current densities achieved by the floating emitter cell, are additional positive signs that silicon can meet the objectives needed for low-cost terrestrial power generation.

High-temperature thermal treatments to dissolve grown-in defects and oxygen-precipitating nucleation sites were employed to prevent the occurrence of subsequent defect nucleation or lifetime-degrading processes.

An advanced solar cell laboratory was established at JPL and was used to evaluate various types of sheet silicon as well as to produce advanced solar cells. Devices with AM1 efficiency >20% were produced and several advanced individual process steps were developed. Similar studies directed at specific goals were conducted by several contractors including Westinghouse (web-dendrite) and ASEC (various sheets and floating emitter cells).

The efforts in this sub-task, although complete and successful in themselves, are of types that are never completed. Not only does the quality of the base silicon sheet continue to change with time, but new process steps and concepts are developed and new cell designs are proposed and proven. The interplay of all of these factors produces a multi-dimensional array of possible high-efficiency approaches. Although modeling and understanding greatly reduce the number of choices to be explored, the remaining number is still substantial.

## H. KEY ACCOMPLISHMENTS

Key accomplishments are:

- (1) Specific cell processes and designs for solar cells made of dendritic web silicon were conceived, developed, and applied. Web cell efficiency of 16.9% was achieved.

- (2) A unique floating emitter cell design was evaluated. Although its proposed advantages were not proven, initial results were encouraging.
- (3) The performance of a variety of unusual silicon sheets was evaluated and compared using baseline methods. Improvement in efficiency in these sheet cell efficiencies after optimized cell processing was determined.
- (4) Rapid temperature processes have been evaluated and are promising for dissolving grown-in defects and nucleation sites, for oxygen precipitation, and for rapid junction actuation following ion implantation.
- (5) A combined double-layer AR coating with surface passivating properties was developed.
- (6) State-of-the-art solar cell facilities were established at JPL to evaluate cells made from various sheet materials on an ongoing basis. These facilities ultimately produced a 20% (AM1) 4 cm<sup>2</sup> cell using FZ silicon.
- (7) A dot contact cell was proposed and developed. Several experimental limitations, however, prevented evaluation of its full potential.

## I. FUTURE NEEDS

Future needs consist of:

- (1) Periodic reassessments of the performance capabilities of unusual silicon sheets with cost potential for terrestrial photovoltaics.
- (2) Assessment of advances and new concepts in control of minority carrier losses. This includes bulk passivation, surface passivation, and contact passivation.
- (3) Development and proof-of-concept of process sequences that incorporate old and new individual steps. This will lead to continual advances in the demonstrated efficiency of crystalline silicon photovoltaics. Special attention should be paid to the impact of choice of specific types of silicon sheet.
- (4) Continual evaluation of the interplay between sheet quality and characteristics, solar cell designs, and process steps and sequences.
- (5) Development of new cell designs that have become possible through better control of losses. Methods to control metal contact losses, for example, would permit designers to consider different contact configurations.

## SECTION V

# Modeling and Measurements

### A. INTRODUCTION

To explore means to approach the theoretical limit of silicon solar cell efficiency, many cell designs need to be analyzed and sensitivity analyses performed to understand the cells' potential. Because experimental evaluation of innumerable alternatives is not practical, the chosen approach is analytical evaluation by numerical modeling. For the numerical model to be accurate, the physics of the device should be correctly represented, the phenomenological relationships of design parameters should be correctly accounted for, and the data input to the numerical model should be accurate. Because the evaluation results obtained by the modeling approach are only as accurate as the data used as input to the model, the correct measurement of the data used in the model is as important as the model itself. The research effort under this sub-task dealing with high-efficiency cells, therefore, was directed toward both the establishment of an accurate numerical analysis model for cell-design evaluation and the improvement of the measurement techniques used to acquire reliable data.

A state-of-the-art silicon solar cell performance-evaluation model was available in the public domain and was procured and made functional at JPL. This model [Solar Cell Analysis Program in One Dimension (SCAP1D) from Purdue University] was used as a primary tool in the evaluation of several new design concepts and in the performance of sensitivity analyses. The in-house research effort at JPL has resulted in several reports dealing with high-efficiency silicon solar cell designs, in identification of key parameters limiting the cell efficiency, and in sensitivity analysis.

When the numerical model is used extensively, the computer cost of using the modeling technique becomes an important issue in cost effectiveness of this approach. A research effort at Research Triangle Institute (RTI) was directed toward development of a comprehensive silicon solar cell evaluation model in one dimension with an emphasis on making the computer program use less central processing unit (CPU) run-time. RTI used a novel solution technique to achieve the objective of a decreased use of the CPU.

The simulation models mentioned above are useful in evaluating the performance of a cell with a given design. The program has to be run repeatedly with each and every variation of the design data set to perform sensitivity analysis. There is no mechanism to optimally modify the design parameters to obtain a best design. A brute force method of evaluating all permutations and combinations of many parameters would be prohibitively expensive. A research effort at UCLA was directed toward developing a code to

optimally vary the design parameters simultaneously and suggest a best design. The code developed at UCLA serves as a front end to a numerical simulation model. The optimization code uses the simulation model as a tool for evaluating the impact of parameter variations internally, and then automatically modifies the parameters optimally until the best design is identified.

The two important input parameters to the above simulation and optimization models are: (1) minority carrier lifetime, and (2) recombination velocities at the front and back surfaces. These parameters directly affect the recombination losses occurring at various regions of the cell, namely, at the front surface, emitter, junction, bulk, and at the back surface. Many research efforts, directed toward development of new and improved techniques of measurement of these and related parameters, are described below.

The research effort at the University of Florida was directed toward developing measurement techniques that accurately measured recombination in various regions of the cell. Although the measurement of recombination properties is difficult, it is important to the understanding of the factors that ultimately limit silicon solar cell performance.

A research effort at University of Southern California (USC) explored the applicability of laser-calorimetric spectroscopy to study deep-level impurities in silicon. These impurities, in turn, will affect the minority carrier lifetime (or diffusion length). The advantage of this method is that it is free from electric field effects such as those used in photoconductivity studies. When the spectroscopic measurements were made, difficulty was encountered in obtaining results for the high-resistivity samples doped with a deep-level impurity of a simple level structure, such as Si:Au.

Research was carried out at the University of Pennsylvania to identify, develop, and analyze useful techniques to measure both bulk recombination rates in all regions and surface recombination velocities of high-efficiency silicon solar cells. Two methods have been identified of selective measurement in multiple layers. One method, Absolute Spectral Light Beam Induced Current (ASLBIC), measures spectral response at selected wavelengths, specifically short wavelengths. Another method, Modulated Light Measurement (MLM), measures the phase shift of currents induced by two AC-modulated light beams each with a different wavelength (penetration depths).

Research efforts at JPL in the area of device measurements included: (1) EBIC characterization of solar cells using a chopped scanning electron microscope beam, (2) EBIC measurements of minority

carrier recombination in the emitter region and at the front surfaces, and (3) measurement of minority carrier lifetime in silicon sheets. A highly sensitive microwave reflection measuring system was designed and built at JPL. Work included efforts to formulate an adequate analysis method to extract quantitative results from experimental data on photoconductive decay. This would allow an estimation of minority carrier lifetime and surface recombination velocity.

All the above studies are described in greater detail in the following sections discussing the individual research activities.

#### B. CPU-EFFICIENT DEVICE MODELING CODE: RESEARCH TRIANGLE INSTITUTE

This effort concentrated on development of a "Comprehensive Silicon Solar Cell Modeling Code." The emphasis was to develop a computer code that would be less expensive to run with a set of design data for a silicon solar cell, compared to that of conventional models that use numerical integration (NI) methods to solve the differential equations that represent the device. In this study, a new method was developed that has been used to simulate the characteristics of semiconductor devices.

In this new method, the set of transport equations is applied to each mesh point, and (through a judicious selection of mesh-point distribution) a relatively accurate closed-form analytical solution is obtained at the assigned mesh point. Application of the boundary conditions to an  $n$ -mesh point field results in  $2n$ -equations that require simultaneous solution. This solution is manifested through the determination of the  $2n$ -constants of integration where each closed-form solution, representing a mesh point, contains two constants of integration. A solar cell transport solution is represented by the complete set of constants obtained in the  $n$  and  $p$  regions. As a result, the complete set of closed-form functions describes the behavior of the photoexcited carrier concentrations for a continuum of  $x$  values in the  $n$  and  $p$  regions. The photoexcited carrier relationships are used to obtain the current-voltage relationship from which are determined the maximum power point and conversion efficiency. Effects of temperature, solar concentration phenomena, submodel parameters, and structure parameters may be studied using this program as a tool. This program is named SICELL.

SICELL is a one-dimensional silicon solar cell analysis program. A model was developed that describes the distribution that establishes a built-in field. The method may be used to calculate built-in fields in generalized cases. Other salient features of this program are as follows: Boltzmann and Fletcher boundary relationships are corrected to account for the net charge distribution in quasi-neutral regions. Phenomena submodels that are incorporated in the simulation program include: (1) lattice, ionized impurity, and carrier-carrier scattering contributions to

mobilities and diffusivities; (2) diffusivity dependency on quasi-Fermi levels; (3) band-to-band Auger, trap-assisted Auger, and SRH recombination processes; (4) oxide-charged insulated surface layers; (5) built-in electric fields under non-equilibrium injection levels; and (6) high solar concentrations and nondegenerate and degenerate contributions to the absorption curve.

The optimum grid point separation is determined. Saturation and depletion region current contributions to dark current are used to determine the equivalent saturation current and diode exponential factor from which the equivalent diode relationship is obtained. A subtraction method is used to obtain the spectral response. Short-circuit currents are determined using the full spectrum and one in which the flux is centered about any wavelength, ( $\lambda_0$ ). The latter is subtracted from the full spectrum. The difference between the two  $I_{SC}$ 's is used to obtain the spectral response at  $\lambda_0$ . This may be repeated for as many  $\lambda_0$ 's as required.

Although this method shares similarities with some aspects of NI methods, it differs markedly in other aspects. Abbreviated forms of analytical relationships, representing the solution of solar cell transport equations obtained using this new method, are presented in the final RTI report (Reference 67). Also discussed in this report are: (1) similarities and differences between the NI and the new methods, (2) recently reported phenomenological submodels that are used in the new simulation program, (3) other phenomena submodels that have been developed in this program, and (4) the operating characteristics of the simulation program that are supported by results obtained from simulations. Validation studies included in this report show the simulation accuracy is in the range of 0.08 to 3.6% for 27 experimental data points over the temperature range of 300 to 421 K.

A copy of the SICELL program was received at JPL and was successfully installed on the GPVAX computer system.

#### C. OPTIMIZATION METHODS FOR SOLAR CELL NUMERICAL MODELS: UNIVERSITY OF CALIFORNIA, LOS ANGELES

The efforts at UCLA were directed toward developing a comprehensive silicon solar cell design optimization model and a companion computer program. Using SCAP1D as a basic tool for evaluating the performance of a given solar cell design, an attempt was made to develop an optimization code in which the design parameters are varied simultaneously in an optimal fashion. The best design is suggested by the program for the given technology limited parameters like bulk lifetimes and surface recombination velocities ( $\tau$ , SF, and SB).

The objective function of the program is to maximize the solar cell efficiency. The decision variables considered are: cell thickness, front junction depth, back junction depth, front surface doping concentration, bulk doping, and back surface concentration.

Given the values for SF, SB, and  $\tau$ , the program will automatically determine the optimal values for these parameters.

The emitter profile options considered by the optimization program are the complementary error function, a step function, and a parabola. Consideration of a gaussian profile and defining the profile point-by-point could also be included. The possibility of varying the objective function suitably, so that the program automatically would decide the design parameters for achieving a cell efficiency of a given value, was explored but not completed. The other variation of the objective function that was considered was the identification of the parameter values for series resistance, etc., to match the experimental I-V curve of an experimental design. The preliminary results of this effort are very promising.

#### D. MEASUREMENT OF RECOMBINATION LIFETIME AND SURFACE RECOMBINATION VELOCITY: UNIVERSITY OF FLORIDA

An improved  $I_{SC}$  decay technique was developed to measure both the recombination time in the base region of silicon solar cell samples and the back surface recombination velocity. The improved technique was called the ESCCD method. Figure 21 shows a schematic diagram of the measuring circuitry of the ESCCD technique (Reference 68). The technique simultaneously measures the carrier lifetime in the bulk of the cell and the recombination velocity at the back interface with the contact. With this method, a forward bias is applied to the solar cell to set up a steady-state condition. Then, by rapidly applying a zero bias across an extremely small resistance, a short circuit is obtained. This causes the p/n junction region and the base and emitter regions to discharge. If the discharge times related to the junction and emitter regions are much smaller than the time related to the base region, the lifetime and recombination velocity can be determined.

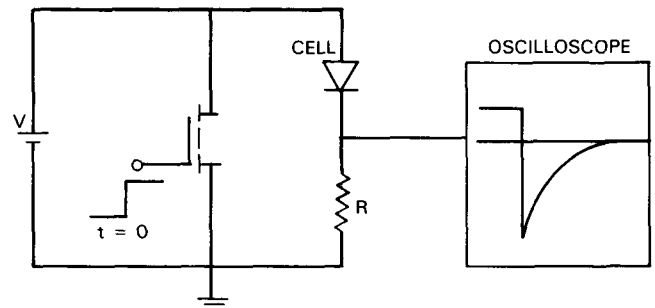
According to the University of Florida, one of the main advantages of this technique is that the discharge time of the p/n junction (on the order of  $10^{-11}$  s) is much less than the discharge times associated with either the emitter or the base. This makes it very easy to interpret the observed transient current. The ESCCD method is simple, fast, and less expensive than other methods used to measure other key solar cell parameters.

In the final phase of this study, work was done on the elusive task of measurement of front surface recombination velocity ( $S_p$ ) in the thin highly doped emitter region. A method was successfully demonstrated on small area n-p-n transistors. The approach included the following steps:

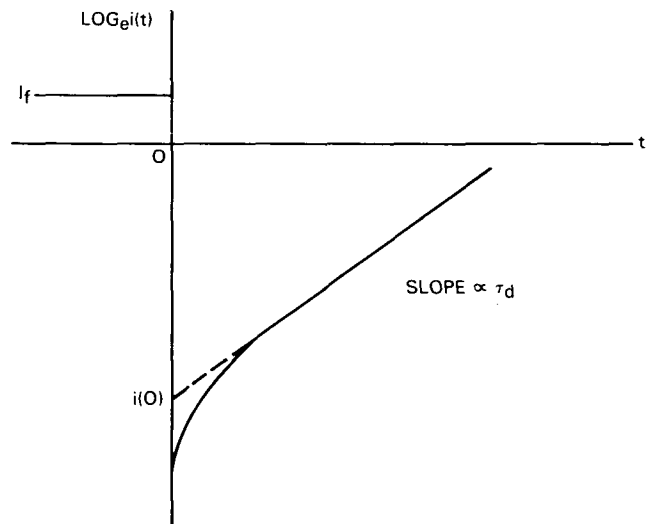
- (1) Obtain the reverse saturation current ( $J_0$ ) from the dark I-V characteristics. Deduct the base component ( $J_b$ ), obtained after measurement of

$\epsilon_n$  and  $S_{eff}$  (technique described in Section II.E.) to obtain the emitter component ( $J_e$ ).

- (2)  $J_e$  is a function of  $D_p/N_{eff}$  and  $\tau_p$ , where  $D_p$  and  $\tau_p$  are the minority carrier diffusivity and lifetime, respectively, and  $N_{eff}$  is the effective carrier density after accounting for heavy doping effects.
- (3) Values of  $D_p/N_{eff}$  and  $\tau_p$  are now available (see Section II.F.). Literature values of  $D_p$  represent the primary uncertainty in this measurement.



(a)



(b)

Figure 21. (a) Electronic Circuit Used in the ESCCD Method, (b) Schematic Illustration of the Current Decay Displayed on a Log Scale

#### E. CRYOGENIC LASER CALORIMETRY FOR IMPURITY ANALYSIS: UNIVERSITY OF SOUTHERN CALIFORNIA

A program was conducted at USC to determine the applicability of laser-calorimetric spectroscopy to the study of deep-level impurities in silicon. There were three parts to the effort: (1) to investigate critical considerations in the application of calorimetric methods to deep-level spectroscopy, (2) to design and build a

cryogenic calorimeter for spectroscopic measurements, and (3) to carry out calorimetric measurements of optical absorption in silicon.

The motivation for using calorimetry is its demonstrated high sensitivity that allows measurement of relative absorption as small as ten parts per million. Cryogenic operation was chosen to control thermal ionization of the deep impurity levels, and to measure the temperature dependence of level energy. An additional advantage of calorimetry is freedom from electric field effects such as those present in photoconductivity studies.

The primary consideration for successful optical absorption spectroscopy of deep-level impurities is that deep-impurity absorption dominates all other optical absorption mechanisms. Possible sources of background absorption include free carrier absorption, absorption by precipitates and inclusions, two photon band-to-band absorption (pulsed sources only), and multiple-phonon band-to-band absorption. The requirement of low free-carrier absorption is especially important; fundamental studies of deep-level impurities are restricted to high-resistivity silicon. The impurity level energy is determined by measuring the photoabsorption cross section as a function of photon energy, and then fitting the data using a line-shape model. Because of coupling to the lattice, the level energy cannot be accurately determined merely by measuring the upper part of the absorption shoulder. It is necessary to follow the curve down as low as possible in the steep region near the threshold energy.

The primary apparatus considerations were found to be optical scattering, and the requirement of a tunable continuous wave (CW) near-IR laser source. Optical scattering causes erroneous heating signals and scattering is especially troublesome at cryogenic temperatures because of the formation of frost on the sample if there is any residual water vapor. It also was found that Raman-shifted radiation from a Q-switched Nd:YAG laser resulted in an undesirable intensity dependence of the optical absorption. Consequently, CW laser sources are preferable. Efforts were concluded when it was realized that major experimental problems remained.

#### F. LOSS MEASUREMENT IN HEAVILY DOPED EMITTERS: UNIVERSITY OF PENNSYLVANIA

Research efforts were conducted to identify, develop, and analyze useful techniques to measure bulk recombination rates, surface recombination rates, and surface recombination velocities in all regions of a high-efficiency solar cell. Of the two methods identified for measuring selectively in multiple layers, ASLBIC measures spectral response at selected wavelengths (primarily at very short wavelengths), and MLM measures the phase shift of currents induced by two AC-modulated light beams with different wavelengths (penetration depths). Both techniques require computer analysis using modeled cell structures and

separately measured doping distributions. Usually, spreading resistance measurements are analyzed to provide the doping distribution data.

The ASLBIC technique does not produce a single answer. Rather, the best answer is determined from the uniqueness of diffusion length: surface loss pairs that fit the spectral data. The thinness of most device emitters limits the usable wavelengths. Figure 22 is an example of a contour plot of the root-mean-square (rms) error of the fit to the data for a specific example for a wide range of lifetime and surface recombination velocity pairs. The thinness of the emitter limited the useful wavelengths to 350, 375, and 400  $\mu$ , with absorption coefficients of  $1.65 \times 10^6$ ,  $0.68 \times 10^5$ , and  $8.2 \times 10^4 \text{ cm}^{-1}$ , respectively. To prepare Figure 22, roughly 80 individual computer runs were necessary. This research addressed the areas of refinement and automation of the DC measurement of ASLBIC, and the theoretical evaluation of dynamic measurements in complex device structures.

ASLBIC measurements require ultraviolet (UV) illumination, specifically in shallow emitters of current cell designs. To improve measurement accuracy, the system was equipped with interference filters to transmit only the various lines of the mercury (Hg) light source for higher spectral purity. This produced repeatability of the measurement of better than half of one percent. Software was implemented to completely sample the parameter space of the unknown with numerous  $s$  and  $\tau$  pairs. The results are displayed three-dimensionally showing the regions of good fit of the model to the experimental data. Also, a Simplex minimization algorithm was available to find the best fit numerically (Reference 69).

#### G. DEVICE MODELING: JET PROPULSION LABORATORY

New ideas of silicon solar cell designs and their potential for improved performance can easily be evaluated by an accurate computer simulation model. Compared to an experimental approach, analytical evaluation techniques can quickly and cost-effectively evaluate many scenarios. Parametric analysis and sensitivity analysis studies are effectively performed by computer simulation.

A Solar-Cell Efficiency Estimation Methodology and Analysis (SEEMA) scheme was established at JPL. It used an existing state-of-the-art silicon solar cell performance evaluation model, SCAP1D. This program was available in the public domain and was procured and installed on the UNIVAC 1180-F computer system at JPL.

Under the SEEMA scheme, the performance of a given silicon solar cell design was evaluated using the SCAP1D program as the basic tool. The one-dimensional process simulation program SUPREM-II formed the basic tool for simulating processes such as diffusion, etc. These analytical tools were used independently and/or in combination for cell design evaluation and sensitivity analysis studies.

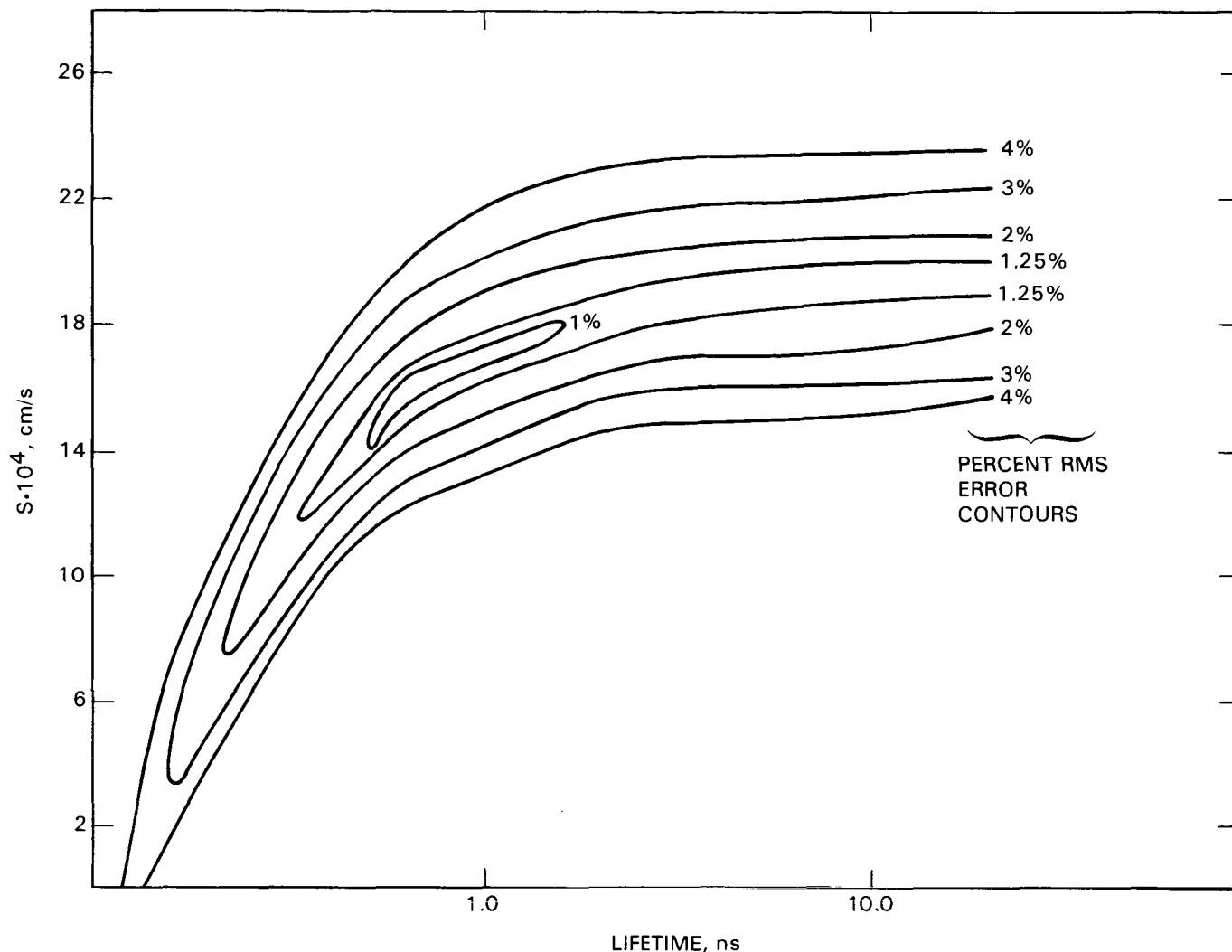


Figure 22. Contour Plot of the rms Data (the ASLBIC Method)

For the one-dimensional analysis by SCAP1D, a solar cell is divided into several nonuniform grid points along the cell thickness, and the set of three differential equations are solved numerically by a conventional finite difference technique. The solution gives the values of hole concentration ( $p$ ), electron concentration ( $n$ ), and electrostatic potential ( $v$ ) as a function of position along the cell thickness. Knowing  $p$ ,  $n$ , and  $v$ , the cell performance parameters  $V_{OC}$ ,  $I_{SC}$ , and  $FF$  can be computed. The doping and geometric details of the silicon solar cell are specified by the user. The minority carrier lifetimes and surface recombination velocities are also specified. The user has the choice of considering Auger recombination and/or bandgap narrowing. Any of the design parameters can be altered individually or collectively for performing sensitivity analysis studies. Details of the SCAP1D program are described (Reference 70) with an example of sensitivity analysis of an experimental high-efficiency silicon solar cell design.

The following is reproduced from the Stanford University Software Distribution Center Directory, October 15, 1983 edition:

"SUPREM-II simulates the processing of silicon semiconductor devices along a one-dimensional axis perpendicular to the surface of the silicon wafer. Most commonly used processing steps are handled by the program such as high-temperature diffusion under both inert and oxidizing ambients, gas source pre-deposition, ion implantation, epitaxial growth, etching, and deposition of doped or undoped silicon dioxide. A numerical solution to the diffusion of up to four impurities is implemented that includes high concentration of oxygen-enhanced diffusion (OED) effects. The oxidation of silicon is modeled according to the Deal-Grove equation, modified to account for high-pressure conditions and high-impurity concentrations at the oxidizing interface. The input commands are input for a user-generated file and are designed to resemble a list of process specifications. Output of resulting impurity distributions can be in either printed or plotted form. Information about junction depths, sheet resistivities, and threshold voltages may be obtained."

A critical part of such modeling is the confirmation of the validity of the predictions. Subsequent to this validation, the models then can effectively be used to determine the effect of parametric variation on device performance. To compare model prediction with experiment, an experimental high-efficiency cell design was considered with a measured efficiency of 18.7%, under illumination of 100 mW/cm<sup>2</sup> at 28°C as published in the literature (Reference 71). It was shown that SCAP1D analysis results agree with the experimental results.

Sensitivity analyses were performed with respect to doping profile, front-surface recombination velocity, minority carrier lifetime, cell thickness, and back surface field. Results of the analysis indicate that with the best possible combination of parameter values for SF,  $\tau$ , and cell thickness, the maximum efficiency achievable is about 20%. It may be noted that the parameters are varied one at a time. True optimization requires simultaneous improvement of all parameters (Reference 72).

Innovative cell design features then were incorporated in this cell to further reduce losses. The schematic of this design is shown in Figure 23. Bulk recombination losses are reduced by making the cell thin (100  $\mu$ m). A BSR compensates for the optical absorption losses caused by cell thinness. Both surfaces (front and back) are considered to be passivated by a silicon dioxide layer to reduce surface recombination velocity, front (SF) and surface recombination velocity, back (SB). Recombination losses under the contact are reduced by providing a heavily doped polysilicon layer between the metal and the silicon surface.

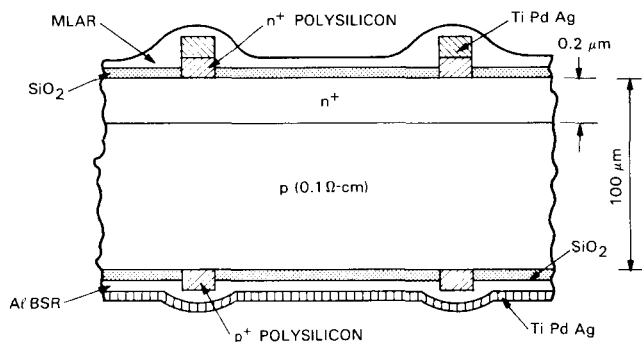


Figure 23. Schematic Cross-Section of a Passivated Thin Silicon Solar Cell Design

The new cell design is shown to be capable of achieving 20% cell efficiency with practically achievable values for  $SF = SB = 1000$  cm/s and  $\tau = 20$   $\mu$ s. Figure 24 shows the sensitivity of cell efficiency as a function of cell thickness with minority carrier lifetime as a parameter. For achieving cell efficiency greater than 20%, substantial reduction in SF and SB and considerable increase in bulk lifetime are essential. Advancement of the state-of-the-art technology is required to realize these values. Details of this study are presented elsewhere (see Reference 72).

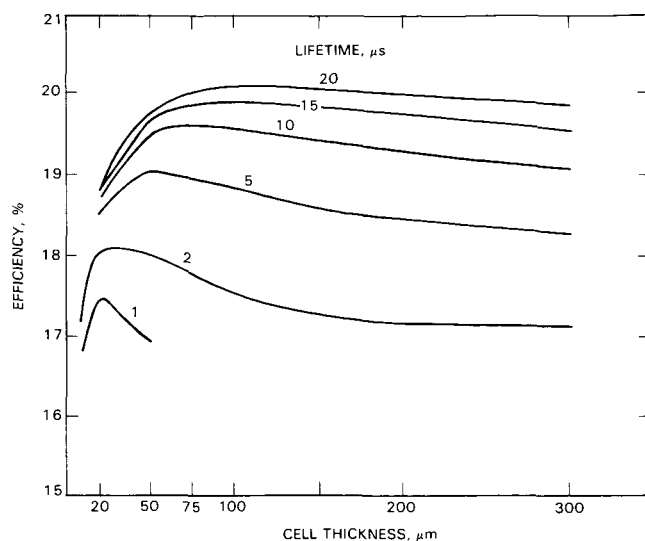


Figure 24. Sensitivity of Efficiency of Solar-Cell Thickness for Various Minority Carrier Lifetime Values

Additional study was performed to investigate the impact of practical barriers such as heavy doping effects, Auger recombination, band-gap narrowing, surface recombination, and shadowing on high-efficiency silicon solar cell performance. An ideal case, considering only radiative recombination losses and ignoring technology limited and fundamental losses, is evaluated to be around 29%. This is comparable to the detailed balance limit maximum efficiency of a p-n junction solar cell of 30%, estimated by Shockley and Queisser (Reference 73). The heavy doping effects, and realizable values of SF and SB and shadowing, are considered in succession and their influence on reducing the cell efficiency is evaluated and quantified. It is shown that these practical barriers cause the cell efficiency to fall to the experimentally achieved value of 19 to 20%. Improvement in  $V_{OC}$  is required to achieve cell efficiency greater than 20%. Increase in value of lifetime reduces reverse saturation current and hence improves  $V_{OC}$ . The impact of practical barriers is shown schematically in Figure 25. The effects of shadowing, SF, and SB is shown in Figure 26. These figures indicate that cell efficiency greater than 20% requires SF and SB to be reduced to 100 cm/s, and  $\tau$  to be increased to 250  $\mu$ s. Other results of this research study are available (References 74 through 77).

#### H. ELECTRON-BEAM INDUCED CURRENT CHARACTERIZATION OF SOLAR CELLS: JET PROPULSION LABORATORY

The EBIC technique has been widely used to measure lattice defect distribution and transport properties of semiconductors. An in-house research task at JPL applied this technique to measure the EBIC signal as a function of distance from the junction with the beam incident on a freshly cleaved (111) surface of silicon solar cells (Reference 78). The results have shown that the effective recombination velocity of the

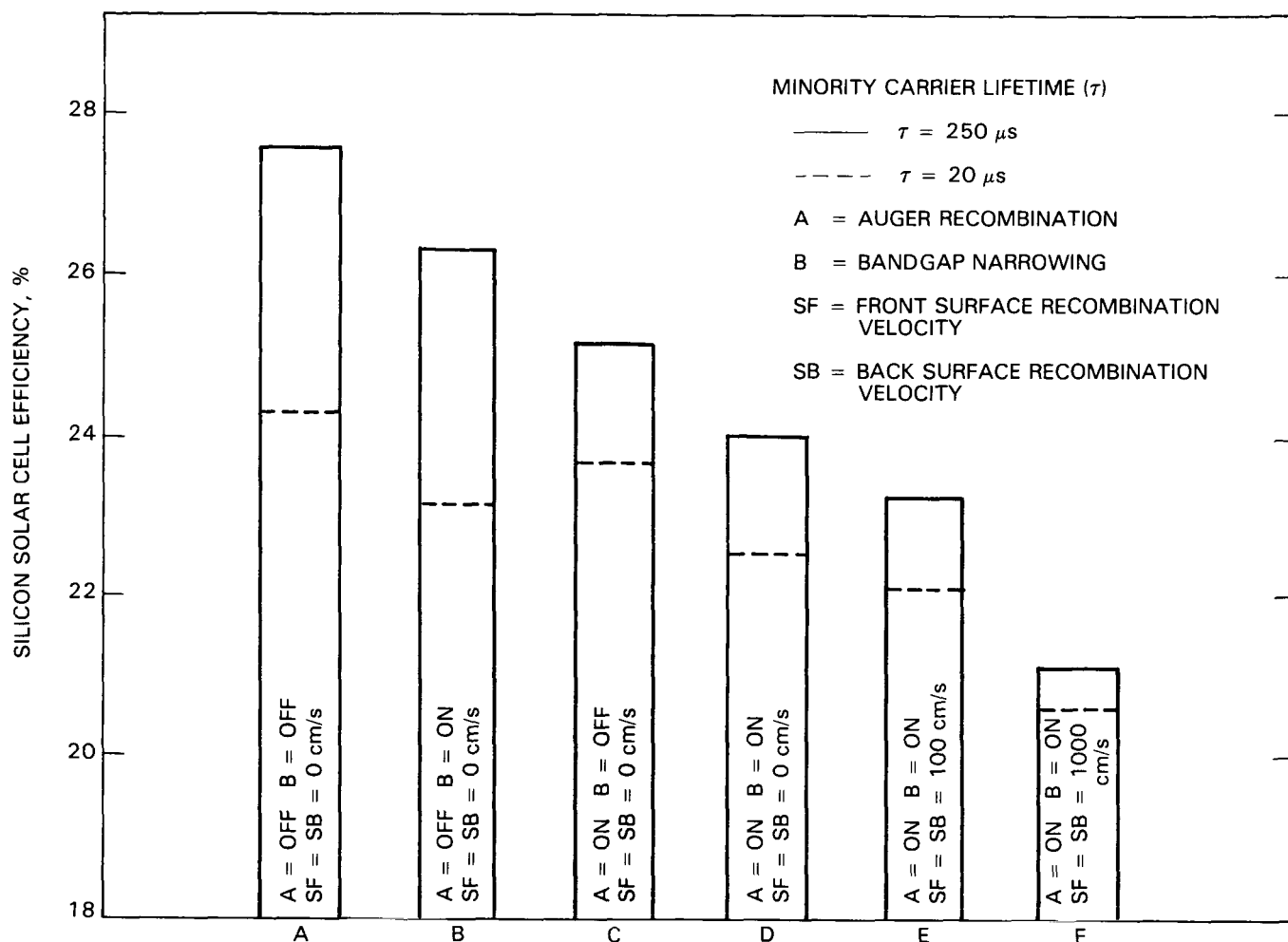


Figure 25. Impact of Practical Barriers on Silicon Cell Performance

low-high junction forming the BSF of silicon solar cells, in addition to the diffusion length and the surface recombination velocity of the surface perpendicular to both the p-n and low-high junctions, can be determined from the data provided by a single EBIC scan. The measured value of the surface recombination velocity in the samples with Al-paste alloy back contacts always was found to be smaller than those of samples with evaporated Al alloy contacts. This observation agrees well with a known fact from solar cell fabrication that the BSF cells with Al-paste alloy contacts are better than those with evaporated Al alloy contacts. This study provides an experimental tool to study the BSF.

A related study for the BSF was conducted at JPL in cooperation with the University of Florida. The first experimental determination and interpretation of the voltage across a high-low junction was obtained as a function of the voltage across a nearby high-low junction (Reference 79). Several  $n^+/p/p^+$  solar cells were measured. Figure 27 shows the typical high-low voltage as a function of the applied voltage. Theoretical analysis showed agreement with these experimental results. A test structure also was proposed for the measurement of the effective surface recombination velocity at the high-low junction.

#### I. ELECTRON-BEAM INDUCED CURRENT MEASUREMENTS OF MINORITY CARRIER RECOMBINATION: JET PROPULSION LABORATORY

An in-house research program at JPL was carried out to explore the potential of the use of EBIC measurements to investigate recombination phenomena of heavily-doped emitter and junction regions of high-efficiency silicon solar cells. It has been shown that this technique is suited to the investigation of the emitter and junction regions. Even though the experimental EBIC data were collected under three-dimensional conditions, it has been shown that the solution obtained with one-dimensional numerical modeling is adequate for the EBIC data analysis (Reference 80). Bare and oxide-covered emitter surfaces were measured and compared with theory. Good agreement was obtained when a cell quality factor of 0.89 was assumed, thus suggesting that about 11 % of the generated carriers recombined in the cell depletion region. This result is similar to published data of silicon diodes with very shallow junctions. The improvement in collection efficiency when an emitter surface was covered with 100-Å-thick silicon oxide film was found to be about 27 % at 2 keV for a cell with a junction depth of 0.35  $\mu m$ .

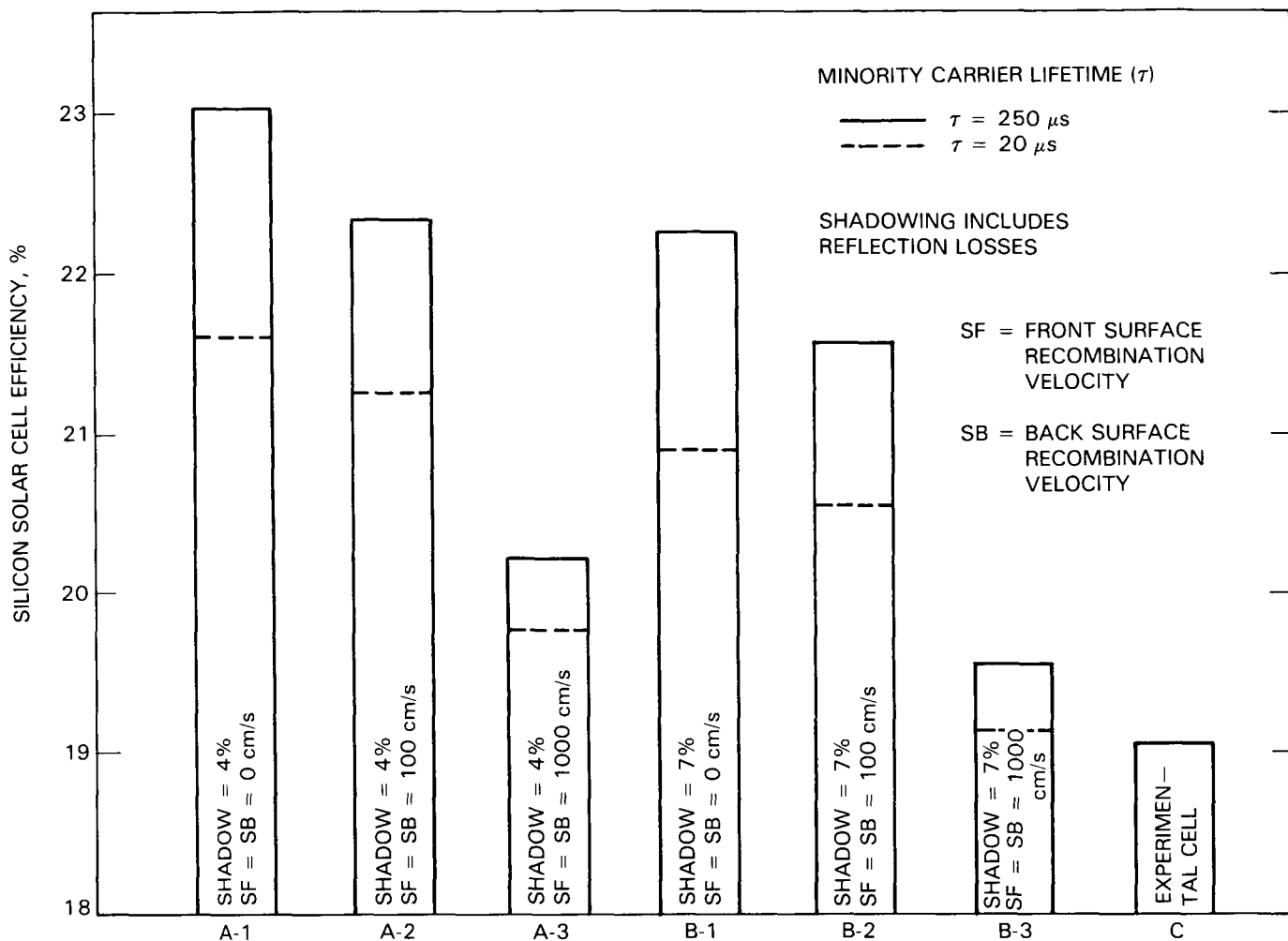


Figure 26. Impact of Shadowing and Surface Recombination Velocities on Silicon Solar Cell Performance

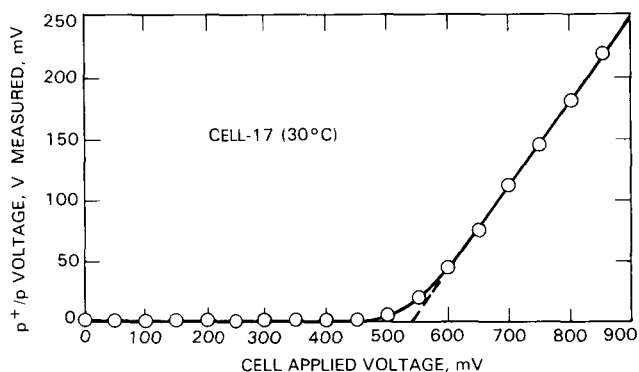


Figure 27. High-Low Junction Voltage (measured) Versus Cell Applied Voltage

#### J. MINORITY CARRIER LIFETIME IN SILICON SHEETS: JET PROPULSION LABORATORY

The measurement of minority carrier lifetime in silicon sheet materials, such as wafers and ribbons, is very important for the characterization of silicon materials for PV applications. A commonly used method, that measures the minority carrier diffusion length by using the

surface photovoltage method, suffers from experimental limitations. To develop a better method to characterize the minority carrier lifetime in silicon wafers and ribbons, in-house research has been carried out to study the applicability of microwave reflectance measurements to monitor the photoconductive decay in silicon wafers and ribbons. From the measured photoconductive decay, one can extract the information of minority carrier lifetime and surface recombination velocity (Reference 81).

A highly sensitive microwave reflectance measuring system with computer data acquisition has been designed and built at JPL. The experimental results illustrate that the microwave technique accurately can probe the decay of photogenerated minority carriers in silicon sheet materials. This decay depends on the minority carrier lifetime and surface recombination velocity. Under controlled surface conditions, one can measure bulk minority carrier lifetime in silicon sheets. With known lifetime in the bulk, the technique has been demonstrated to be an effective tool for monitoring the surface recombination velocity. Preliminary results reveal that Cz and FZ silicon wafers have small surface recombination velocities when they are freshly etched in a dilute hydrofluoric acid solution, but the recombination velocity

increases significantly when the surface is exposed to the air. The effect becomes saturated after several hours. Work is incomplete at this time to provide an adequate analysis method to extract quantitative results from experimental data.

#### K. PRESENT STATUS

In the modeling research, a one-dimensional numerical analysis model was considered to be adequate to evaluate the performance of a given silicon solar cell design for use in flat-plate solar array modules. A state-of-the-art numerical analysis code, available in the public domain, was used successfully in analyzing many high-efficiency silicon solar cell designs. A modeling effort to develop an efficient computer code with emphasis on minimum computer time (CPU) consumption per run was completed, but the efficiency of the code was not proven. Another effort developed an optimization code to be used as a front end of a simulation model to modify optimally the design parameters simultaneously until the best design is identified.

Many research efforts were directed toward the development of methods, techniques, or procedures to measure directly or indirectly the two key input parameters: the minority carrier lifetime (a measure of recombination losses in all regions of the cell) and surface recombination velocities at the front and back surfaces. Measurement techniques developed at the University of Florida yield better values for minority carrier lifetime, effective surface recombination velocity at the back surface, and the high-low junction behavior in a BSF cell. One improved technique, the electronic  $I_{SC}$  decay method, had special interest because it simultaneously measures the recombination lifetime in the base and the back surface recombination velocity.

Two methods, the ASLBIC technique and the MLM technique, have been identified by research efforts at the University of Pennsylvania to measure bulk recombination rates and surface recombination velocities.

In the area of measurement, JPL in-house research studies include: (1) EBIC characterization of solar cells using a chopped scanning electron microscope beam, (2) EBIC measurements of minority carrier recombination in the emitter region and at the front surface, and (3) study of applicability of microwave reflectance measurements to monitor the photoconductive decay in silicon wafers and ribbons to extract minority carrier lifetime and surface recombination velocity.

#### L. KEY ACCOMPLISHMENTS

Following is a summary of accomplishments:

- (1) A state-of-the-art, numerical, one-dimensional analysis model (SCAP1D) has been identified,

procured, and made functional at JPL. Several high-efficiency silicon solar cell designs and concepts have been evaluated and results published.

- (2) A novel numerical analysis code in one dimension, with emphasis on economy in computer time used per run, has been developed for evaluating the performance of a silicon solar cell of a given design.
- (3) An optimization code has been developed as a front end to the simulation model to modify the design parameters optimally until a best design is identified.
- (4) An improved  $I_{SC}$  decay method was developed that simultaneously was able to measure carrier lifetime in the bulk of a cell and recombination velocity at the back interface.
- (5) EBIC techniques were shown to be effective tools to investigate carrier recombination parameters in the bulk and at the interfaces.
- (6) Considerable progress was made in the application of the scanning laser-beam induced current (SLBIC) technique to measure diffusion length in heavily doped emitter regions.

#### M. FUTURE NEEDS

The following items have been identified for future work:

- (1) Basic modeling should be upgraded to use a two-dimensional numerical analysis model such as SCAP2D. This requires modifications to provide more efficient computer utilization.
- (2) The RTI computer program, designed to save computer time, needs to be evaluated. If this code is efficient, a similar two-dimensional code should be developed.
- (3) Improvements of all models are needed including consideration of new phenomenological relationships.
- (4) The optimization model should be used for other simulation models for both solar cells and for different materials like gallium arsenide or amorphous silicon.
- (5) Measurement techniques for key input data values should be emphasized, especially those related to minority carrier lifetime.

## SECTION VI

# Overview Status

As a result of studies and support from the High-Efficiency Device Research Task, major advances were made in all aspects of solar cell science. Because many efforts were terminated before completion much significant work remains to be done. During the active years of this Task, the conversion efficiency of crystalline-silicon solar cells advanced significantly with final devices exhibiting efficiencies greater than 22% (AM1). Although this Task cannot claim direct credit for all of this progress, many of the advances can be traced to its activities. Major accomplishments and unfinished work are summarized below.

### A. KEY ACCOMPLISHMENTS

Following is a summary of accomplishments:

- (1) Modeling techniques for solar cells were developed and proved effective for evaluation of devices.
- (2) New high-efficiency solar cells were conceived, modeled, and evaluated.
- (3) New techniques were developed to measure simultaneously minority carrier lifetime and surface recombination velocity.
- (4) Key barriers to obtain high-efficiency cells were identified and, in many cases, reduced.

### B. ADDITIONAL RESEARCH NEEDED

Although much understanding and improvement in crystalline-silicon solar cells has been accomplished because of the research in this Task, the work is far

from completed as noted in the Summary section of this report. The general nature and sources of loss mechanisms are known. What is not known is their detailed response to processing and their variation from changes in silicon sheet type, especially low-cost varieties of sheet. The studies in this Task were very active at the time of termination of the FSA Project and, in many cases, need to be completed. After completion of the FSA Project, continued U.S. Department of Energy (DOE) support for research addressing a limited number of these problems is anticipated.

Specifically needed are:

- (1) Determination of the remaining low-cost, silicon-sheet recombination mechanisms in bulk, in all layers, and at all surfaces.
- (2) Establishment of quantitative relationships between defects and recombination mechanisms.
- (3) Development of new device structures and their verification using device modeling and experiment.
- (4) Establishment of correlations among material defects, device fabrication steps, and device performance.
- (5) Characterization of defects in silicon sheets as their quality improves.
- (6) Development of cost-effective and reliable passivation techniques for bulk and surface recombination sites in appropriate forms of silicon sheet.

PRECEDING PAGE BLANK NOT FILMED

## SECTION VII

# References

For acquisition of DOE/JPL documents listed below, see Appendix A.

1. Sah, C.T., "Recombination Phenomena in High-Efficiency Silicon Solar Cells," *Proceedings of the Flat-Plate Solar Array Project Research Forum on High-Efficiency Crystalline Silicon Solar Cells*, DOE/JPL-1012-103, p. 37, 1985.
2. Sah, C.T., "High-Efficiency Crystalline Silicon Solar Cells," *Solar Cells*, October 1985.
3. Corbett, J.W., "Oxygen and Carbon-Related Defects in Silicon," *Final Report of Contract*, DOE/JPL-956989-86/01, State University of New York at Albany, 1986.
4. Wang, P.W., and Corbett, J.W., "Studies of Oxygen Thermal Donor Formation Under Stress," *Proceedings of Symposium on Oxygen, Carbon, Hydrogen, and Nitrogen in Crystalline Silicon*, Vol. 59, p. 167, Materials Research Society, Pittsburgh, Pennsylvania, 1986.
5. Borenstein, J.T., and Corbett, J.W., "A Unified Treatment of the Thermal Donor Hierarchies in Silicon and Germanium," *Proceedings of Symposium on Oxygen, Carbon, Hydrogen, and Nitrogen in Crystalline Silicon*, Vol. 59, p. 159, Materials Research Society, Pittsburgh, Pennsylvania, 1986.
6. Borenstein, J.T., Peak, D., and Corbett, J.W., "Formation Kinetics of Thermal Donors in Silicon," *Proceedings of Symposium on Oxygen, Carbon, Hydrogen, and Nitrogen in Crystalline Silicon*, Vol. 59, p. 173, Materials Research Society, Pittsburgh, Pennsylvania, 1986.
7. Goesele, U., and Ast, D.G., *Carbon, Oxygen, and Their Interaction with Intrinsic Point Defects in Solar Silicon Ribbon Materials*, Annual Report, DOE/JPL-956046-83/9, 1983.
8. Sullivan, T., and Ast, D.G., *EBIC Investigation of Hydrogenation of Crystal Defects in EFG Solar Silicon Ribbons*, Quarterly Report, DOE/JPL-956046-83/5, 1983.
9. Ast, D.G., *Electrical, Structural and Chemical Characterization of Silicon Sheet Material*, Annual Report, DOE/JPL-956046/86-1, 1986.
10. Gleichmann, R., Vaudin, M.D., and Ast, D.G., "Interactions of Twin Boundaries and Dislocations in Solar Silicon," *Phil. Mag.* Vol. A, pp. 51, 449, 1985 (also topical technical report, DOE/JPL-956046-84/10).
11. Ast, D.G., *The Structure of <110> Tilt Boundaries in Large Area Solar Silicon*, Annual Report, DOE/JPL-956046-82/5, 1982.
12. Lindholm, F.A., Liou, J.J., Neugroschel, A., and Jung, T.J., *Proc. 18th IEEE Photovoltaic Specialists Conf.*, Las Vegas, Nevada, p. 611, 1985.
13. Neugroschel, A., and Lindholm, F.A., *Appl. Phys. Letters*, Vol. 42, p. 176, 1983.
14. Park, J-S, Neugroschel, A., and Lindholm, F.A., *IEEE Transactions on Electronic Devices*, ED-33, p. 240, 1986.
15. Landsberg, P.T., Neugroschel, A., Lindholm, F.A., and Sah, C.T., "A Model for Band-Gap Shrinkage in Semiconductors with Application to Silicon," *Physics Status Solidi a*, Vol. 130, p. 285, 1985.
16. Misiakos, K., and Lindholm, F.A., *J. Applied Physics*, Vol. 58, p. 4743, 1985.
17. Misiakos, K., and Lindholm, F.A., *J. Applied Physics*, Vol. 59, p. 4091, 1986.
18. Neugroschel, A., Jung, T.J., and Lindholm, F.A., *IEEE Electron Device Letters*, EDL-6, p. 253, 1985.
19. Swanson, R.M., *Measurement of Carrier Transport and Recombination Parameters in Heavy Doped Silicon*, Final Report of Contract 957159, DOE/JPL-957159-85/1, 1985.
20. del Alamo, J., and Swanson, R.M., *Proc. 18th IEEE Photovoltaic Specialists Conf.*, Las Vegas, Nevada, p. 584, 1985.
21. del Alamo, J., Swichun, S., and Swanson, R.M., *IEEE IDEM Conf.*, Washington, D.C., p. 290, 1985.
22. Streil, D., Metzger, R.A., and Allen, F.G., *J. Appl. Phys. Letters*, Vol. 44, p. 234, 1984.
23. Sparks, P.D., Allen, F.G., and Daud, T., *Proc. 17th IEEE Photovoltaic Specialists Conf.*, Kissimmee, Florida, p. 726, 1984.
24. Fonash, S.J., *Use of Low Energy Hydrogen Ion Implants in High Efficiency Crystalline Silicon Solar Cells*, DOE/JPL 957126-TBD, The Pennsylvania State University, University Park, Pennsylvania, 1986.
25. Cheng, L.J., Dumas, K.A., Su, B.M., and Leipold, M., *J. Crystal Growth*, Vol. 70, p. 314, 1984.

PRECEDING PAGE BLANK NOT FILMED

26. Hopkins, R., Seidensticker, R., and Schruher, J., *J. Crystal Growth*, Vol. 65, p. 307, 1983.
27. Duncan, S., Seidensticker, R.G., McHugh, J.P., Hopkins, R.P., Meier, D., and Schruher, J., *Annual Report on Advanced Dendritic Web Growth Development*, DOE/JPL-955843/82/4, p. 14, 1982.
28. Cheng, L.J., "Structural Defect Characterization of Silicon Dendritic Web Ribbons," *Proceedings of the 18th Photovoltaic Specialists Conference*, p. 1084, Las Vegas, Nevada, 1985.
29. Cheng, L.J., *Proceedings of the 13th International Conference on Defects in Semiconductors*, p. 403, The Metallurgical Society of AIME, Warrendale, Pennsylvania, 1985.
30. Cheng, L.J., "Impurity Diffusion and Gettering in Semiconductors," *Materials Research Society Symposia Proceeding*, Vol. 36, p. 199, Materials Research Society, Pittsburgh, Pennsylvania, 1985.
31. Dumas, K.A., Briglio, A., and Cheng, L.J., "Annealing Effects in Low- and High-Stress Silicon Ribbons," *Proceedings of Symposium on Oxygen, Carbon, Hydrogen, and Nitrogen in Crystalline Silicon*, Vol. 59, p. 359, Materials Research Society, Pittsburgh, Pennsylvania, 1986.
32. Swimm, R.T., and Dumas, K.A., "Optical Absorption Coefficient and Minority Carrier Diffusion Length Measurements in Low-Cost Silicon Solar Cell Material," *J. Appl. Phys.* Vol. 53, p. 7502, 1982.
33. Olsen, L.C., and Addin, F.W., "Measurement and Analysis of High Efficiency Silicon MINP Solar Cells," *Solar Cells*, Vol. 17, pp. 1-11, 1986.
34. Olsen, L.C., and Addin, F.W., "Measurement and Analysis of Solar Cell Voltage and Current Characteristics," *Proceedings of the 18th IEEE Photovoltaic Specialists Conference*, p. 72, Las Vegas, Nevada, 1985.
35. Olsen, L.C., and Addin, F.W., *Investigation of Inversion-Layer Solar Cells and Carrier Lifetime Measurement*, JPL/DOE Report 955614-86/01, 1986.
36. Misiakos, K., Lindholm, F.A., and Neugroschel, A., "Solution for Continuity Equation in Planar Symmetry Cases and Assessment of Photoluminescence Decay," *J. Appl. Phys.*, Vol. 58, p. 1647, 1985.
37. Misiakos, K., and Lindholm, F.A., "Generalized Reciprocity Theorem for Semiconductor Devices," *J. Appl. Phys.*, Vol. 58, p. 4743, 1985.
38. Lindholm, F.A., and Neugroschel, A., *Heavy Doping Effects in High Efficiency Silicon Solar Cells*, JPL/DOE Report 956525-86/01, 1986.
39. Iqbal, A., and Bates, C.W., Jr., "Electron Spectroscopy Study of the Si-O Bonding and the Polarization Screening Near the Si-SiO<sub>2</sub> Interface," *Appl. Phys. Letters*, Vol. 47, No. 10, p. 1064, 1985.
40. Bates, C.W., Jr., *Interfacial Barriers in High-Efficiency Crystalline Silicon Solar Cells*, JPL/DOE Report 956960-86/1, 1986.
41. Iles, P., and Fang, P.H., *Microcrystalline Growth for Heterojunction Solar Cells*, JPL/DOE Report 956369/84-03, 1984.
42. Vasquez, R.P., Madhuker, A., Grunthaner, F.J., and Naiman, M.L., "An X-ray Photoelectron Emission Study of the Thermal Nitridation of SiO<sub>2</sub>/Si Interface," *J. Appl. Phys.*, July 1986.
43. Vasquez, R.P., Madhuker, A., Grunthaner, F.J., and Naiman, M.L., "Distribution of Nitrogen and Defects in SiO<sub>x</sub>Ny/Si Structures," *J. Appl. Phys.* Vol. 59, pp. 972, 3933, 1986.
44. Wynne, K.J., and Street, G.B., "Conducting Polymers," *N.R. Reviews*, 38, 1981.
45. Greene, L., and Street, G.B., "Conducting Organic Materials," *Science*, pp. 226, 651, 1984.
46. Wegner, G., Angew, K., "Polymers with Metal-like Conductivity -A Review of Their Synthesis Structure and Properties," *Chem. Int. Ed., Engl.*, a20, B361, 1981.
47. Kanazawa, K.K., Diaz, A.F., Giess, R.H., Gill, W.D., Kwak, J.F., Logan, J.A., Rabolt, J.F., and Street, B., "Organic Metals, A Stable Synthetic Metallic Polymer," *J. Chem. Soc., Chem. Commun.*, p. 894, 1979.
48. Diaz, A.F., and Hall, B., "Mechanical Properties of Electrochemical Polypyrrole Films," *IBM. J. Res. Dev.*, a27, B342, 1983.
49. Lai, H., Jenekhe, S.A., Jensen, R.J., and Royer, M., "Polymers in Electronics," *Solid State Technol.*, a12, B149, 1984.
50. Fan, F.-R. F., Wheeler, B.L., Bard, A.J., and Noufi, R.N., "Techniques for Stabilization of n-silicon Electrodes in Solution Photochemical Cells," *J. Electrochemical Soc.*, a128, B2024, 1981.
51. Noufi, R.N., Frank, A.J., and Nozik, A.J., "Stabilization of n-type Silicon Photoelectrodes to Surface Oxidation in Aqueous Electrolyte Solution and Mediation of Oxidation Reaction," *J. Am. Chem. Soc.*, B1849, 1981.
52. Noufi, R.N., Nozik, A.J., White, J., and Warren, L.F., "Enhanced Stability of Photoelectrodes with Electro-generated Polyaniline Films," *J. Electrochemical Soc.*, a129, B2261, 1982.

53. White, H.S., Abruna, H.D., and Bard, A.J., "Improvement in Performance of n-WSe<sub>2</sub> by Electrochemical Polymerization of o-phenylenediamine at Surface Imperfections," *J. Electrochemical Soc.*, a129, B265, 1982.
54. Parkinson, B.A., Furtak, T.E., Canfield, D., Kam, K., and Kline, G., "Evaluation and Reduction of Efficiency Losses at Tungsten Diselenide Photoanodes," *Discuss. Faraday Soc.*, a70, B233, 1980.
55. Canfield, D., and Parkinson, B.A., "Improvement of Energy Conversion Efficiency by Special Chemical Treatments of n-MoSe<sub>2</sub> and n-WSe<sub>2</sub> Photoanodes," *J. Am. Chem. Soc.*, a 103, B1279, 1981.
56. Nagasubramanian, G., DiStefano, S., and Moacanin, J., "Effect of Counter Ions on the Formation of Ohmic Contact between p-Si and Poly(pyrrole) Films; An AC Impedance Analysis," *J. Electrochemical Soc.*, 133, 305, 1986.
57. Nagasubramanian, G., DiStefano, S., and Moacanin, J., "Determination of the Si-conducting Polymer Interfacial Properties Using AC Impedance Technique," *J. Electronic. Mat.*, 15, 21, 1986.
58. Rohatgi, A., et al., *Development of High-Efficiency Solar Cells on Silicon Web*, Final Report, DOE/JPL 956786-86/10, Westinghouse Electric Corp., Pittsburgh, Pennsylvania, 1986.
59. Ho, F., Chu, C., Iles, P., *Development of High Efficiency Cells*, Final DOE/JPL 957098-86/7, Applied Solar Energy Corp., City of Industry, California, 1986.
60. Yoo, H.I., Iles, P.A., and Leung, D.C., *Silicon Solar Cell Process Development, Fabrication, and Analysis*, Annual Report, DOE/JPL-955089-81/12, 1981; Annual Report DOE/JPL-955089/82-15, 1982.
61. Rozgonyi, G.A., *Rapid Thermal Effects on CZ Substrates: Effects, Denuded Zones and Minority Carrier Lifetimes*, North Carolina State University, Raleigh, North Carolina. Final Report DOE/JPL-957175-86/1, 1986.
62. Crotty, G., Daud, T., and Kachare, R. "Front Surface Passivation of Silicon Solar Cells with Anti-reflection Coating," accepted for publication in *Appl. Phys. Letters*.
63. Hyland, S., and Uno, F., *Baseline Solar Cell Fabrication Procedure for Evaluation of Silicon Sheets*, JPL Document 5101-206, Jet Propulsion Laboratory, Pasadena, California, July 1982.
64. Daud, T., and Crotty, G., *New High Efficiency Solar Cells*, Final Report, JPL Publication 85-6, Jet Propulsion Laboratory, Pasadena, California, February 1985.
65. Crotty, G., and Daud, T., "Fabrication and Analysis of Dot Junction Silicon Solar Cells," *Proceedings of the 18th IEEE Photovoltaic Specialists Conference*, p. 424, Las Vegas, Nevada, 1985.
66. Daud, T., and Crotty, G., "Dot Junction Solar Cells," *J. Appl. Phys.*, Vol. 59, p. 2566, 1986.
67. Lamorte, M.F., *Comprehensive Silicon Solar Cell Modeling*, JPL Contract 956741, Final Report DOE/JPL-956741-86/1, 1986.
68. Lindholm, F.A., *Surface and Allied Studies in Silicon Solar Cells*, Quarterly Report of Contract 956525, DOE/JPL-956525-83/1, 1983.
69. Wolf, M., *Development and Analysis of Silicon Solar Cells of Near 20% Efficiency*, University of Pennsylvania, Philadelphia, Pennsylvania. Final Report DOE/JPL-956290-86/1, 1986.
70. Mokashi, A.R., Daud, T., and Kachare, R.H., *High-Efficiency Silicon Solar-Cell Design Evaluation and Sensitivity Analysis*, JPL Publication 85-46, JPL Document 5101-267, DOE/JPL-1012-107, Jet Propulsion Laboratory, Pasadena, California, October 15, 1985.
71. Green, M.A., et al., "High-Efficiency Silicon Solar Cells," *IEEE Transactions on Electron Devices*, Vol. ED-31, No. 5, pp. 679-683, Institute of Electrical and Electronic Engineers, Inc., New York, 1984.
72. Mokashi, A.R., Daud, T., and Kachare, R.H., *Sensitivity Analysis of a Passivated Thin Silicon Solar Cell*, JPL Publication 85-48, JPL Document 5101-269, DOE/JPL-1012-108, Jet Propulsion Laboratory, Pasadena, California, November 1, 1985.
73. Shockley, W., and Queisser, H.J., "Detailed Balance Limit of Efficiency of p-n Junction Solar Cells," *J. Appl. Phys.*, Vol. 32, pp. 510-519, March 1961.
74. Mokashi, A.R., Daud, T., and Kachare, R.H., "Simulation Analysis of a Novel High Efficiency Silicon Solar Cell," *Proceedings of the 18th IEEE Photovoltaic Specialists Conference*, p. 573, Las Vegas, Nevada, 1985.
75. Mokashi, A.R., Daud, T., and Kachare, R.H., *High-Efficiency Silicon Solar Cell Design and Practical Barriers*, JPL Publication 85-75, JPL Document 5101-281, DOE/JPL-1012-112, Jet Propulsion Laboratory, Pasadena, California, November 15, 1985.
76. Mokashi, A.R., Daud, T., and Kachare, R.H., "Identification of Some Key Parameters Limiting the Performance of High-Efficiency Silicon Solar Cells," (accepted for publication in *Solar Cells*).
77. Lin, E.I.H., "Sensitivity Analysis of Low Resistivity Solar Cells," *Proceedings of the 18th IEEE Photovoltaic Specialists Conference*, p. 715, Las Vegas, Nevada, 1985.

78. Luke, K.L., and Cheng, L.J., "Electron Beam-Induced-Current Characterization of Back-Surface-Field Solar Cells Using a Chopped Scanning Electron Microscope Beam," *J. Appl. Phys.*, Vol. 55, pp. 555-559, January 1984.
79. Daud, T., and Lindholm, F.A., "Direct Experimental Determination of Voltage Access High-Low Junction", *J. Appl. Phys.*, Vol. 59, p. 285, 1985.
80. Luke, K.L. and Cheng, L.J., "Characterization of the Heavily Doped Emitter and Junction Regions of Silicon Solar Cells Using an Electron Beam," *J. Appl. Phys.*, Vol. 32, pp. 2589-2595, October 1986.
81. Johnson, M.S., and Culik, J.S., "The Measurement of Variation in Minority Carrier Lifetime Due to Microstructural Defects in Large Area Polysilicon Wafers," *Proceedings of the 17th IEEE Photovoltaic Specialists Conference*, p. 548, San Diego, California, 1982.

## APPENDIX A

# Acquisition of References

Most of the references used in this report fall into one of four generic types: (1) JPL published reports, (2) reports prepared for JPL by an outside contractor, (3) articles in the proceedings of professional meetings, and (4) articles in professional journals.

### JPL PUBLISHED REPORTS

These reports nearly always contain an FSA Project document number of the form 5101-xxx, and many also contain a JPL Publication number (such as JPL Publication 83-52) and/or a Federal Government sponsor number in the form of DOE/JPL-1012-xx. Only those reports contain a JPL Publication number can be easily obtained from JPL. These can be obtained from:

Jet Propulsion Laboratory  
Documentation and Materiel Division  
4800 Oak Grove Dr.  
Pasadena, CA 91109

JPL reports containing the Federal Government sponsor number DOE/JPL-1012-xx can be obtained from:

U.S. Department of Commerce  
National Technical Information Service  
5285 Port Royal Rd  
Springfield, VA 22161

or

U.S. Department of Energy  
Technical Information Center  
Publication Request Section  
P.O. Box 62  
Oak Ridge, TN 37831

JPL reports without a JPL Publication number or Federal Government sponsor number are internal JPL reports. They are sometimes available from the Documentation and Materiel Division, which determines their releasability with the author's organization, assuming copies are still in print.

### JPL CONTRACTOR REPORTS

These reports are available from the National Technical Information Service (NTIS) at the Springfield, Virginia, address given above, using the Federal Government sponsor number (DOE/JPL 9xxxxx-xx) associated with the reference. They are generally not available from either JPL or the contractor who prepared the report.

## APPENDIX B

### Glossary

AC	alternating current	m-Si	microcrystalline silicon
AES	Auger electron spectroscopy	NI	numerical integration
AR	antireflective	OCVD	open-circuit voltage decay
ASEC	Applied Solar Energy Corp.	OED	oxygen-enhanced diffusion
ASLBIC	Absolute Spectral Light-Beam-Induced Current	PECVD	plasma-enhanced chemical vapor deposition
BIS	Brehmstrahlung Isochromat Spectroscopy	PV	photovoltaic(s)
BSC	back-surface contact	QMS	quadrupole mass spectroscopy
BSF	back-surface field	R&D	research and development
BSR	back-surface reflector	RF	radio frequency
CPU	central processing unit	rms	root-mean-square
c-Si	single-crystalline silicon	RTI	Research Triangle Institute
C-V	capacitance voltage	RTP	rapid thermal process
CVD	chemical vapor deposition	S	surface recombination velocity
CW	continuous wave	SB	back surface recombination velocity
Cz	Czochralski	SCAP1D	Solar Cell Analysis Program in One Dimension
DLTS	deep-level transient spectroscopy	SCCD	short circuit current delay
DC	direct current	sccm	standard cubic centimeters per minute
DOE	U.S. Department of Energy	SCT	solar cell transistor
DW	dendritic web	SEEMA	Solar-Cell Efficiency Estimation Methodology and Analysis
EBIC	electron-beam-induced current	SF	surface recombination velocity, front
EFG	edge-defined film-fed growth	Seff	effective surface recombination velocity
ESCCD	Electrical Short-Circuit Current Delay	SIMS	Scanning Ion Microprobe Spectroscopy
FF	fill factor	SLBIC	scanning laser-beam induced current
FSA	Flat-Plate Solar Array (Project)	Sp	front surface recombination velocity
FSC	front-surface contact	SPV	surface photovoltage
FZ	float-zone	SRH	Shockley-Reed-Hall
HEM	heat exchange method	SUNYA	State University of New York at Albany
IR	infrared	TEM	transmission electron microscopy
I <sub>sc</sub>	short-circuit current	UCLA	University of California, Los Angeles
I-V	current-voltage	UCP	ubiquitous crystallization process
J <sub>sc</sub>	junction current density	USC	University of Southern California
JCGS	Joint Center for Graduate Studies	UV	ultraviolet
JPL	Jet Propulsion Laboratory	VFE	vertical floating emitter
JRR	Junction Reverse Recovery	VLSI	very large scale integration
LBIC	light-beam-induced current	V <sub>oc</sub>	open-circuit voltage
LEED	low-energy electron diffraction	XPS	x-ray photoelectron spectroscopy
MBE	Molecular-Beam Epitaxy		
MLM	Modulated Light Measurement		

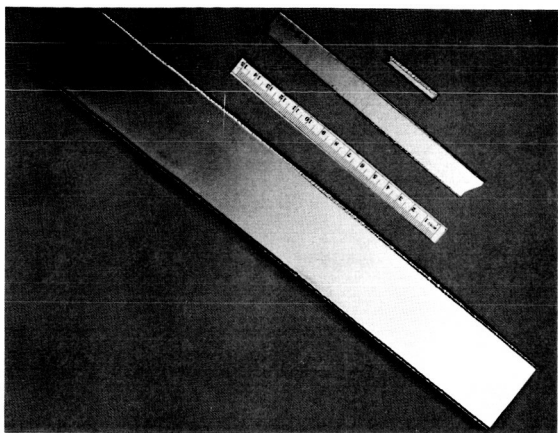
Prepared by the Jet Propulsion Laboratory, California Institute of Technology,  
for the U.S. Department of Energy through an agreement with the National  
Aeronautics and Space Administration.

The JPL Flat-Plate Solar Array Project is sponsored by the U.S. Department of  
Energy and is part of the National Photovoltaics Program to initiate a major  
effort toward the development of cost-competitive solar arrays.

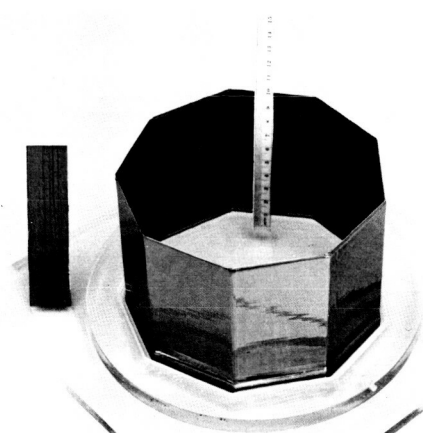
This report was prepared as an account of work sponsored by an agency of the  
United States Government. Neither the United States Government nor any  
agency thereof, nor any of their employees, makes any warranty, express or  
implied, or assumes any legal liability or responsibility for the accuracy, com-  
pleteness, or usefulness of any information, apparatus, product, or process  
disclosed, or represents that its use would not infringe privately owned rights.

Reference herein to any specific commercial product, process, or service by trade  
name, trademark, manufacturer, or otherwise, does not necessarily constitute or  
imply its endorsement, recommendation, or favoring by the United States  
Government or any agency thereof. The views and opinions of authors expressed  
herein do not necessarily state or reflect those of the United States Government  
or any agency thereof.

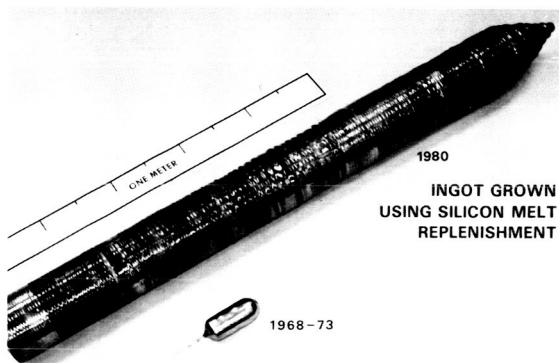
# More Technology Advancements



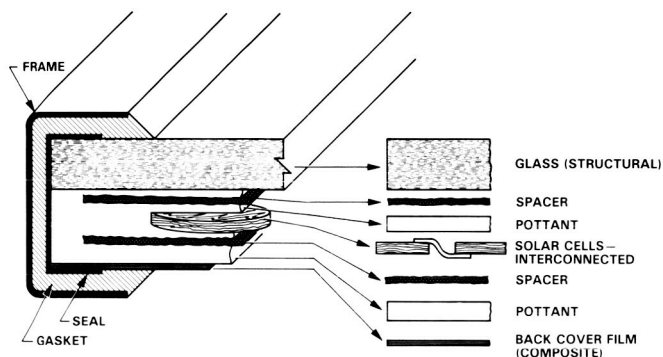
*Dendritic web silicon ribbons are grown to solar-cell thickness. Progress is shown by experimental ribbons grown in 1976 and 1978 and a ribbon grown in a Westinghouse Electric Corporation pilot plant.*



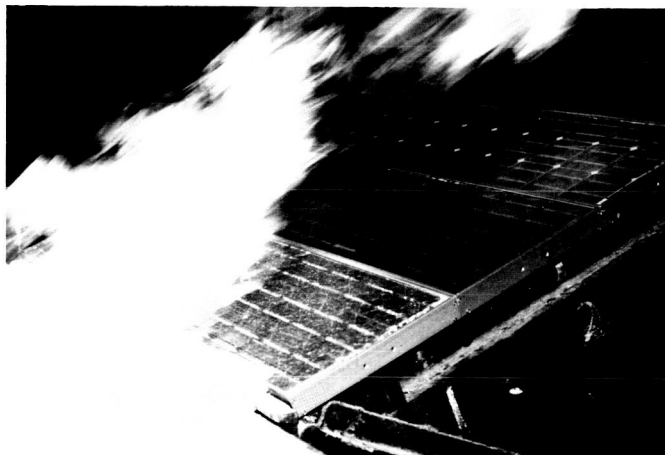
*The edge-defined film-fed growth silicon ribbons are grown to solar-cell thickness. A DOE/FSA-sponsored research ribbon grown in 1976 is shown next to a nine-sided ribbon grown in a Mobil Solar Energy Corporation funded configuration.*



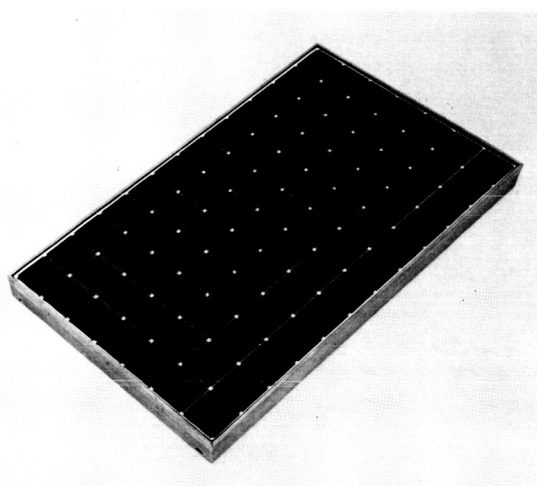
*Czochralski silicon crystals as grown are sawed into thin circular wafers. (Support for this effort was completed in 1981.)*



*Typical superstrate module design is shown with the electrically interconnected solar cells embedded in a laminate that is structurally supported by glass. Materials and processes suitable for mass production have been developed using this laminated design.*



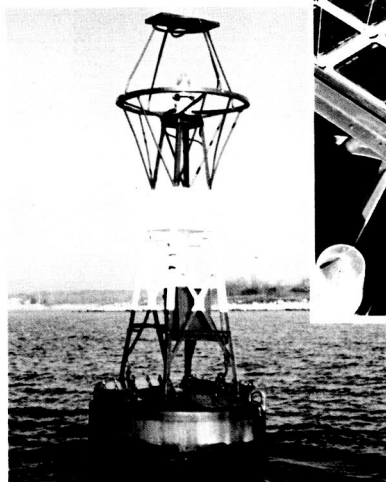
*Prototype modules have passed UL 790 Class A burning brand tests which are more severe than this spread of flame test.*



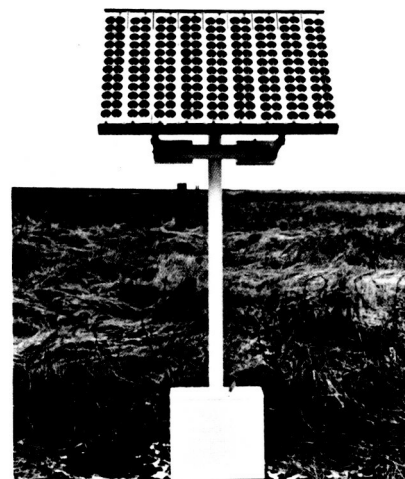
*A 15.2% efficiency prototype module (21 x 36 in.) was made by Spire Corp. using float-zone silicon wafers. Recently, similarly efficient modules were fabricated from Czochralski silicon wafers.*

# Photovoltaic Applications

1975



*U.S. Coast Guard buoy with photovoltaic-powered navigational light.*



*Photovoltaic-powered corrosion protection of underground pipes and wells.*

Later...



*House in Carlisle, Massachusetts, with a 7.3-kW photovoltaic rooftop array. Excess photovoltaic-generated power is sold to the utility. Power is automatically supplied by the utility as needed.*



*A 28-kW array of solar cells for crop irrigation during summer, and crop drying during winter (a DOE/University of Nebraska cooperative project).*

1985



*1.2 MW of photovoltaic peaking-power generation capacity for the Sacramento Municipal Utility District. (The 8 x 16 ft panels are mounted on a north-south axis for tracking the sun.)*